TUNABLE FREQUENCY MICROSTRIP ANTENNAS BY RF-MEMS TECHNOLOGY

A THESIS SUBMITTED TO
THE GRADUATE SCHOOL OF APPLIED AND NATURAL SCIENCES
OF
MIDDLE EAST TECHNICAL UNIVERSITY

BY

EMRE ERDİL

IN PARTIAL FULFILMENT OF THE REQUIREMENTS
FOR
THE DEGREE OF MASTER OF SCIENCE
IN
ELECTRICAL AND ELECTRONICS ENGINEERING

MAY 2005

Approval of Graduate School of Natural and Applied Sciences.

_____

Prof. Dr. Canan ÖZGEN

Director

I certify that this thesis satisfies all the requirements as a thesis for the degree of Master of Science.

_____

Prof. Dr. İsmet ERKMEN

Head of Department

This is to certify that we have read this thesis and that in our opinion it is fully adequate, in scope and quality, as a thesis for the degree of Master of Science.

_____

Assoc. Prof. Dr. Özlem AYDIN ÇİVİ

Supervisor

Examining Committee Members

Assoc. Prof. Dr. Gülbin DURAL (METU, EE) _____

Assoc. Prof. Dr. Özlem AYDIN ÇİVİ (METU, EE) _____

Assoc. Prof. Dr. Sencer KOÇ (METU, EE) _____

Assoc. Prof. Dr. Şimşek DEMİR (METU, EE) _____

Assoc. Prof. Dr. Vakur ERTÜRK (BİLKENT, EE) _____

I hereby declare that all information in this document has been obtained and presented in accordance with academic rules and ethical conduct. I also declare that, as required by these rules and conduct, I have fully cited and referenced all material and results that are not original to this work.

Name, Last name: Emre ERDİL

Signature :

ABSTRACT

TUNABLE FREQUENCY MICROSTRIP ANTENNAS BY RF MEMS TECHNOLOGY

Erdil, Emre

M.Sc., Department of Electrical and Electronics Engineering
Supervisor: Assoc. Prof. Dr. Özlem Aydın Çivi

May 2005, 97 pages

This thesis presents the design, fabrication, and measurement of tunable frequency microstrip antennas using RF MEMS (Microelectromechanical Systems) technology. The integration of RF MEMS components with radiators enable to implement tunable systems due to the adjustable characteristics of RF MEMS components.

In the frame of this thesis, different types of structures have been investigated and designed. The first structure consists of a microstrip patch antenna which is loaded with a microstrip stub whose length is controlled by RF MEMS switches. In the other structure, the length of a microstrip patch antenna is changed by connecting a metal plate using RF MEMS switches. The third structure is composed of a microstrip patch antenna and a microstrip stub on

which RF MEMS variable capacitors are placed periodically to control the resonant frequency. In order to maintain an easier integration with RF MEMS capacitors, another structure consisting of a microstrip patch antenna and a coplanar waveguide (CPW) stub which is loaded with variable RF MEMS capacitors is designed. The final structure is a dual frequency CPW-fed rectangular slot antenna whose resonant frequencies are shifted by RF MEMS variable capacitors placed on a short circuited stub inserted inwards the antenna.

The fabrication of CPW-fed rectangular slot antenna is completed in the MEMS fabrication facilities of METU using RF MEMS process based on electroforming on glass substrate. The measurement results show that RF MEMS components might be a proper solution to obtain tunable frequency antenna structures.

Keywords: RF MEMS, reconfigurable antennas, microstrip antennas, multi-frequency antennas, capacitive loading.

ÖZ

RF MEMS TEKNOLOJİSİ İLE FREKANSI AYARLANABİLİR MİKROŞERİT ANTENLER

Erdil, Emre

Yüksek Lisans, Elektrik ve Elektronik Mühendisliği Bölümü
Tez Yöneticisi: Doç. Dr. Özlem Aydın Çivi

Mayıs 2005, 97 Sayfa

Bu tez RF MEMS teknolojisi ile frekansı ayarlanabilir mikroşerit antenlerin tasarımını, üretimini ve ölçümünü sunmaktadır. Antenlerin RF MEMS devre elemanları ile bütünleştirilmesi RF MEMS devre elemanlarının ayarlanabilir özelliklerinden dolayı ayarlanabilir sistemlerin gerçekleştirilmesini mümkün kılmaktadır.

Bu tez çerçevesinde farklı tipte yapılar incelenmiş ve tasarlanmıştır. İlk yapı, uzunluğu RF MEMS anahtarlarla kontrol edilen mikroşerit kütük ile yüklenen mikroşerit yama antenden oluşmaktadır. Diğer yapıda, mikroşerit yama antenin uzunluğu metal bir plakanın RF MEMS anahtarlar ile birleştirilmesi kaydıyla değiştirilmektedir. Üçüncü yapı, mikroşerit yama anten ve rezonans frekansı kontrol etmek için kütük üzerine periyodik olarak yerleştirilmiş RF

MEMS değişken sığalardan oluşmaktadır. Ayrıca, RF MEMS sığalarla daha kolay bütünleşme sağlayabilmek için mikroşerit yama anten ve değişken RF MEMS sığalarla yüklenmiş eşdüzlemsel dalga kılavuzu (EDK) kütükten oluşan bir yapı tasarlanmıştır. Son yapı rezonans frekansı anten içine doğru sokulan kısa devre kütük üzerine yerleştirilen RF MEMS sığalar ile kaydırılan EDK beslemeli çift frekanslı dikdörtgen yarık antendir.

RF MEMS sığalarla yüklenmiş yarık anten üretimi ODTÜ MEMS üretim tesislerinde, cam taban üzerine elektroşekillendirmeye dayanan RF MEMS süreciyle üretilmiştir. Ölçüm sonuçları göstermektedir ki RF MEMS devre elemanları frekansı ayarlanabilir anten yapılarının elde edilebilmesi için uygun bir çözümdür.

Anahtar kelimeler: RF MEMS, yeniden şekillendirilebilir antenler, mikroşerit antenler, çoklu-frekans antenler, sığasal yükleme.

To my family

ACKNOWLEDGMENTS

I would like to thank Prof. Özlem Aydın Çivi for her supervision, valuable guidance, support and tolerance during the thesis study.

I also would like to thank Prof. Altunkan Hızal for providing the millimeter wave laboratory and contribution to the research. I would like to acknowledge Prof. Şimşek Demir for contribution to the research.

I wish to express my sincere gratitude to Kağan Topallı for his contribution not only for the thesis but also in my whole life. I would like to express my appreciation to Mustafa Seçmen, Orhan Akar, Mehmet Ünlü, and Yusuf Tanrıkulu for their help.

I would like to thank specially my family for their very love and support at my hard times.

TABLE OF CONTENTS

LIST OF TABLES

TABLES

LIST OF FIGURES

FIGURES

CHAPTER 1

INTRODUCTION

With the development of the systems operating at different frequencies, there is a growing need for a single antenna that can be tuned dynamically to operate at different frequencies. The usage of a single antenna on the system for various applications reduces the system size and cost. Due to these advantages, frequency tunable antennas are preferred both in military and commercial systems. For instance, an antenna whose resonant frequency can be tuned in an analog manner can be used in radar applications for frequency hopping. A discretely tuned antenna can be used in telecommunications systems to maintain different system frequencies. Tunable antennas also find application area in satellite communications systems for adjusting one operating frequency as transmitter and the other as receiver.

To tune the resonant frequency of the antenna in a dynamic manner tunable components are required. Microelectromechanical systems (MEMS) and the application of this technology to RF systems enable production of these tunable components with low power consumption, high linearity and high performance. Tunable circuit elements produced by RF MEMS technology makes the realization of dynamically reconfigurable structures more efficiently in terms of lower insertion losses, integration on low dielectric-constant substrates. Also, the monolithic fabrication of the antenna together with these tunable components reduces the power losses and parasitic effects compared to integration of discrete

components. MEMS switches and MEMS tunable capacitors are used in reconfigurable antennas to control the resonant frequency, bandwidth, polarization and radiation pattern of these antennas.

Reconfigurable antenna structures designed and fabricated in the frame of this thesis include tunable RF MEMS components integrated with microstrip antennas. Microstrip antennas are preferred in frequency tunable antenna applications for their advantages such as;

- Being lightweight and having small volume and low-profile planar configuration.
- Ease of mass production using printed-circuit technology leading to a low fabrication cost.
- Easy integration with other MMICs on the same substrate.
- Allowing both linear and circular polarization.
- Ability to being made compact for use in personal mobile communication.
- Allowing for dual and triple-frequency operation [1].

The aim of this thesis is to demonstrate the advantages of RF MEMS technology in terms of tuning the resonant frequency of the microstrip antennas when they are integrated with tunable RF MEMS components such as switches and capacitors. For that purpose, design, fabrication, and measurements of different reconfigurable antenna structures using RF MEMS technology are accomplished in the frame of this thesis. The simulation and measurement results obtained from these designs prove that the integration of tunable RF MEMS components with the radiators enables significant amount of tuning of resonant frequency of the antennas.

Section 1.1 gives a brief summary about RF MEMS. Section 1.2 explains RF MEMS capacitor and its application areas. Section 1.3 summarizes previous

work on reconfigurable antennas and methods for tuning the resonant frequency of an antenna.

1.1 RF MEMS: General View

The 1970s were the starting time for developing microelectromechanical systems (MEMS) structures. Several kinds of sensors, accelerometers were developed using MEMS technology. However, the first MEMS switch for microwave applications was produced in 1991, and the relatively very high performance of the switch with respect to GaAs devices made several research groups take attention on this research area [2]. Time on, several kinds of components were produced using MEMS technology such as; switches [3]-[7], capacitive switches [8]-[10], tunable capacitors [11]-[18], transmission lines, high-Q resonators, and filters [2].

There are several advantages of RF MEMS devices such as:

- Extremely low power consumption: RF MEMS switches consume 0.05-0.1 mW power including the voltage upconverter or drive circuitry necessary for raising the input 3-5 V control voltage to the 20-80 V actuation voltage of the MEMS switches which is a very good performance with respect to PIN diode as PIN diode consume 5-100 mW power [2].
- Linearity: Since the MEMS switches do not contain a semiconductor junction and do not have an exponential current versus voltage relationship, they are extremely linear devices [2].
- Low loss: The loss range of RF MEMS switches are 0.05-0.2 dB for 1-100 GHz band whereas the loss range is 0.3-1.2 dB for GaAS PIN diode and 0.4-2.5 dB for transistor switches [2].

- Isolation: RF MEMS switches offer very high isolation in 1-40 GHz band (~45 dB) and high isolation in 60-100 GHz band, (~25 dB), with respect to GaAs PIN diode and transistor switches having only 20 dB isolation [2].

By these advantages RF MEMS find application in communication systems, radar systems and switching networks, reconfigurable antennas, reconfigurable matching networks, tunable filters, phase shifters, low phase-noise oscillators subsystems [2].

Tunable circuit elements produced by RF MEMS technology make the realization of dynamically reconfigurable structures more efficiently in terms of lower insertion losses, integration on low dielectric-constant substrates. MEMS switches and MEMS tunable capacitors are used in reconfigurable antennas to control the resonant frequency, bandwidth, polarization and radiation pattern of these antennas.

Besides the advantages of RF MEMS technology there are some disadvantages. Since the operation of RF MEMS devices can be affected by the environmental conditions, i.e. water vapor, oxygen, contaminants, and other hydrocarbons, good packaging of these devices are required for commercial applications. Since the cost of hermetic packages for RF MEMS is $2-50 per unit, the possibility of nonhermetic packaging for RF MEMS devices is considered to determine the application areas of RF MEMS devices [2]. Also for many applications, the required actuation voltage for RF MEMS switches is 20-80 V which is a very high value for most of the systems that RF MEMS is being considered to be implemented. The reliability of RF MEMS components is one of the main research area in the field of RF MEMS. Lifetime, RF power handling, failure modes are all investigated in the frame of reliability by many researchers. For example, the failure of RF MEMS switch after 10 Billion cycles of operation

have been demonstrated which can be a limiting case for the use of RF MEMS devices for the applications requiring higher number of switching.

1.2 RF MEMS Tunable Capacitors

Tunable capacitor is a capacitor of which the capacitance can be tuned by applying DC voltage. The application areas of MEMS tunable capacitors are tunable matching networks, tunable filters, loaded-line phase shifters and reconfigurable antennas. Since the dielectric material in RF MEMS tunable capacitors is air, these components have lower losses and higher quality factor. Excellent linearity is shown by RF MEMS tunable capacitors, as the interference between the capacitance variations and the applied RF signal is small [19].

Tuning of MEMS capacitance is done basically by two methods:

- Gap-tuning, tuning the spacing between the two plates.
- Area-tuning, tuning the overlapping area between the two plates. The plates form finger-like structures and by actuating the plates the overlapping area changes forming a tunable capacitance.

In the gap-tuning method, by applying a DC voltage between the plates, an attractive electrostatic force between the plates occurs resulting in reducing the distance between the plates that is increasing the capacitance. Pull-in instability occurs when the gap between the plates reduces to 2/3 of its original value which is limiting the tuning range of the capacitor [19]. Dussopt and Rebeiz [11] present two tunable capacitors based on electrostatic actuation. One of the tunable capacitors is an extended tuning range MEMS varactor showing a capacitance ratio of 1.46. The other varactor is a discrete-position varactor with a capacitance ratio of 1.90. Both designs result in a quality-factor of 95-100 at 34 GHz.

In the area tuning method, basically by applying electrostatic force, the area between the plates moves resulting in changing the area and tuning the capacitance. Figure 1.1 shows the typical schematics of an area-tuning MEMS capacitor. Yao et al. [20] proposed an interdigitated comblike structure of which movement based on the electrostatic force between the movable comb and the fixed comb. The overlapping area is a function of the applied voltage. Measurement results of the structure shows a tuning ratio of %100 at 5V.

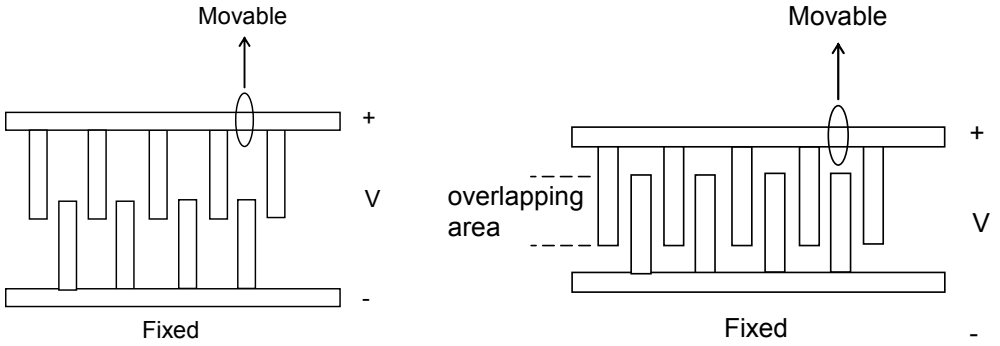

(a) (b)

Figure 1.1 Parallel-plate area-tunable MEMS capacitor. (a) Schematic representation of an unactuated comb-like structure. (b) By applying electrostatic force, i.e. actuation, the movable plate drifts into the fixed plate forming an increase in the overlapping area. The change in the overlapping area results in change in the capacitance.

To avoid pull-in instability, different actuation types rather than electrostatic actuation have also been used. Park et al. [12] describes a tunable capacitor using piezoelectric actuators. C_{max}/C_{min} ratio of 3.1 with quality-factor 210 (at 1 GHz) is obtained. Thermal actuators have also been used for the same problem. Wu et al. [13] describes a tunable MEMS capacitor actuated thermally. The gap variation for the described MEMS capacitor is from 2 to 0.2 μm. Feng et al. [14] also describes a tunable capacitor actuated electrothermally. The measured

quality-factor is 256 and the C_{max}/C_{min} ratio is 2. C_{max}/C_{min} ratio achieved by electrothermally actuation is higher than the ratio achieved by using piezoelectric actuators.

1.3 Previous Work on Reconfigurable Antennas

With the development of the military and telecommunications systems operating at different frequencies, there is a growing need for the reconfigurable antennas to operate at these different frequencies for reducing the size and cost of these systems. To dynamically tune the resonant frequency of the antenna, tunable components are needed.

Tunable characteristics of the RF MEMS devices and the integration of these devices with the antennas enable reconfigurability of the antennas in terms of resonant frequency, polarization and radiation pattern. Simons et al. [21] describes MEMS actuators to tune the resonant frequency of a patch antenna. Patch antennas with two independent MEMS actuators and with two MEMS actuators in series are designed and the measurement results show that with two independent MEMS actuators the patch can be reconfigured dynamically to operate at frequency separated by 0.8 percent of the nominal frequency whereas the frequency separation is 15 percent with two series MEMS actuators.

Simons et al. [22] also describes a polarization reconfigurable patch antenna with integrated MEMS actuators. The actuator consists of a metal overpass suspended over a metal stub, and the actuator is actuated by an electrostatic force of attraction occurred by applying voltage between the overpass and the metal stub. When the MEMS actuator is in the OFF state, the antenna radiates circularly polarized whereas in the ON state the electrostatic force pulls down the overpass, resulting in perturbation in the phase relation between the two modes which causes the radiation to be reconfigured as linearly polarized.

1.3.1 Resonant Frequency Tuning Methods for Antennas

This section gives some methods to be used to tune the resonant frequencies of various antennas such as dipoles, slot antennas, microstrip antennas.

1.3.1.1 Dipole and Slot Antennas

The idea to control the resonant frequency of a dipole antenna is to change the length of the antenna by using MEMS switches. In order to adjust the length of the antenna for the desired resonant frequency range, MEMS switches for the corresponding length are taken into down-state position. This application has been done using PIN diode or FET switches at 0.1-3 GHz, but the frequency range can be extended to 120 GHz using MEMS series switches [2]. Figure 1.2 shows the schematics of a dipole antenna whose length is controlled by RF MEMS switches. Due to the change in the length of the antenna the resonant frequency can be tuned.

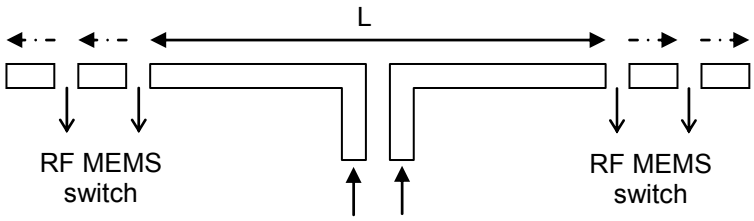

Figure 1.2. Frequency tunable dipole antenna with RF MEMS switches.

The resonant frequency of the slot antennas can be controlled by changing the slot length using MEMS series switches with a similar approach used for dipole antennas. As the switch is not large enough to short circuit the gap, indentations is required for this approach [2].

1.3.1.2 Microstrip Antennas

Changing the dimensions of the antenna: This method is based on changing the physical dimensions of the microstrip antenna by using RF MEMS switches. This can be realized as placing metal plates near one of the radiating edges of the microstrip antenna and binding these plates by MEMS switches. For each different combination of MEMS switches the resonant frequency of the antenna shifts to a different value [2].

Loading by stub: The resonant frequency of a microstrip antenna can be tuned by changing its resonant dimension. Stub can be used to change the effective resonant length of the antenna. Using stubs having different lengths it is possible to tune the resonant frequency of the antenna [1]. Changing the length of the stub can be done by series MEMS switches. The stub can be placed along the radiating edges or nonradiating edges of the microstrip antenna.

If the antenna is loaded by a stub at the center of one of its radiating edges, the overall effective resonant length of the antenna increases which makes the resonant frequency decrease. Changing the dimensions of the stub, the resonant frequency and bandwidth can be tuned. For this configuration the cross-polar level increases since the symmetry is disturbed by adding a single stub [1].

The resonant length of the antenna can be changed also by loading the antenna by stubs on both of the radiating edges. In this case the radiation pattern is more like the pattern for the unloaded microstrip antenna [1].

In microstrip antennas the electric field varies along the nonradiating edges. So, the location of the stub on these edges has effect on the input impedance together with the resonant frequency of the antenna [1].

Loading by varactor diode: In this method, the antenna is loaded by a tunable capacitor to change the equivalent capacitance of the antenna which results in changing the resonant frequency [1].

Using shorting posts: Shorting post changes the field distribution and provides inductive loading to the patch therefore it changes the resonant frequency of the antenna. The position and the number of the shorting posts determine the tuning of the resonant frequency [1].

The thesis is composed of four chapters. Chapter 2 presents the design considerations of the tunable antenna structures designed in the frame of thesis by giving simulation results. Chapter 3 gives the fabrication process and the measurement results of the structures fabricated. Finally, chapter 4 summarizes the work throughout the thesis.

CHAPTER 2

DESIGN OF RECONFIGURABLE MICROSTRIP ANTENNA STRUCTURES USING RF MEMS TECHNOLOGY

This chapter presents the design considerations of tunable frequency microstrip antennas. The performances of antennas in terms frequency tuning are examined when they are integrated with RF MEMS components such as switches and capacitors. The designs include tunable microstrip patch antenna and slot antenna. These structures are finalized according to the fabrication process optimized at the facilities of METU which is presented in the next chapter.

First, the frequency tuning methods presented in the previous chapter are employed on microstrip patch antennas. The designs using the method of loading the patch antenna with stub and the method of changing the dimensions of the patch antenna are examined. The description of these designs together with the simulation results are presented in section 2.1.

Section 2.2 presents the circuit model analyses based on basic transmission line model of the patch antenna. The circuit model analyses are used to get idea about the effect of the capacitors on the resonant frequency since one of the approaches in the frame of the thesis is employing RF MEMS capacitors for tuning the resonant frequency of the antennas. An analysis of the patch antenna loaded with a stub terminated by a capacitor is investigated by using transmission line method. As RF MEMS capacitors are placed onto stubs in our designs to

control the characteristic impedance of the stub, the effects of characteristic impedance of the stub on the resonant frequency are examined.

Section 2.3 presents a frequency tunable microstrip patch antenna loaded with microstrip stub on which RF MEMS capacitors are placed. Simulation results concerning the change in the resonant frequency due to the capacitive loading are given. In section 2.4 the resonant frequency of a microstrip patch antenna loaded with open ended CPW stub is tuned by using RF MEMS capacitors. Section 2.5 presents a dual frequency rectangular slot antenna whose resonant frequencies are tuned by loading the antenna with a short circuited stub on which RF MEMS cantilever type capacitors are placed.

2.1 Tuning the Resonant Frequency of the Microstrip Patch Antenna using RF MEMS Series Switches

The resonant frequency of a microstrip patch antenna can be tuned by using stubs with variable length which can be realized by RF MEMS switches. This section starts with the design of a microstrip patch antenna operating at 10 GHz and presents two approaches on the use of RF MEMS series switches to tune resonant frequency. The first approach employs the idea of loading the microstrip patch with a stub whose length can be controlled using RF MEMS series switch. In the other approach, a metallic plate is connected to the patch antenna using RF MEMS switches resulting in a change in the electrical length.

2.1.1 Stub Loaded Microstrip Patch Antenna

This section gives the results of the analysis on the stub loaded microstrip patch antenna. The dimensions of the unloaded microstrip patch antenna and the reflection coefficient characteristic of the antenna are shown in Figure 2.1 (a) and

Figure 2.2, respectively. Antenna is terminated by a 2 mm length open-ended stub on the midpoint of the radiating edge opposite to the feeding line as shown in Figure 2.1 (b). Due to the effect of the stub the resonant length of the antenna increases resulting in a decrease in the resonant frequency. According to the simulations done by Ansoft Ensemble 8.0^{TM} the resonant frequency of the antenna loaded by 2 mm length stub occurs at 9.45 GHz which is at 10 GHz without the stub. The length of the stub can be adjusted by using MEMS cantilever type switches, whose anchors are attached on the patch antenna. These switches are actuated by applying DC voltage between the patch antenna and the stub which results in electrostatic attraction force exerted on the cantilever. The up-state and down-state positions of the MEMS switches determine the length of the stub loading the antenna. To understand the effect of the up-state position of the MEMS switch to be applied on the structure, as can be seen in Figure 2.1 (c), the stub is divided into two equal length pieces having lengths 0.8 mm with a spacing 0.4 mm. The resonant frequency is at 9.85 GHz for this case. The spacing between the pieces is then connected with 0.1 mm width conductor to observe the down-state effect of the MEMS switch. As seen from Figure 2.2, the resonant frequency of the structure occurs at 9.45 GHz which is the same value as the antenna loaded by 2 mm length stub. According to the simulation results for a single MEMS switch structure the resonant frequency changes between 9.85 GHz-9.45 GHz, corresponding to 4 % change, for up-state and down-state.

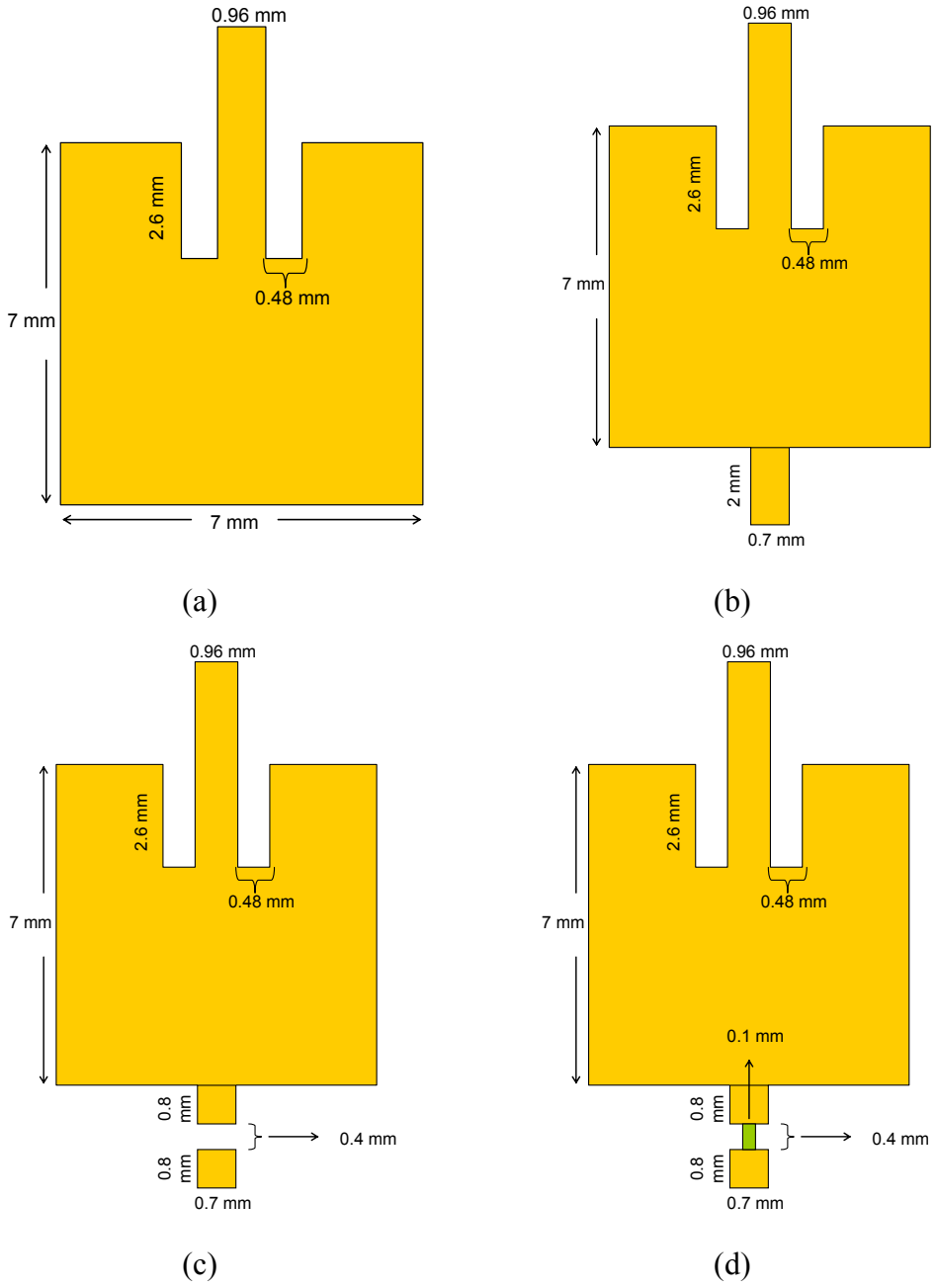

Figure 2.1. (a) Geometry of the microstrip patch antenna operating at 10 GHz. (b) The microstrip patch antenna loaded by 2 mm length stub. (c) The RF MEMS switch at up-state position. (d) The RF MEMS switch at down-state position.

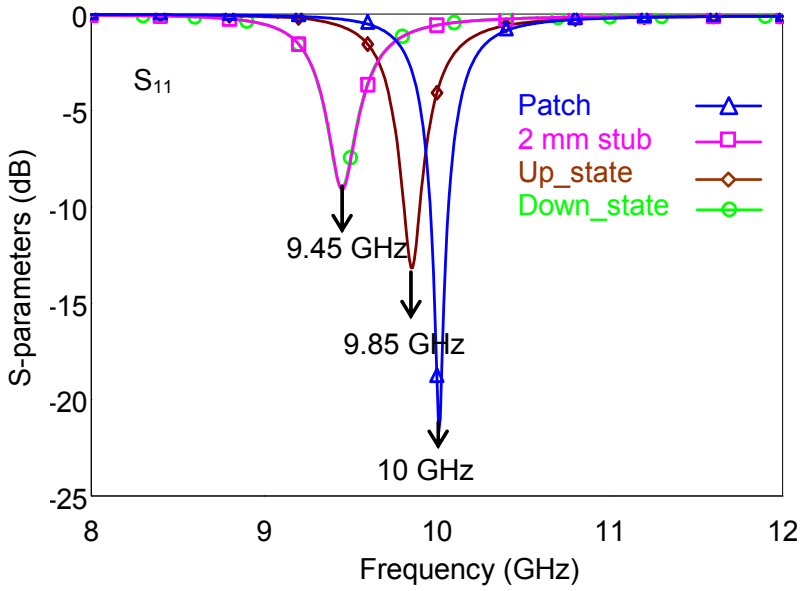

Figure 2.2. The reflection coefficient characteristics of the antennas.

2.1.2 Changing the Physical Dimension of a Microstrip Patch Antenna Using RF MEMS Switches

On the other structure, the resonant frequency of the microstrip patch antenna is tuned by changing the physical dimensions of the antenna. A metal plate having dimensions 7 mm width and 1 mm length is placed 0.4 mm apart of the radiating edge opposite to the feeding line of the patch antenna. MEMS cantilever type switches are used to make a connection between the patch and the plate to increase in the length of the antenna. These switches are actuated by applying DC voltage between the patch antenna and the plate resulting in attraction of the cantilevers. The structure without MEMS switches is shown in Figure 2.3 (a). This figure also corresponds to the up-state position of the MEMS switches which are considered to be ideal in the simulations. The reflection coefficient characteristic and the radiation patterns for the E- and H- planes are given in Figure 2.4 and in Figure 2.5 (a)-(b), respectively.

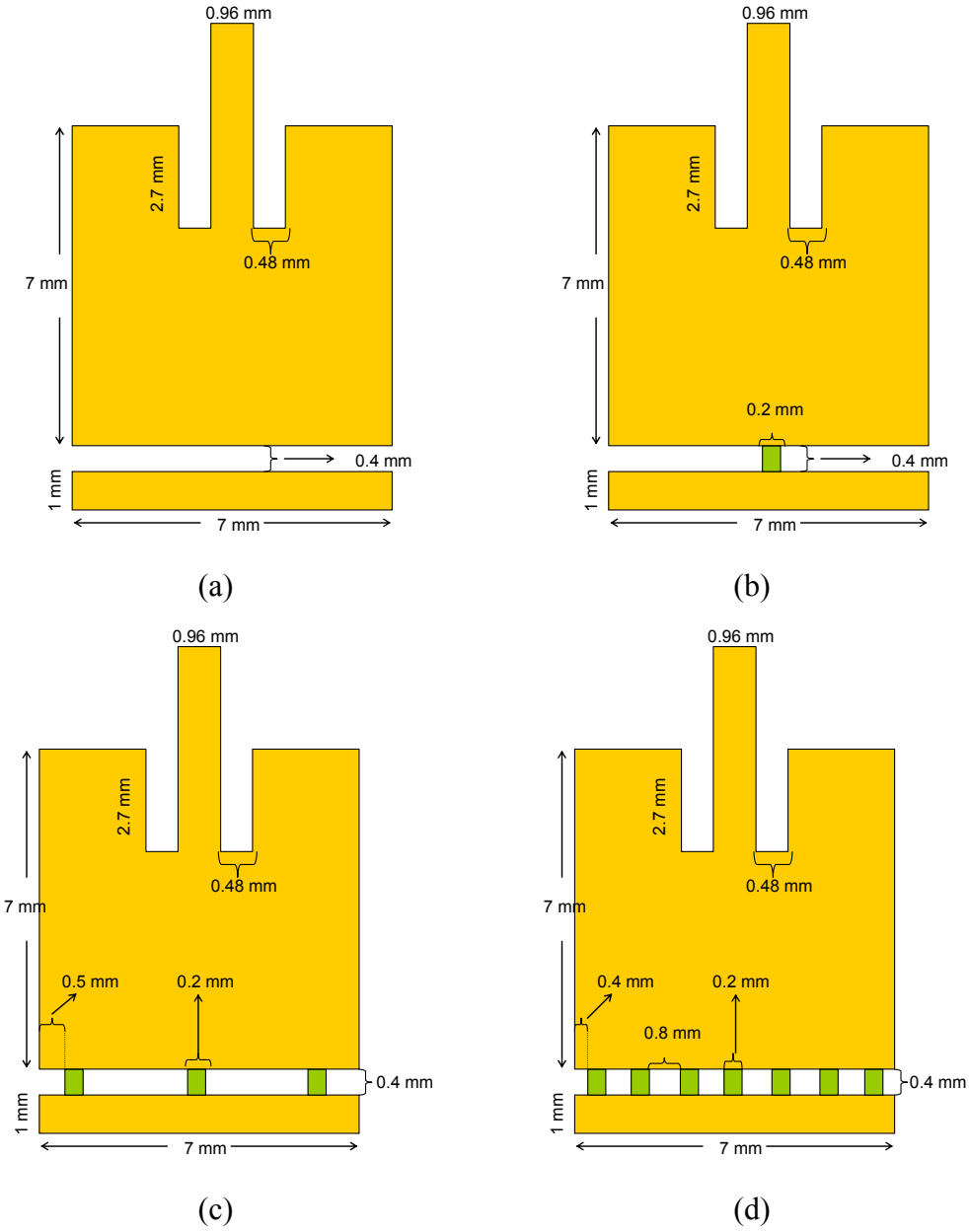

Figure 2.3. (a) Microstrip patch antenna when RF MEMS switches are up-state position. (b) Microstrip patch antenna to which metal plate is connected with single RF MEMS switch. (c) Microstrip patch antenna to which metal plate is connected with 3 RF MEMS switches. (d) Microstrip patch antenna to which metal plate is connected with 7 RF MEMS switches.

Firstly, the connection between the plate and the patch is made by a single MEMS switch having a width of 0.2 mm. The structure is shown in Figure 2.3(b) and the related reflection coefficient characteristic is given in Figure 2.4. The resonant frequencies of the structure occur at 6 GHz and 10.66 GHz with distorted matching. The radiation patterns of the structures for the given resonant frequencies given in Figure 2.6 (a)-(d) show similar behavior for both of the frequencies in E- and H- plane.

Then, the effect of the number of RF MEMS switches on the connection of the patch and the plate is investigated. The structure with 3 RF MEMS switches is shown in Figure 2.3 (c). The reflection coefficient characteristic of the structure when the switches are in down-state position is in Figure 2.4. The resonant frequencies of the antenna are at 8.2 GHz and 14.2 GHz. As can be seen from the radiation patterns for the related frequencies in Figure 2.7 (a)-(d), the antenna radiates nearly broadside at 8.2 GHz whereas the radiation is not broadside for E-plane and cross-polar component is high in H- plane at 14.2 GHz. Figure 2.3 (d) shows the structure that the plate is connected to the patch via 7 RF MEMS switches. Reflection coefficient characteristic and related radiation patterns are given in Figure 2.4 and Figure 2.8 (a)-(d), respectively. The antenna radiates nearly broadside at the lower resonant frequency, which is 8.44 GHz. The reason for the slight deviation of maximum radiation for E- plane at broadside might be due to the asymmetric geometry of the structure for this plane.

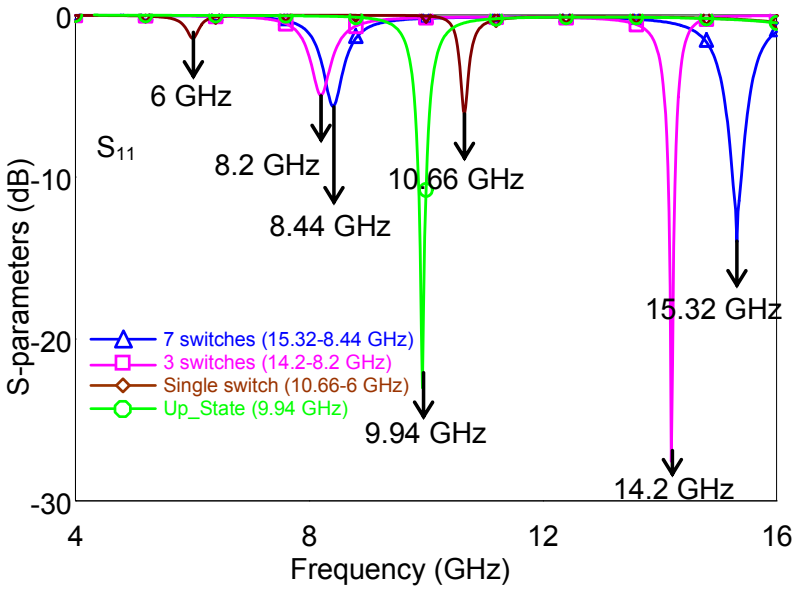

Figure 2.4. The reflection coefficient characteristics of the structures in Figure 2.3.

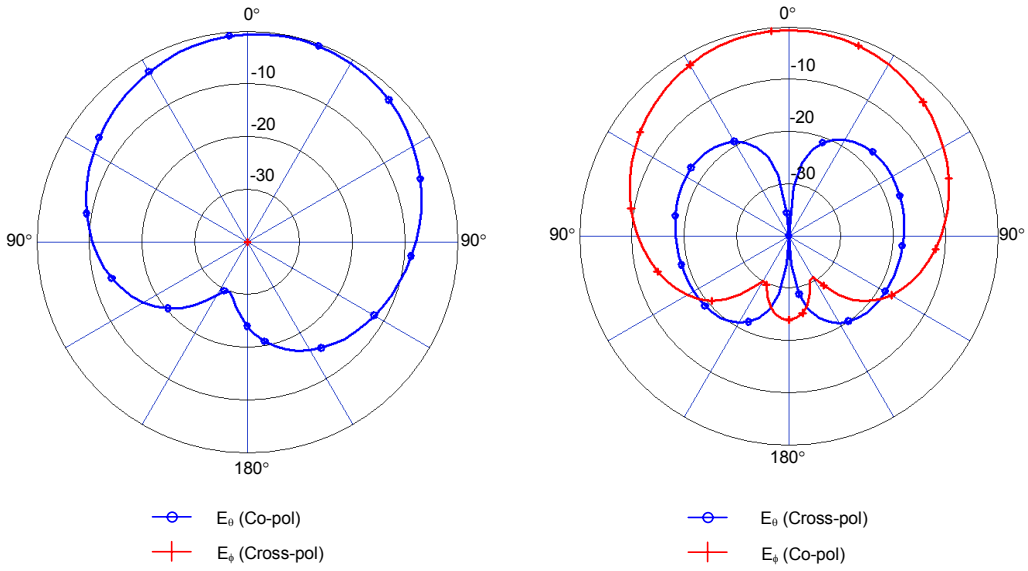

(a) E- plane at 9.94 GHz (b) H- plane at 9.94 GHz

Figure 2.5. The radiation patterns of the antenna in Figure 2.3 (a) for the resonant frequency at 9.94 GHz. (a) E-plane at 9.94 GHz. (b) H- plane at 9.94 GHz.

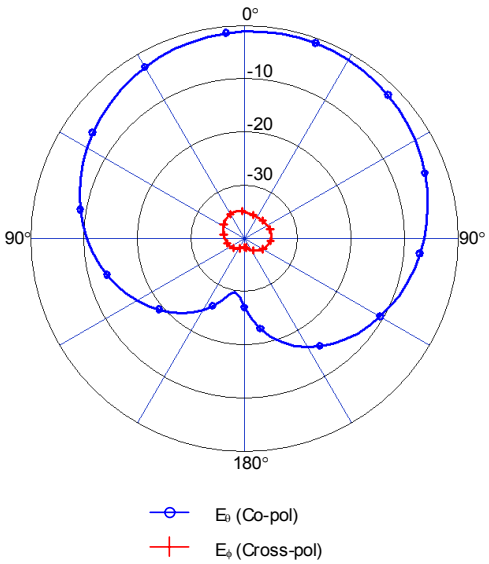

(a) E- plane at 6 GHz

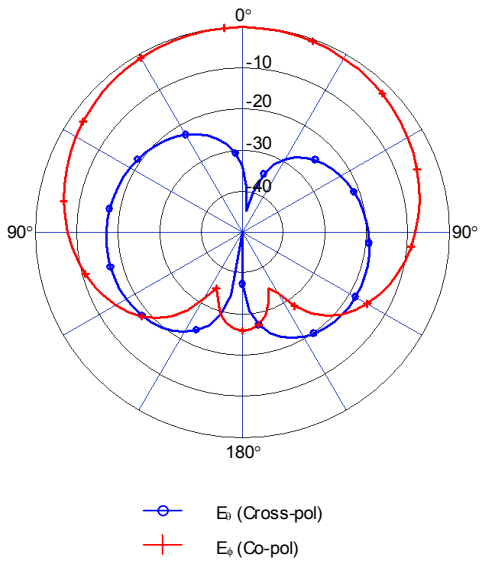

(b) H- plane at 6 GHz

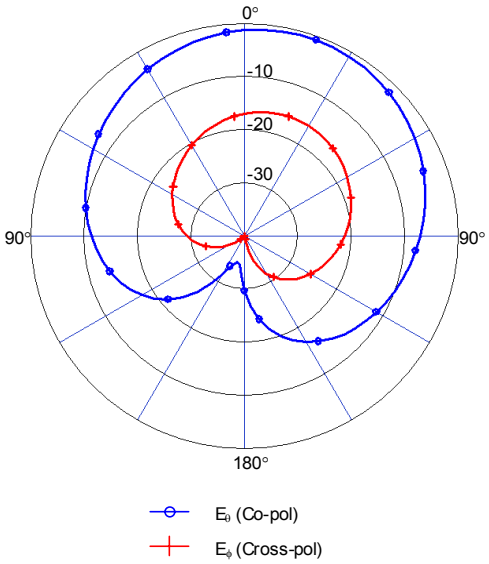

(c) E- plane at 10.66 GHz

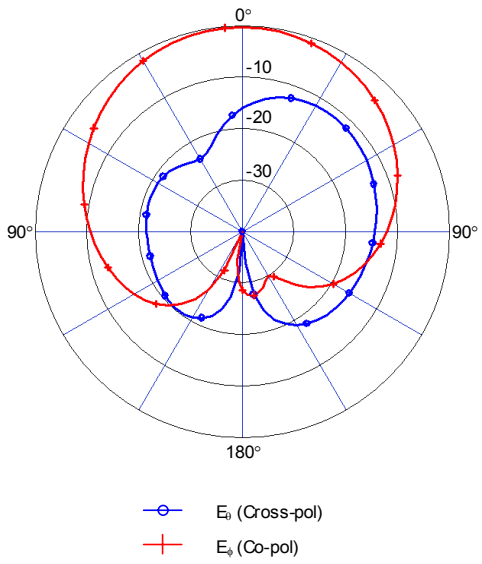

(d) H- plane at 10.66 GHz

Figure 2.6. The radiation patterns of the antenna in Figure 2.3 (b) for the resonant frequencies at 6 GHz and 10.66 GHz. (a) E- plane at 6 GHz. (b) H- plane at 6 GHz. (c) E- plane at 10.66 GHz. (d) H- plane at 10.66 GHz.

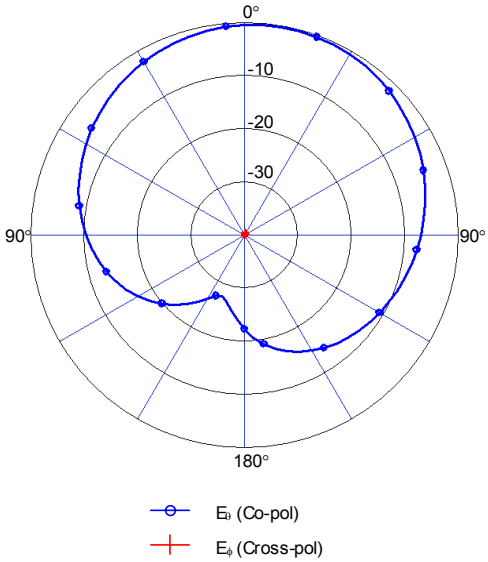

(a) E- plane at 8.2 GHz

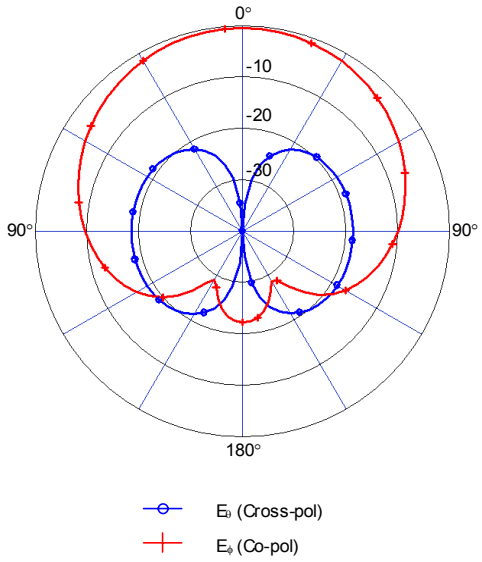

(b) H- plane at 8.2 GHz

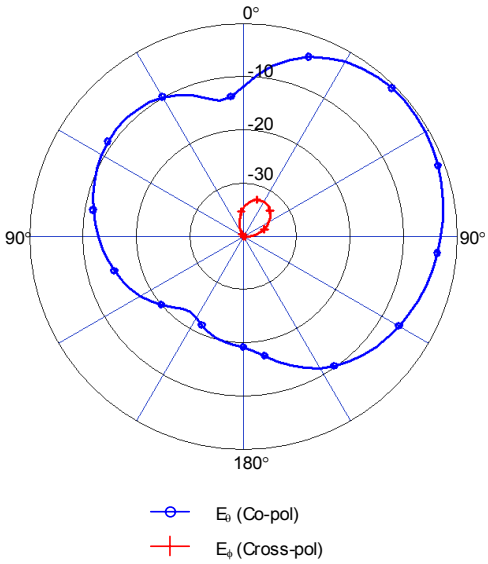

(c) E- plane at 14.2 GHz

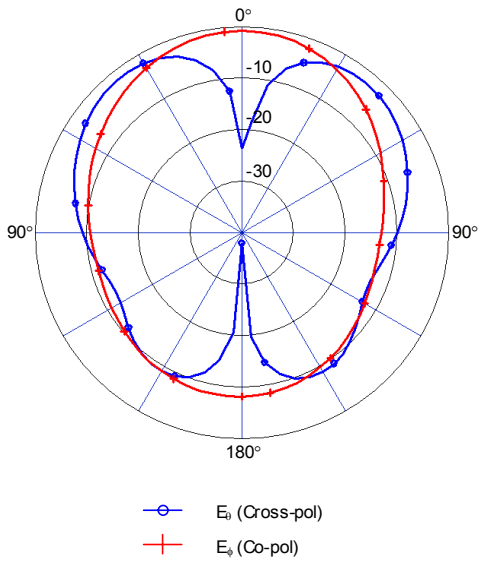

(d) H- plane at 14.2 GHz

Figure 2.7. The radiation patterns of the antenna in Figure 2.3 (c) for the resonant frequencies at 8.2 GHz and 14.2 GHz. (a) E- plane at 8.2 GHz. (b) H- plane at 8.2 GHz. (c) E- plane at 14.2 GHz. (d) H- plane at 14.2 GHz.

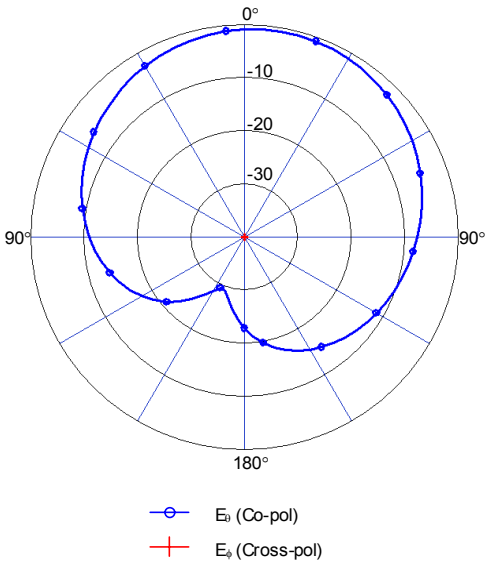

(a) E- plane at 8.44 GHz

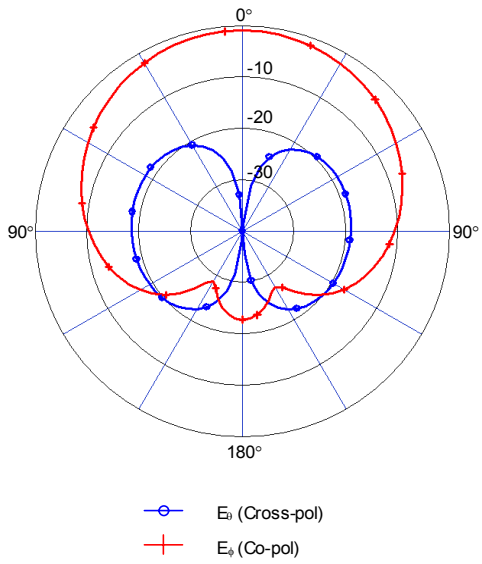

(b) H- plane at 8.44 GHz

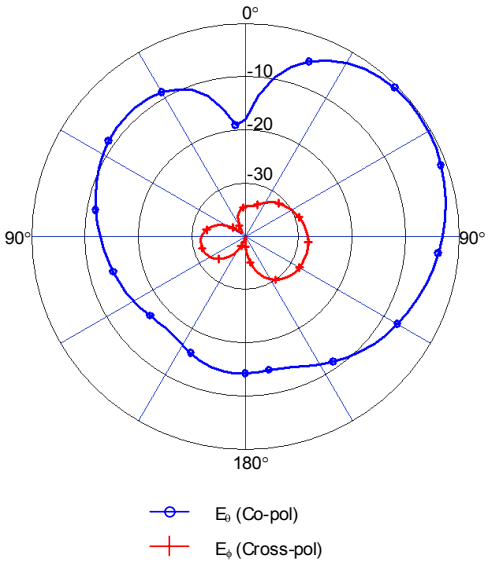

(c) E- plane at 15.32 GHz

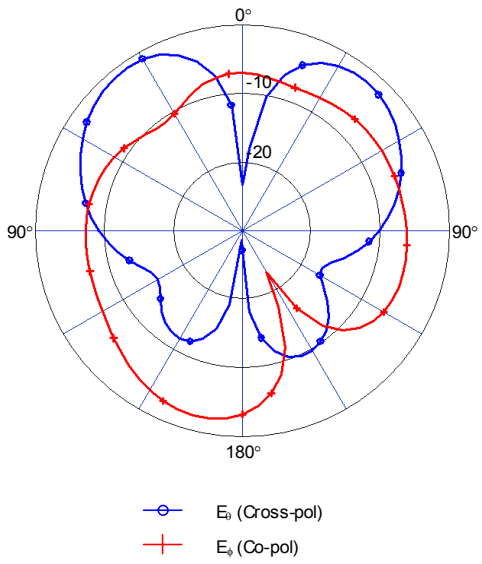

(d) H- plane at 15.32 GHz

Figure 2.8. The radiation patterns of the antenna in Figure 2.3 (d) for the resonant frequencies at 8.44 GHz and 15.32 GHz. (a) E- plane at 8.44 GHz. (b) H- plane at 8.44 GHz. (c) E- plane at 15.32 GHz. (d) H- plane at 15.32 GHz.

As a result of these examinations, we can observe that by increasing the number of RF MEMS switches the resonant frequency of the antenna approaches to a value as if there is no space between the metal plate and the patch, that is, the length of the patch is 8.4 mm. Reflection coefficient characteristics of the microstrip patch antenna having length 8.4 mm is shown in Figure 2.9.

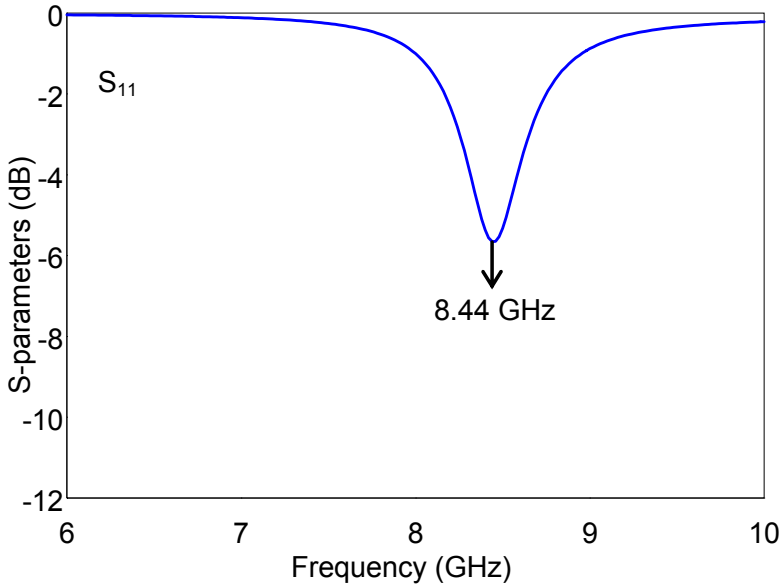

Figure 2.9. The reflection coefficient characteristics of a microstrip patch antenna with a length of 8.4 mm.

By this approach, with 7 RF MEMS switches the resonant frequency of the antenna changes from 9.92 GHz when switches are off to 8.44 GHz when switches are on which corresponds to 14.9% change. Also by actuating the RF MEMS switches independently, it is possible to obtain different up-state and down-state combinations that can support wide range of tuning of the resonant frequency.

2.2 Circuit Model Analyses on Tuning the Resonant Frequency of a Microstrip Patch Antenna

This section presents the analyses on the circuit models to provide an idea how the resonant frequency of a microstrip patch antenna can be tuned. These analyses are essential to introduce the concept of tuning the resonant frequency by using capacitors which is the aim of the designs that will be presented in the following sections.

2.2.1 Transmission Line Model

A microstrip patch antenna and its transmission line model are given in Figure 2.10. Basically the transmission line model represents the microstrip antenna by two slots, separated by a low-impedance transmission line of length of L and a characteristic impedance of Z_c, [24]. In the Figure 2.10 R, C models the impedance of the radiating slots. Z_o is the characteristic impedance of the transmission line between the slots with an electrical length of θ at the frequency of f_o. The electrical length of the transmission line is approximately equal to 180º (~λg/2) at the resonant frequency providing a cancellation of the reactive part of the impedance seen at the first radiating slot since both of the slots have identical electrical parameters.

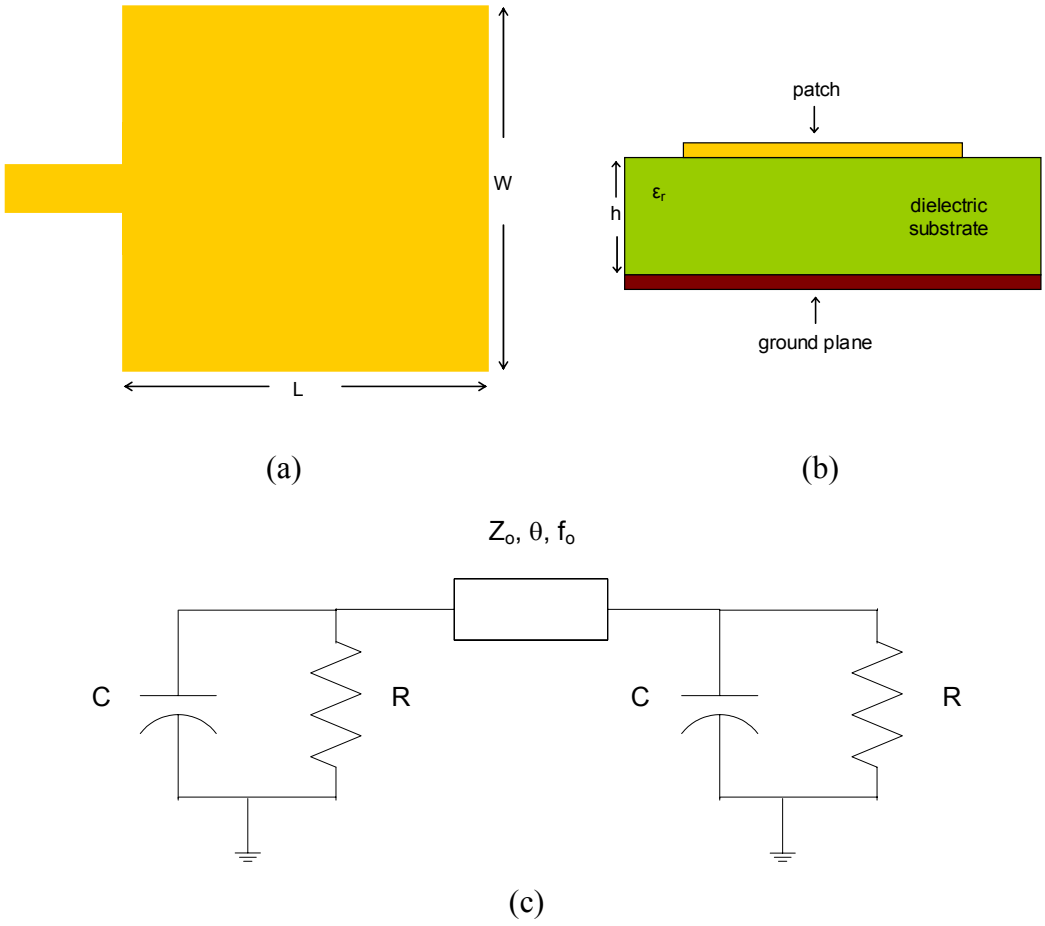

Figure 2.10. (a) Top-view of a microstrip patch antenna. (b) Side-view of a microstrip patch antenna. (c) The transmission line model of a microstrip patch antenna.

In order to make analyses about the effect of the capacitor on the resonant frequency, the values of the circuit model parameters are found. To find the values of the circuit model parameters, electromagnetic simulation of a microstrip patch antenna having L=W=4.3 mm is performed using Ansoft HFSSv9.0^{TM}. The inset at the feeding transmission line of the patch antenna is 1.5 mm. Then matching is provided between the reflection coefficient characteristics of the electromagnetic simulation and the circuit model by the optimization tool of Microwave Office^{TM}. The results of EM simulation and the transmission line model are given in Figure

2.11. Table 2.1 presents the circuit model parameters found by optimization. These values provide nearly the same reflection coefficient characteristics with the EM simulation shown in Figure 2.11.

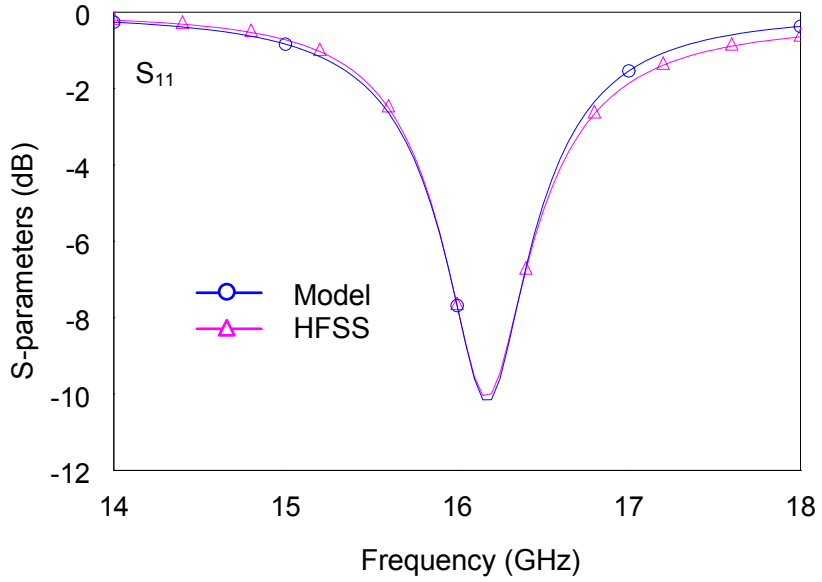

Figure 2.11. Reflection coefficient characteristics of simulation and circuit model results for a microstrip patch antenna with L=W=4.3 mm.

Table 2.1. The circuit model parameters extracted by the optimization tool of Microwave Office™.

C	R	Z_o	θ	f_o
40 fF	189 Ω	3.67 Ω	180°	16.33 GHz

2.2.2 Loading with Capacitor

This section verifies the validity of the approach about tuning the resonant frequency of the microstrip antenna with RF MEMS capacitors. First, the

transmission line model of the antenna with the given parameters in Table 2.1 is loaded with a capacitor of 350 fF capacitance in order to observe the effect of the loading capacitor. Figure 2.12 gives the circuit model of the patch antenna loaded with capacitor. The reflection coefficient characteristics of the model loaded with 350 fF capacitor is shown in Figure 2.13. The resonant frequency occurs at 15.5 GHz whereas the resonant frequency for the unloaded case occurs at 16.1 GHz. This shift in the resonant frequency is because of the change of the impedance at the 2nd slot since the transformed impedance of the 2nd slot and 1st slot provides matching at a different frequency at the feeding port.

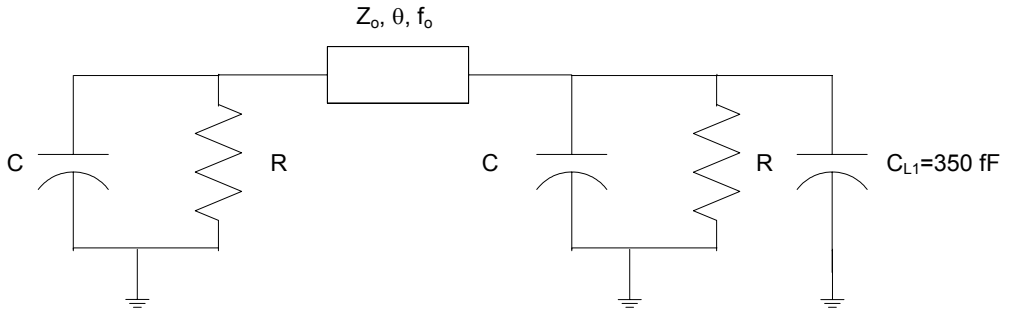

Figure 2.12. Transmission line model of the microstrip patch antenna loaded with 350 fF capacitor.

To achieve 500 MHz difference which corresponds to 3.2% change in the resonant frequency, the capacitance value has to be increased to 650 fF from 350 fF. The reflection coefficient characteristics when the loading capacitance values are 350-650 fF are shown in Figure 2.13. However, the change from 350 fF to 650 fF is beyond the value that can be achieved by fixed-fixed beam type RF MEMS capacitors operating electrostatically due to mechanical instability.

In order to achieve nearly 300 fF additional capacitance mentioned in the previous example which is required to shift the resonant frequency of the antenna 500 MHz at 16 GHz band without exceeding the mechanical instability

limitations, the initial value of the capacitor has to be increased. Figure 2.14 shows the reflection coefficient characteristics of the patch antenna loaded with 800 fF and 1185 fF capacitors. For the initial capacitance value of 800 fF, the resonant frequency of the structure is at 14.8 GHz. A shift of 500 MHz can be achieved by increasing the capacitance to 1185 fF. However, a single 800 fF capacitor covers very large area which is hard to implement with MEMS technology. Actuation problems and bending faults of bridges might occur which can cause the structures not to operate properly. To avoid these problems, distributed capacitors should be used for such large capacitance values.

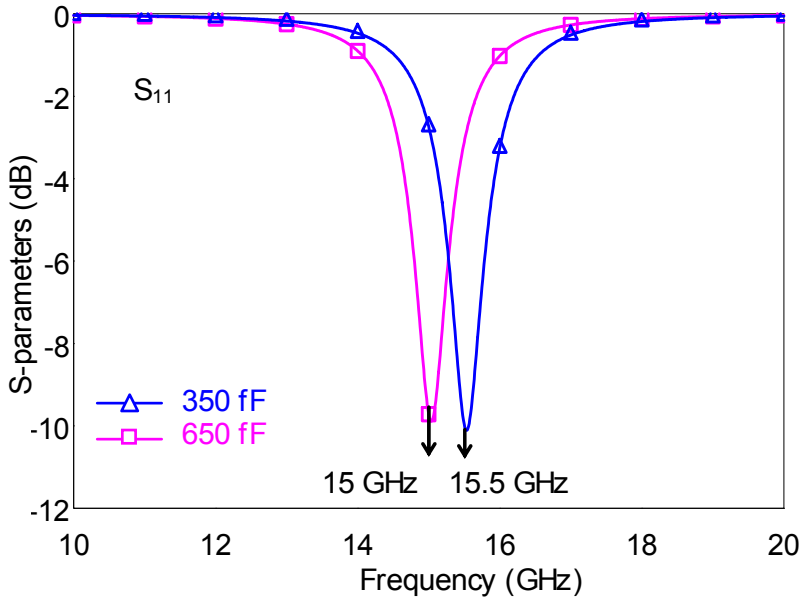

Figure 2.13. The reflection coefficient characteristics of the patch antenna loaded with 350 fF and 650 fF capacitance.

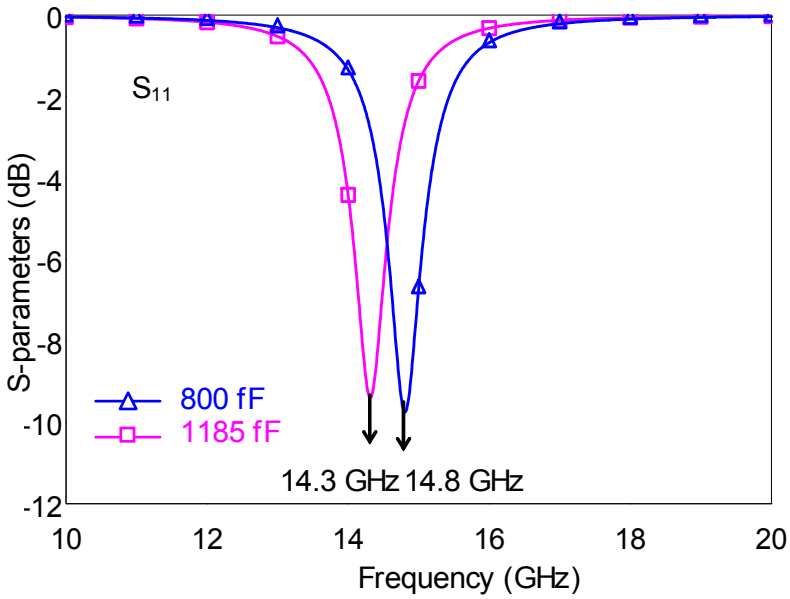

Figure 2.14. The reflection coefficient characteristics of the patch antenna loaded with 800 fF and 1185 fF capacitance.

The effect of capacitive loading on tuning the resonant frequency is more significant for a microstrip patch antenna operating at higher frequencies. The change in the resonant frequency is 2.9 GHz for an antenna operating at 58 GHz with a capacitance change from 800 fF to 1185 fF, which provides only 500 MHz change for the patch around 16 GHz. Figure 2.15 shows the reflection coefficient characteristics of the microstrip patch antenna operating at 58 GHz loaded with 800 fF and 1185 fF capacitance. By increasing the loading capacitance from 800 fF to 1185 fF, the resonant frequency of the structure changes from 45.4 GHz to 42.5 GHz which corresponds to a difference of 6.4%. The reason behind this difference is the dependency of the capacitive loading on frequency. As the loading impedance of a capacitance is:

$$Z_{load} = \frac{1}{j\omega C}$$

the loading effect is frequency dependent. Therefore, the amount of shift in the resonant frequency with respect to same additional capacitance is different for different resonant frequencies. As the operating frequency of the antenna is increased, the amount of shift increases keeping capacitance values same.

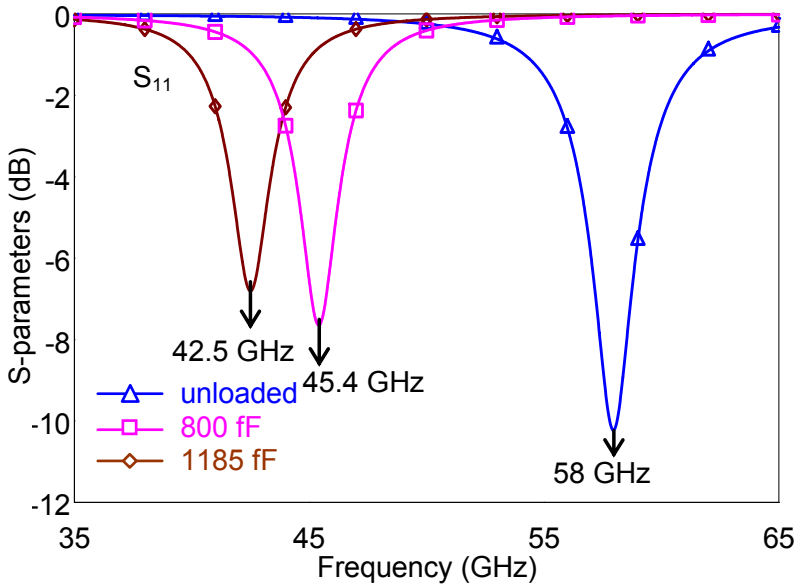

Figure 2.15. The reflection coefficient characteristics of the patch antenna operating at 58 GHz loaded with 800 fF and 1185 fF capacitance.

2.2.3 Loading with Stub

This section gives the analyses on the transmission line model when an open-ended stub is added to one of the radiating slots. The analyses on the effect of the stub are required since the stub is essential to integrate the MEMS capacitors with the antennas. These stubs can be realized with open-ended microstrip or CPW transmission line on which MEMS capacitors can be placed periodically.

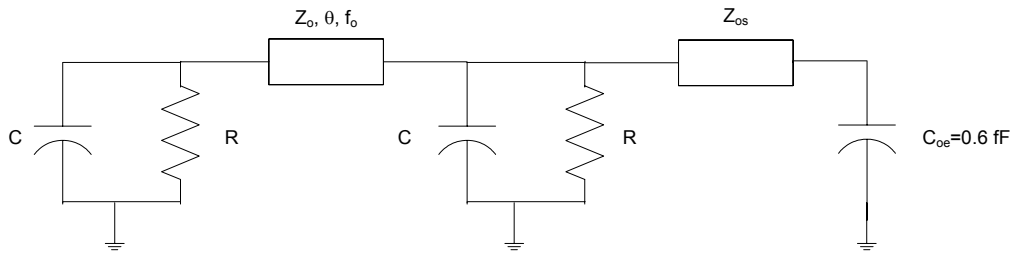

Figure 2.16. The circuit schematics of a microstrip patch antenna loaded with stub.

The circuit schematics of an antenna loaded with a stub can be seen in Figure 2.16. Figure 2.17 shows an example to the effect of loading stub on the resonant frequency. The unloaded structure has a resonant frequency at 16.2 GHz and it shifts down to 15.5 GHz due to the loading effect. The stub has an electrical length of $\lambda_g/8$ at 16 GHz with a characteristic impedance of 50 Ω. These parameters of the stub are important since the transformation of the open-ended transmission line capacitance denoted as C_{oe} on Figure 2.16 determines the impedance at the 2nd slot. The electrical length and the characteristic impedance of the loading stub are effective on the resulting resonant frequency. For example, when the characteristic impedance of the stub is reduced to 30 Ω from 50 Ω which can be achieved by the movement of distributed MEMS capacitances, the resonant frequency occurs at 15.3 GHz, which shows the ability of the stub to tune the resonant frequency of a microstrip patch antenna. Figure 2.18 shows the reflection coefficient characteristics where the characteristic impedance of the stub is varied from 50 Ω to 30 Ω. Using this concept, if the electrical parameters of the loading stub can electrically be controlled using a distributed structure, the resonant frequency of a microstrip patch antenna can be tuned dynamically.

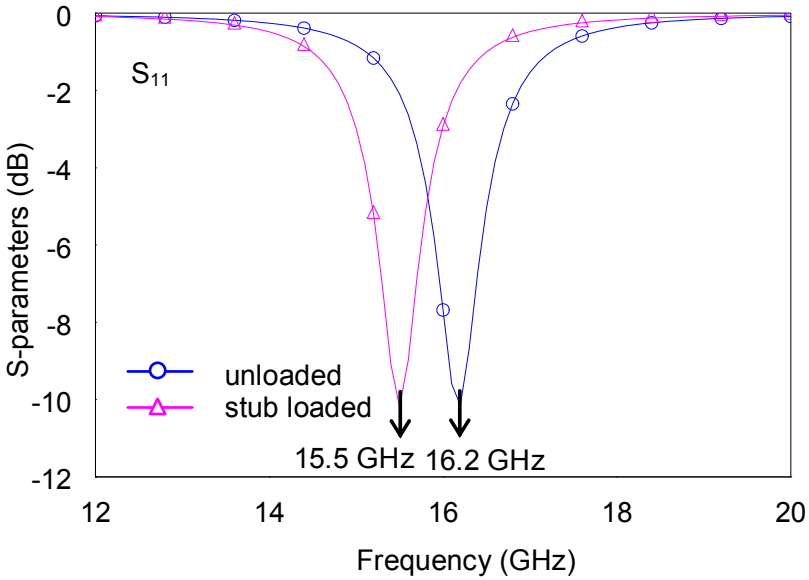

Figure 2.17. Reflection coefficient characteristics of the unloaded antenna and the antenna loaded with stub having 50 Ω characteristic impedance.

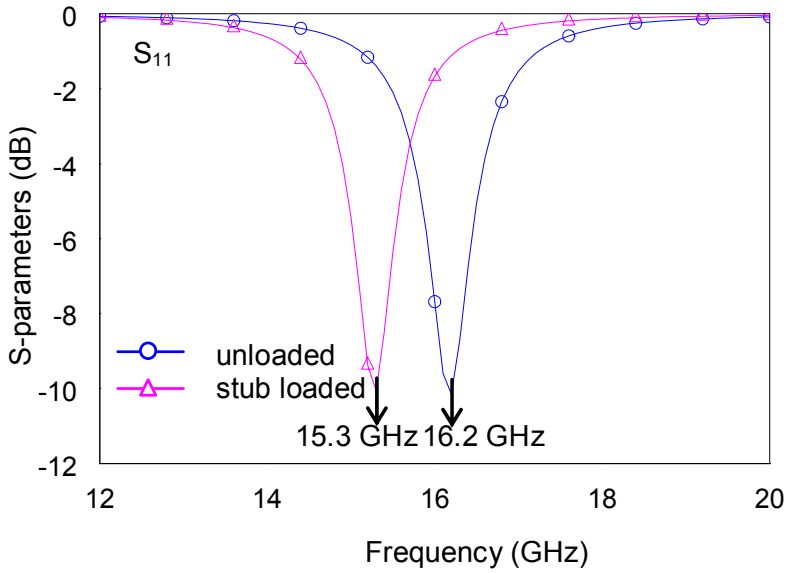

Figure 2.18. Reflection coefficient characteristics of the unloaded antenna and the antenna loaded with stub having 30 Ω characteristic impedance.

2.3 Tuning the Resonant Frequency of the Microstrip Patch Antenna Loading with RF MEMS Capacitors on Microstrip Stub

As the analyses on the transmission line model of a patch antenna presented in section 2.2 are considered, the resonant frequency of a patch antenna can be changed with an open-ended stub which can be implemented with microstrip or CPW transmission lines. In these analyses, it is shown that the resonant frequency of an antenna can be tuned by adjusting the electrical parameters such as the electrical length and the characteristic impedance of the stub. The design in this section uses these concepts and is composed of a microstrip patch antenna loaded with a microstrip transmission line at the radiating edge opposite to the feeding line of the antenna. RF MEMS capacitors are placed periodically on the stub to obtain a distributed transmission line whose electrical parameters can be adjusted using these variable RF MEMS capacitors.

Figure 2.19 shows the general view of the microstrip patch antenna loaded with two RF MEMS capacitors placed periodically over a stub. The length of the stub is selected to be 4.3 mm which is nearly half of the guided-wavelength. RF MEMS capacitors are formed by placing a metal bridge over the open-ended stub at 2 μm height which is specified by the fabrication process. The capacitance takes place on the overlapping area between the metal bridge and the open-ended stub carrying the RF signal. When microstrip transmission line is used as a stub, to load the antenna at the radiating edge opposite to the feeding line of the antenna grounded via has to be opened through the substrate to provide grounding of the MEMS bridges suspended on top of the stub. Due to these difficulties in the processing vias in glass substrates, radial stubs are attached to the anchors of the bridges to provide grounding to the MEMS bridges. These radial stubs have lengths nearly $\lambda_g/4$ at 16 GHz and they show grounding effect around 16 GHz [2].

Figure 2.20 shows the transmission coefficient characteristics of the radial stub used in our designs which has a length of 1.7 mm and radial angle of 45°. Transmission coefficient characteristic shows that the radial stub does not transmit the signal at 16.6 GHz.

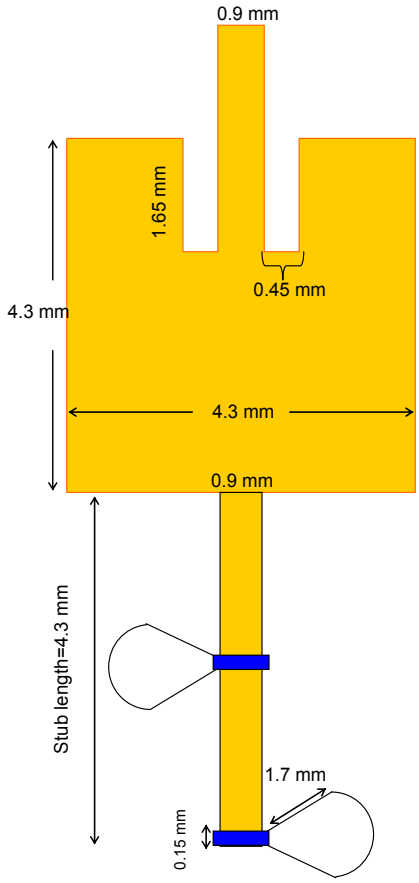

Figure 2.19 The general view of the tunable frequency microstrip patch antenna loaded with a microstrip line stub on which RF MEMS capacitors are placed periodically.

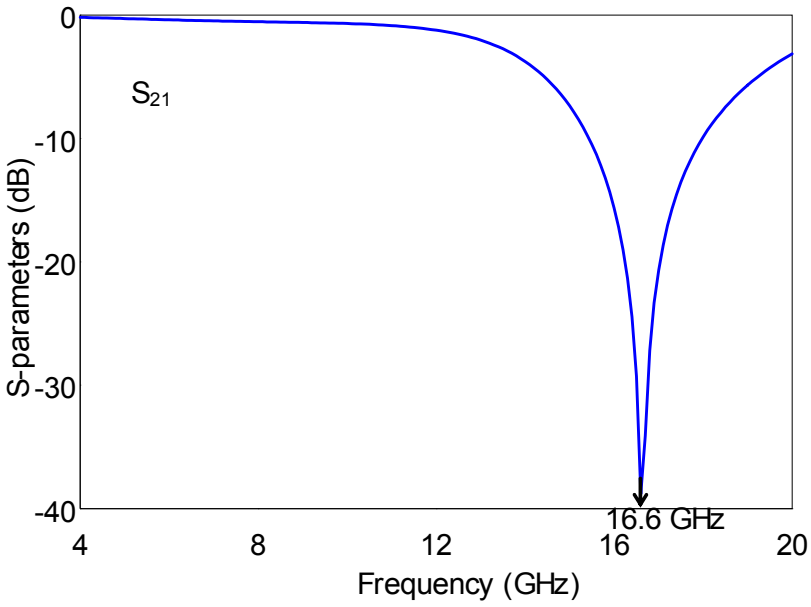

Figure 2.20. Transmission coefficient characteristic of the radial stub.

In order to adjust the electrical parameters of the loading stub, the height of the MEMS bridges are lowered to increase the capacitance. These bridges can be moved by applying DC voltage between the stub and the bridge. The active polarity of the DC voltage is applied to the stub via bias tee feeding the antenna. The passive (ground) polarity of the DC voltage is connected to the radial stub by using a resistive line. The reflection coefficient characteristics for the capacitor at 2 μm and 1 μm height are shown in Figure 2.21 (a). It should be noted here that it is actually not possible to change the bridge height from 2 μm to 1 μm using fixed-fixed beams. However the aim is to observe the effect of the increase of the loading capacitance by a ratio 2:1 although it is not physically realizable. As can be seen in the figure, the resonant frequency of the structure shifts 100 MHz, corresponding to 0.6% change, by increasing the capacitance. Figure 2.21 (b)-(c) shows the radiation pattern at 16.3 GHz for E- and H- planes. The radiation is broadside at this frequency.

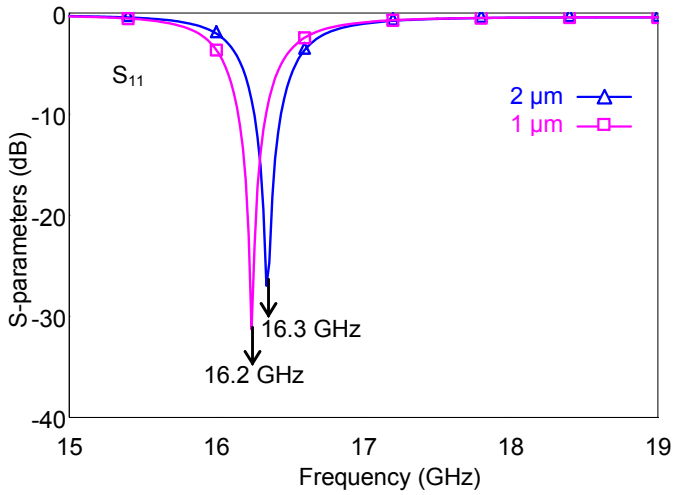

(a)

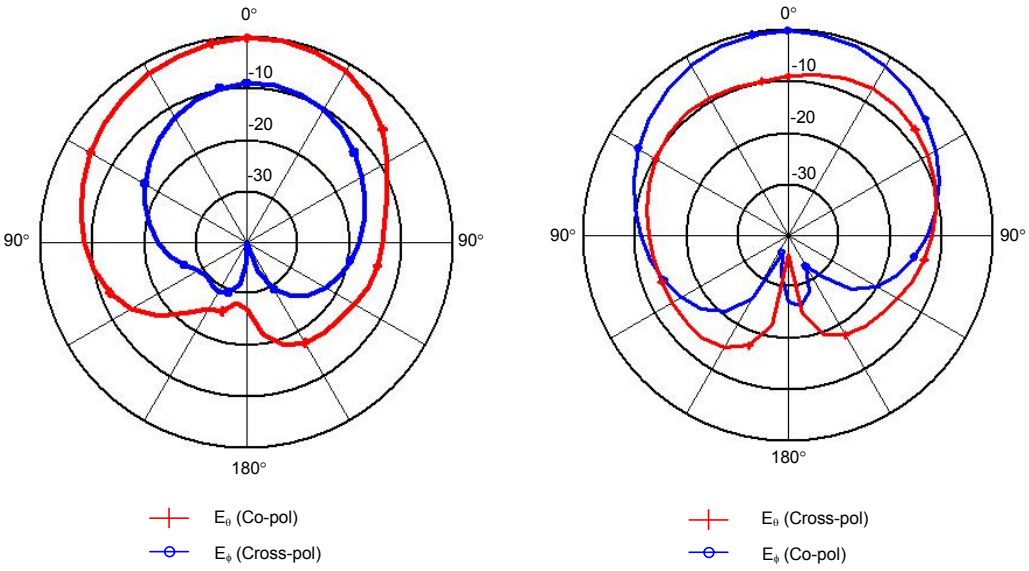

(b) E- plane at 16.3 GHz (c) H- plane at 16.3 GHz

Figure 2.21. (a) The reflection coefficient characteristics of the structure for the capacitor height 1 µm and 2 µm. (b) The radiation patterns for the resonant frequency at 16.3 GHz for E-plane (c) The radiation patterns for the resonant frequency at 16.3 GHz for H- plane.

In order to investigate the effect of number of MEMS capacitors and stub length on the resonant frequency, various simulations are performed in Ansoft

HFSS v9.0^{TM}. Table 2.2 summarizes the results of these analyses. The bridge heights are varied from 2 μm to 1 μm including 1.4 μm in order to observe the amount of shift.

Table 2.2. Simulation results of the antenna loaded with different numbers of capacitors having different dimensions.

# of capacitors	Capacitor width (μm)	Capacitor height (μm)	Stub length (μm)	Stub width (μm)	Resonant frequency (GHz)
2	200	2	2.15	900	17.36
2	200	1	2.15	900	16.92
4	200	2	8.6	900	16.28
4	200	1	8.6	900	16.40
2	400	2	4.3	450	16.32
2	400	1.4	4.3	450	16.20
4	400	2	8.6	450	16.50
4	400	1.4	8.6	450	16.38

According to the results obtained from the simulations, even with high number of capacitors, there is no significant effect on the amount of shift in resonant frequency by the increase in the loading capacitance. Also, a desirable tuning in the frequency band cannot be achieved by these designs. This might be due to the narrow bandwidth of grounding stubs even their performance have been improved by their radial geometry. This narrow bandwidth cannot provide proper grounding in the vicinity of the resonant frequencies. Therefore, as the number of MEMS capacitors increased the tunability of the antenna cannot be improved.

Another disadvantage of this design is as radial stubs are used for grounding, the structure is not suitable for loading with large number of

capacitors. Because the dimensions of the radial stub determine the separation between the MEMS capacitors. Hence, the overall dimensions of the structure grow as more MEMS capacitors are used for loading, which is a problematic issue in terms of fabrication. This is because the yield and the probability of realizing a working device at the end of process decrease as the device dimensions increase.

2.4 Tuning the Resonant Frequency of the Microstrip Patch Antenna Replacing RF MEMS Capacitors on CPW

2.4.1 General View

In order to get rid of the problems of capacitors with radial stubs, a modified antenna structure has been proposed in this section. The antenna is again loaded with a microstrip stub at the radiating edge opposite to the feeding line. A tapered line is employed for the transition from microstrip to the CPW line where the MEMS capacitors are placed periodically. Figure 2.22 shows the structure without MEMS capacitors. The use CPW line ensures the ease of grounding properly within smaller chip size compared to radial stub grounding approach. Also, the number of loading capacitors can be increased which provides an improved tunability on the resonant frequency.

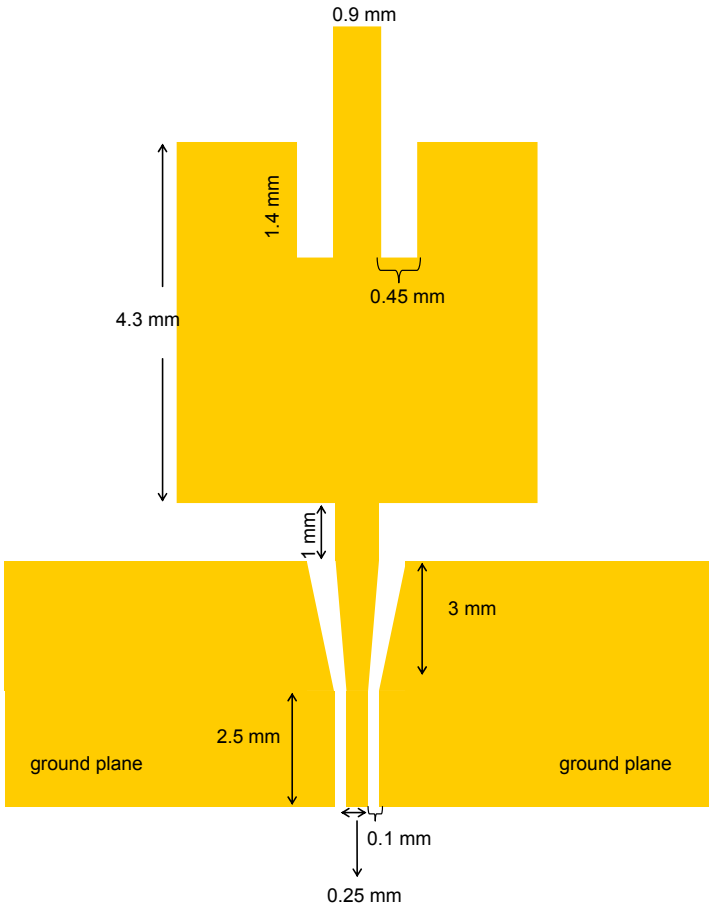

Figure 2.22. The microstrip patch antenna loaded with open ended CPW without MEMS capacitors.

2.4.2 Loading of Patch antenna With CPW Stub

To load the microstrip patch antenna with a coplanar waveguide, the antenna is loaded by a microstrip stub and a tapered line to provide the appropriate transition from microstrip stub to the CPW. The length of the tapered line for the compatibility should not be less than $\lambda_g/4$. In the design, the length of the taper is 3 mm as $\lambda_g/4$=2.44 mm at 16 GHz for a 900 μm width microstrip stub on Pyrex 7740 substrate having dielectric constant of 4.6 and height of 500 μm. The microstrip stub-tapered line-open ended CPW part of the structure is

simulated and the reflection coefficient characteristic is shown on the Figure 2.23. The level of reflection coefficient implies that the tapered line is suitable for this transition.

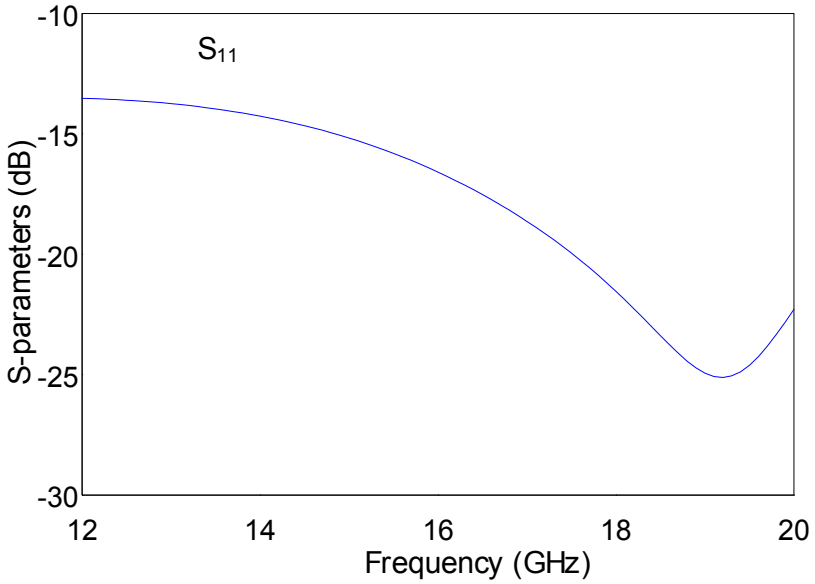

Figure 2.23. Reflection coefficient characteristics of microstrip stub- tapered line-CPW structure.

The reflection coefficient characteristics and the radiation patterns of microstrip patch antenna loaded by open-ended CPW in Figure 2.22 is given in Figure 2.24 and in Figure 2.25, respectively. According to the Figure 2.24, the resonant frequency of the microstrip patch antenna shifts due to the capacitive loading of the stub structure.

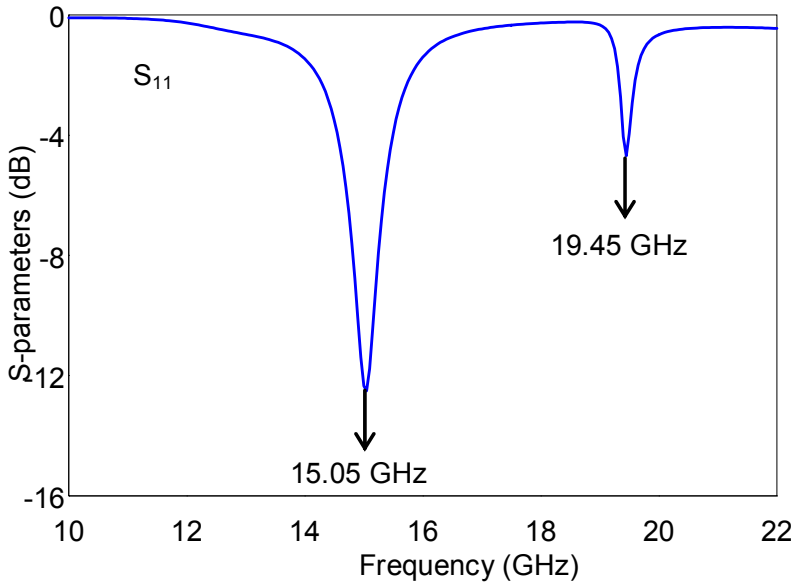

Figure 2.24. The reflection coefficient characteristics for the microstrip patch antenna loaded with open ended CPW without MEMS capacitors.

The radiation patterns of the structure imply that the antenna radiates broadside at 15.05 GHz. The cross-polar component at this frequency is at -20 dB level for both E- and H- planes. However, the higher resonant frequency at 19.45 GHz has large cross-polar component in the H- plane and the antenna does not radiate broadside.

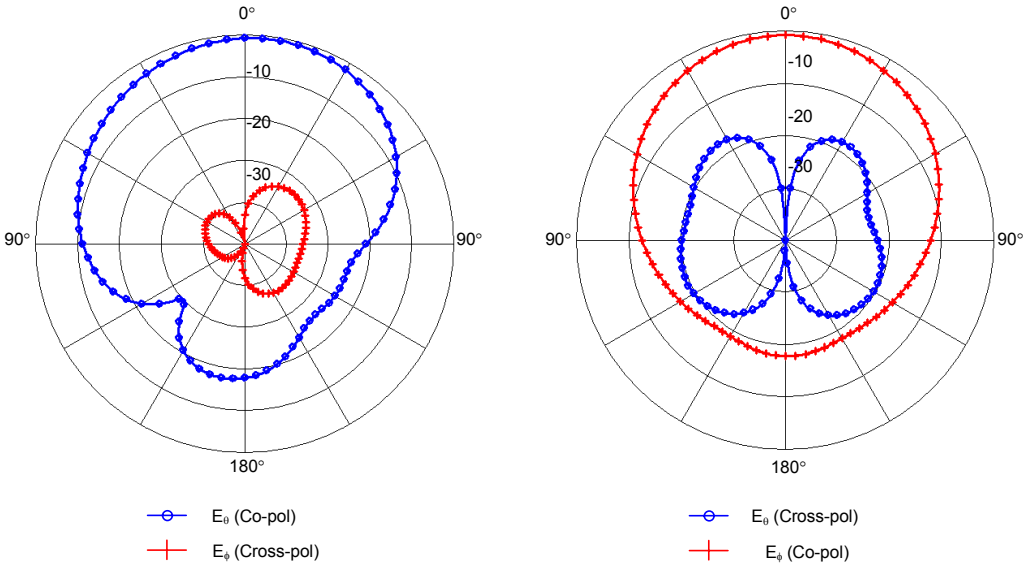

(a) E- plane at 15.05 GHz (b) H- plane at 15.05 GHz

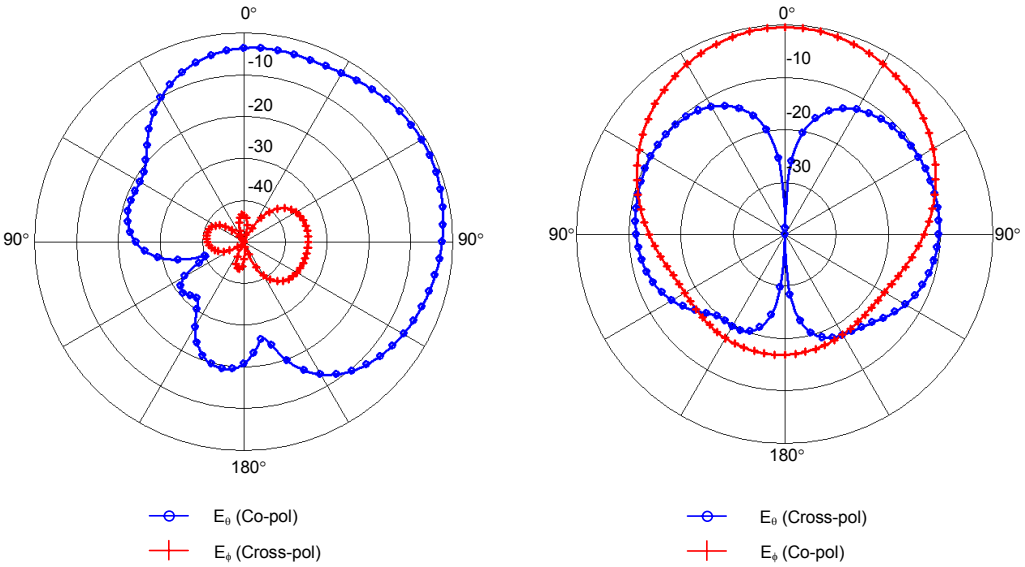

(c) E- plane at 19.45 GHz (d) H- plane at 19.45 GHz

Figure 2.25. Radiation patterns for the structure loaded with open ended CPW at the termination. (a) E- plane at 15.05 GHz. (b) H- plane at 15.05 GHz. (c) E- plane at 19.45 GHz. (d) H- plane at 19.45 GHz.

2.4.3 Loading With MEMS Capacitors

In order to analyze the effect of number and dimensions of MEMS capacitors on the resonant frequency, various simulations are performed. The capacitors are placed periodically on the CPW section of the stub which has a signal width of 250 μm and a gap of 100 μm. Table 2.3 gives the results of these simulations.

Table 2.3. Simulation results of the antenna loaded with different numbers of capacitors having different dimensions.

# of capacitors	MEMS bridge height (μm)	MEMS bridge width (μm)	f_c (GHz)
1	2	100	14.60
1	1.4	100	14.48
2	2	100	14.40
2	1.4	100	14.16
2	2	200	14.24
2	1.4	200	14.04
3	2	100	14.25
3	1.4	100	13.75
3	2	200	18.65
3	1.4	200	18.00
5	2	100	17.9
5	1.4	100	17.3
5	2	200	17.1
5	1.4	200	15.95

According to the data on Table 2.3, the number of capacitors and the dimensions of the capacitors play a significant role on tuning the resonant frequency of the antenna. As the number and the dimensions of the MEMS capacitors increase, i.e. the loading effect increases, the shift on the resonant frequency of the antenna increases.

Figure 2.26 shows the final geometry of the structure. In the final structure, the width of the signal line of the CPW is 250 µm and the gap between the signal line and the ground lines is 100 µm. 5 bridge type MEMS capacitors having width 200 µm and length 600 µm are placed on the open ended CPW with 400 µm from periodic spacing.

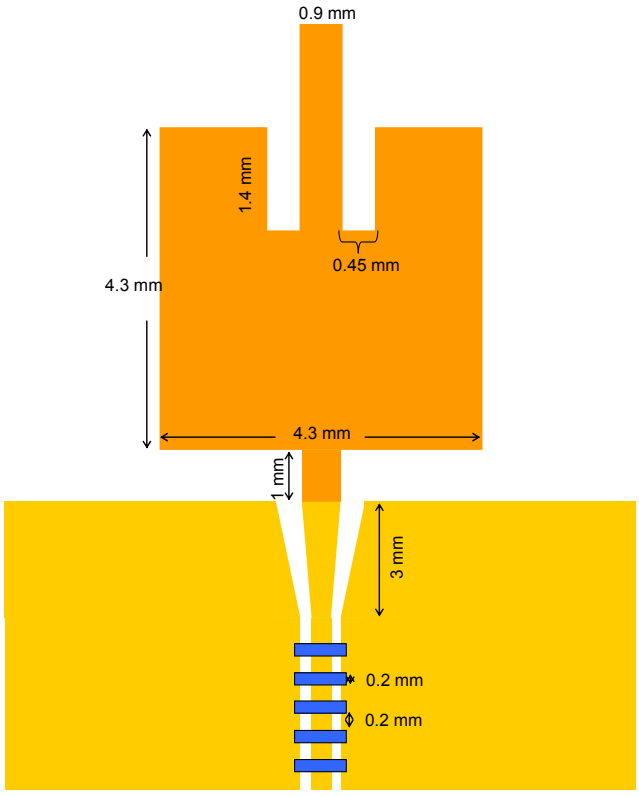

Figure 2.26. The microstrip patch antenna loaded with 5 bridge type MEMS capacitors.

In this design, the capacitance is formed by the overlapping area between the bridges and the signal line of the open ended CPW which is 200 μm × 250 μm. The height of the capacitors is changed from 2 μm to 1.4 μm to tune the resonant frequency. The capacitors cannot be lowered to less height below 1.4 μm because of the mechanical instability. The MEMS bridges are electrostatically actuated using DC voltage applied between the signal line of CPW and the MEMS bridges. The active polarity of the DC voltage is connected to the signal line of CPW via bias tee feeding the antenna. The passive (ground) polarity of the DC voltage is connected to the planar ground either using a resistive line or wire bond. The reflection coefficient characteristics and the radiation patterns for both of the conditions are shown in Figure 2.27 and in Figure 2.28, respectively.

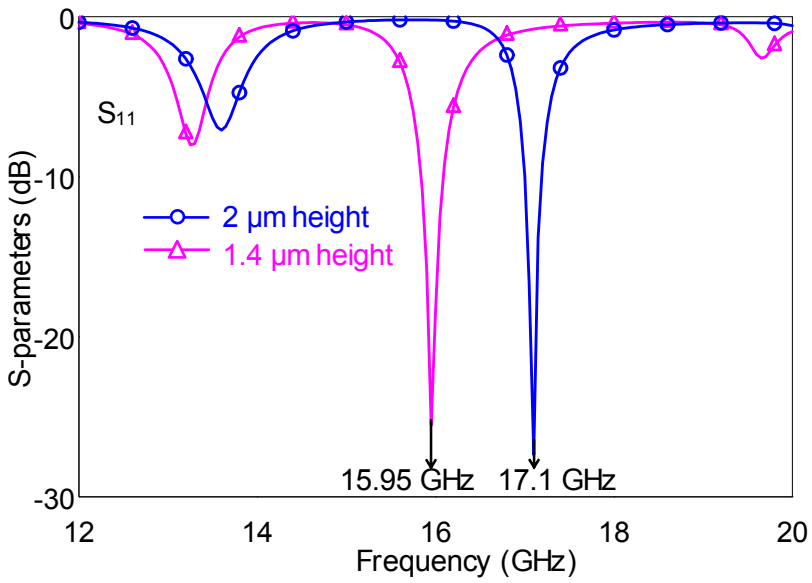

Figure 2.27. Reflection coefficient characteristics of the structure for the height of the capacitors at 2 μm and 1.4 μm.

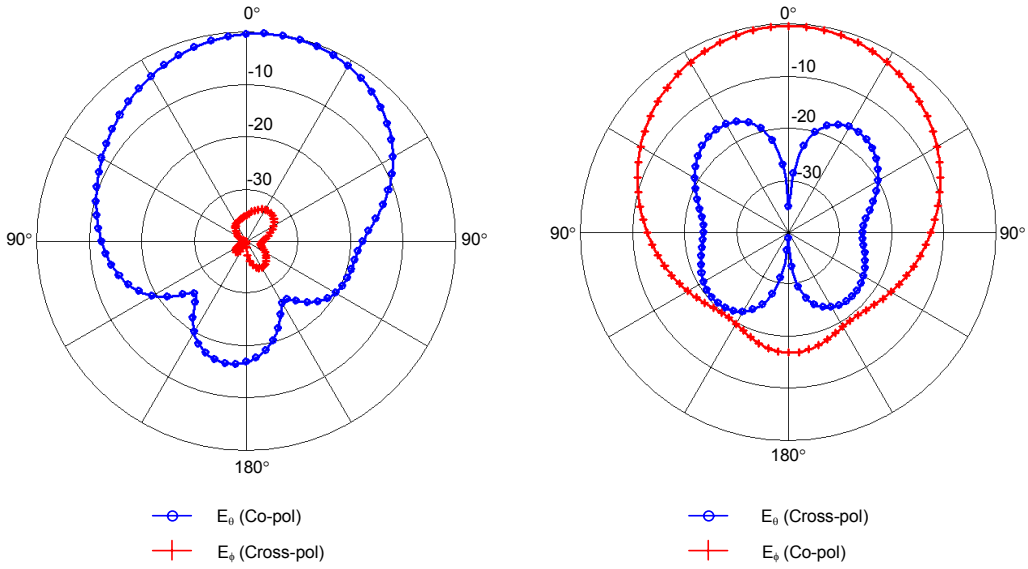

(a) E- plane at 17.1 GHz (b) H- plane at 17.1 GHz

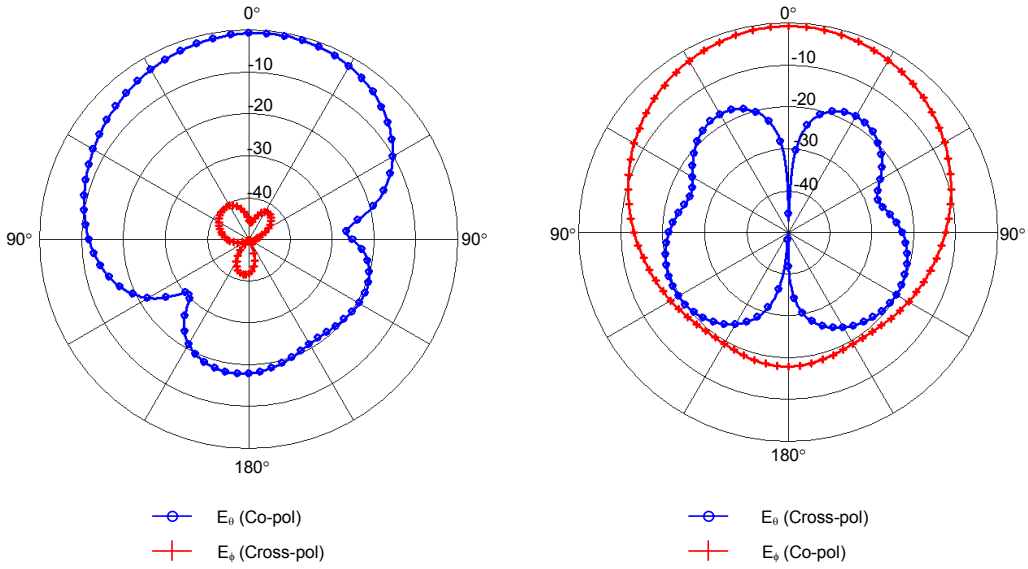

(c) E- plane at 15.95 GHz (d) H- plane at 15.95 GHz

Figure 2.28. Radiation patterns of the structure for the height of the capacitors at 2 μm and 1.4 μm. (a) E- plane for 17.1 GHz when capacitors are at 2 μm height. (b) H- plane for 17.1 GHz when capacitors are at 2 μm height. (c) E- plane for 15.95 GHz when capacitors are at 1.4 μm height. (d) H- plane for 15.95 GHz when capacitors are at 1.4 μm height.

As can be seen from the radiation patterns, for the resonant frequencies at 17.1 GHz and 15.95 GHz the radiation is broadside with cross-polar components below –20 dB. Hence, by this approach we shift the resonant frequency of the microstrip patch antenna by 1.15 GHz, corresponding to 6.7 % change, without any sacrifice from reflection. The main disadvantage of the system is as the loading with MEMS capacitors is done on the CPW for a microstrip fed antenna, the overall dimensions of the structure increase due to the usage of the tapered line to make a good transition from the antenna to the CPW.

2.5 Tuning the Resonant Frequency of the Rectangular Slot Antenna

2.5.1 CPW Fed Approach

In this section frequency tunable CPW fed rectangular slot antenna is presented. In the previous design, microstrip line has been employed as the feeding transmission line. But, a major drawback of microstrip line is that it is not compatible with monolithic fabrication and therefore easier integration with active solid-state devices is not possible [25]. Also, in the other design the stub is added outwards the antenna and to make the transition a tapered line is used which makes the system dimensions larger. However, CPW fed approach is more suitable for loading with capacitors as it does not require a stub outwards the slot of the antenna.

2.5.2 General View and Simulation Results of Rectangular Slot Antenna

Due to their ease of implementation and low profiles, slot antennas with different geometries have been investigated by several researchers [26-31]. The

general view of the rectangular slot antenna fed by a 50 Ω line is given in Figure 2.29 which has been examined as the basic structure. The antenna is designed on glass substrate (ε_r=4.6, tanδ=0.005) having a thickness of 500 μm.

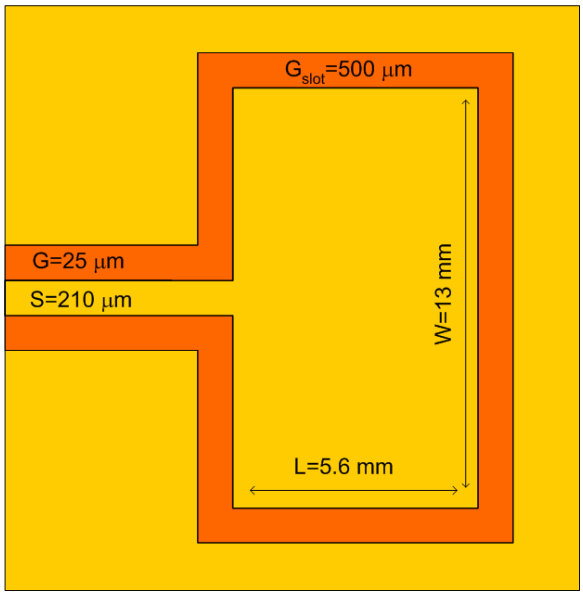

Figure 2.29. The rectangular slot antenna implemented on glass substrate. The feed line is a 50 Ω CPW. The total area of the structure including the ground plane around the antenna is 17.5 mm × 21 mm.

The antenna which is simulated using Ansoft HFSS v9.0™ has a resonant frequency at 7.9 GHz and 12.98 GHz. The rectangular slot antenna itself shows a dual frequency behavior as the radiation patterns are considered. However, there is a significant amount of cross-polar component on the H-plane for the higher resonant frequency. The reflection coefficient and the radiation patterns for E- and H- planes are given in Figure 2.30 and Figure 2.31, respectively.

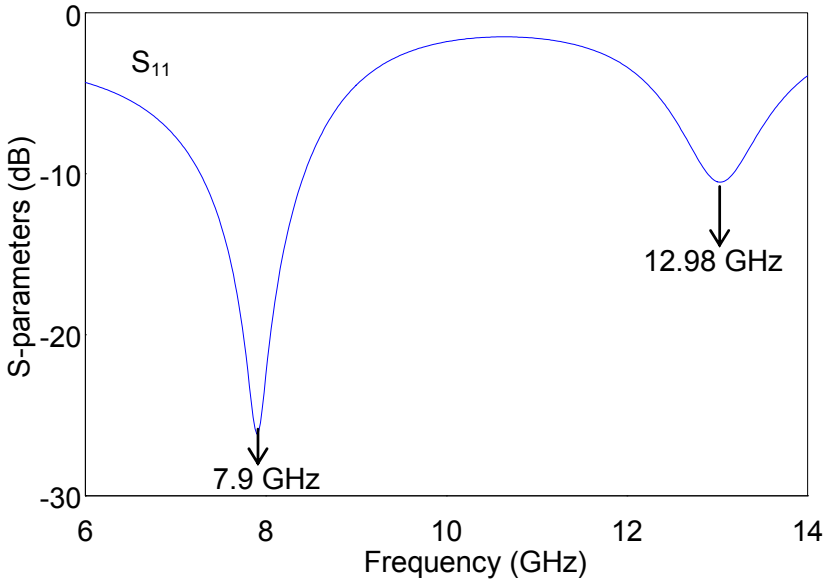

Figure 2.30. The reflection coefficient characteristics of the rectangular slot antenna.

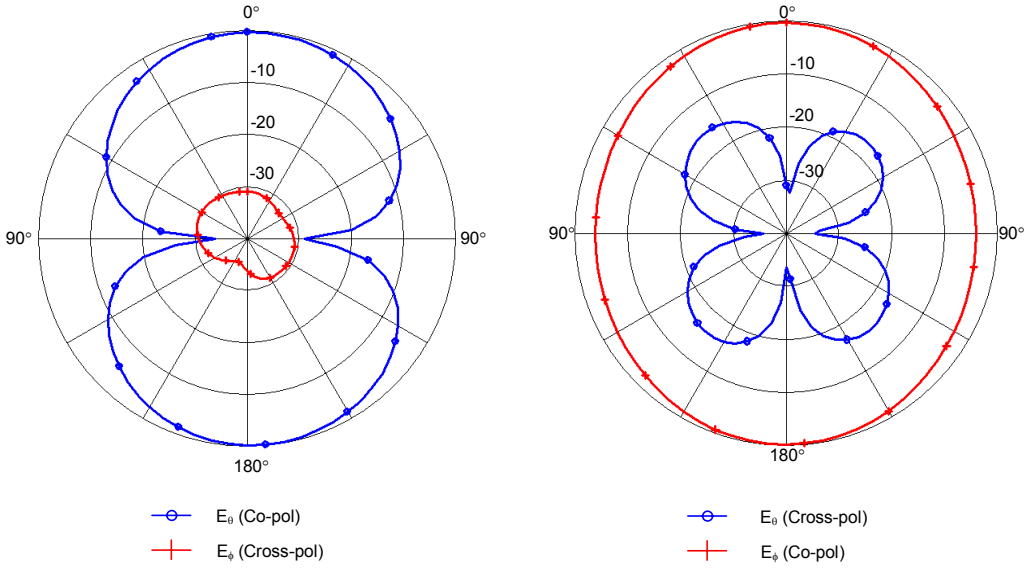

(a) E- plane at 7.9 GHz

(b) H- plane at 7.9 GHz

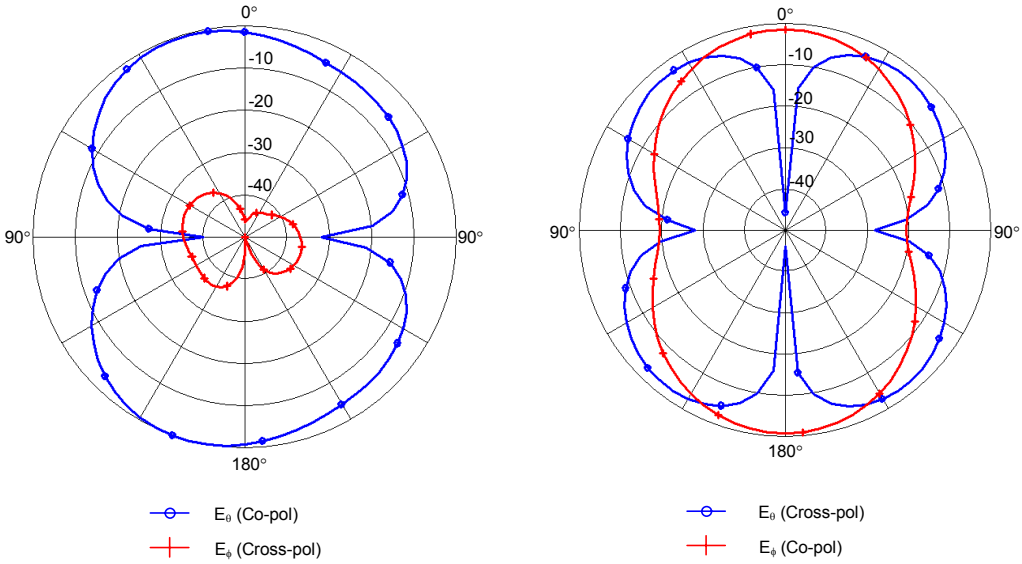

(c) E- plane at 12.98 GHz (d) H- plane at 12.98 GHz

Figure 2.31. Radiation patterns of the rectangular slot antenna shown in Figure 2.29. (a) E- plane at 7.9 GHz. (b) H- plane at 7.9 GHz. (c) E- plane at 12.98 GHz. (d) H- plane at 12.98 GHz.

As seen from Figure 2.31, at 12.98 GHz the cross-polar component in the H-plane is significantly large, even larger than the co-polar component. This is mainly due to the electric field distribution on the slots parallel to the feeding line of the antenna. For these two slots, the equivalent magnetic currents do not cancel each other and the mean value of the magnetic currents is not equal to zero for the slots individually.

2.5.3 Loading With Stub

As in the design given in section 2.3 and 2.4, a stub is used for loading the antenna and MEMS capacitors are placed on stub to tune the resonant frequency of the antenna. The stub is the insertion of the ground plane to the slot opposite to

the feeding transmission line inwards the antenna. The related structure can be seen in Figure 2.32.

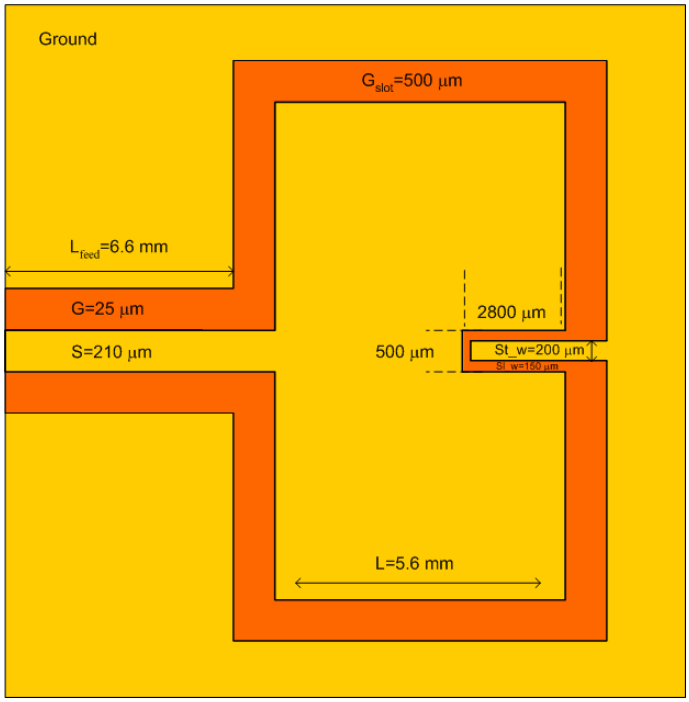

Figure 2.32. Stub loaded rectangular slot antenna.

The stub inserted opposite to the feeding line has a positive effect in terms of reducing the cross-polar component. The length of the stub is selected to be nearly quarter-guided wavelength in the upper band [23]. As can be observed from the given reflection coefficient characteristics in Figure 2.33, there is a shift in the resonant frequencies down to 6.82 GHz and 11.29 GHz.

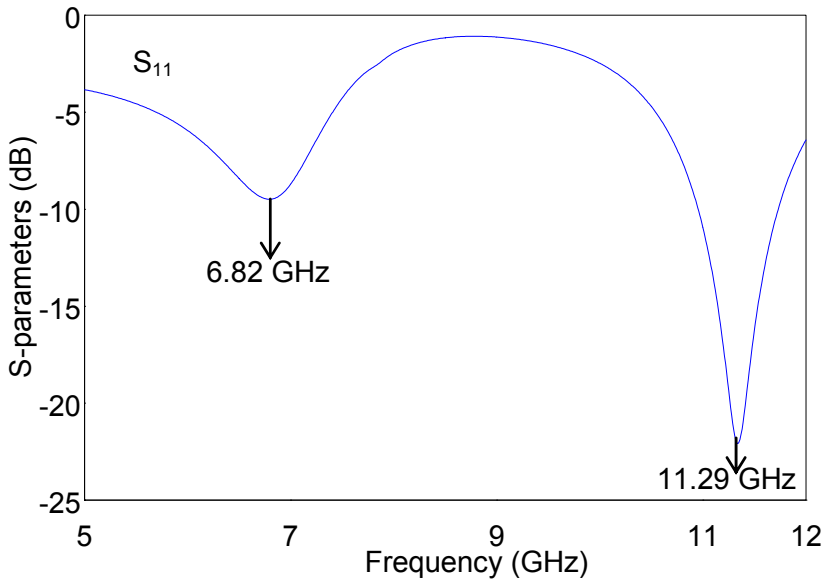

Figure 2.33. Reflection coefficient characteristics of stub loaded rectangular slot antenna.

The reason for this shift is the capacitive loading of the slot antenna by stub. The major advantage obtained with the aid of this stub is the reduction of the cross-polar component in the H-plane at the higher resonant frequency. Figure 2.34 shows the radiation patterns for the resonant frequencies of the stub loaded antenna. As can be seen in the radiation patterns the cross-polar component in the H- plane for the higher resonant frequency is reduced to a level lower than -20 dB. The radiation patterns at both of the resonant frequencies show similar characteristics so that this antenna can be used as a dual-frequency antenna.

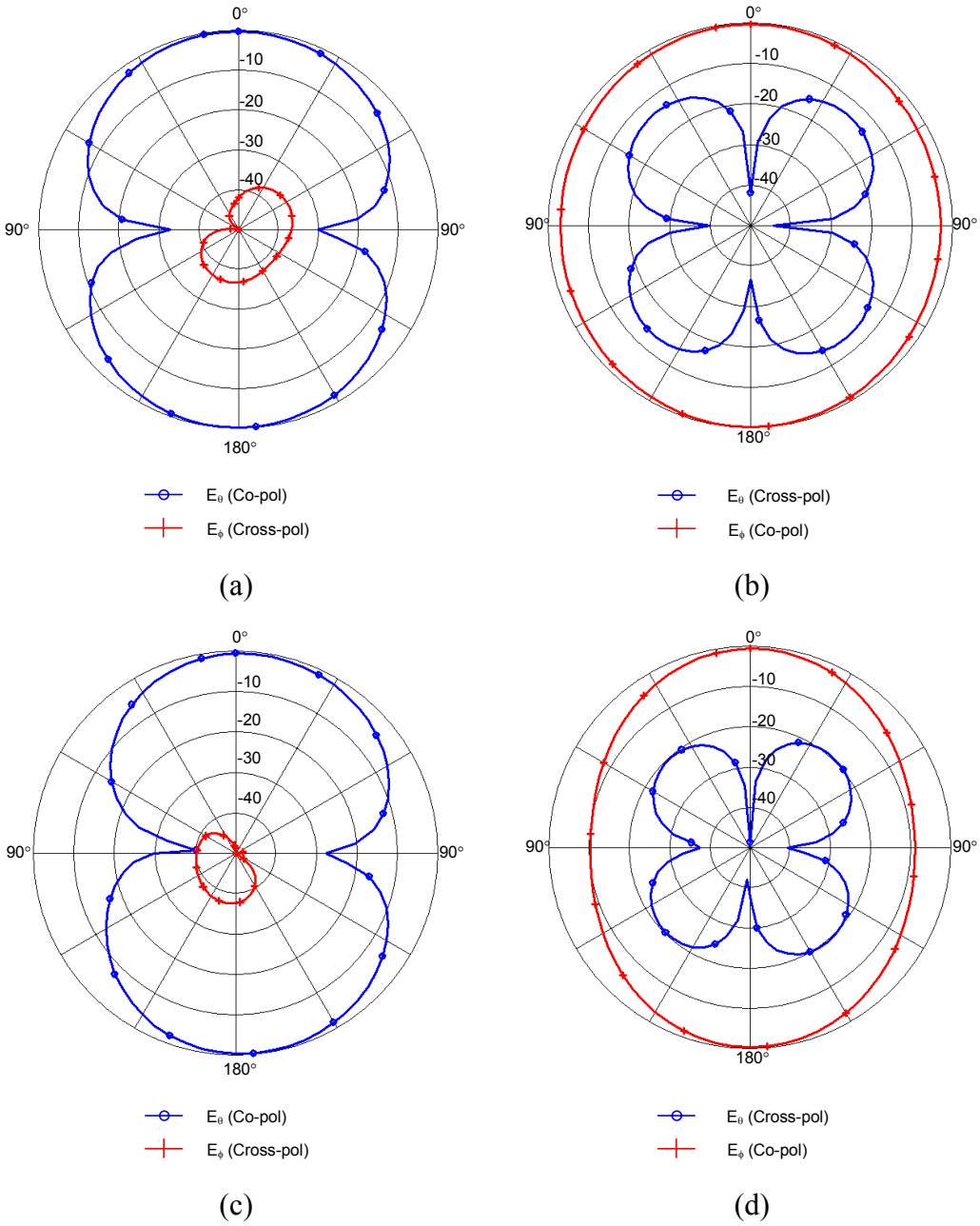

Figure 2.34. The radiation patterns of the antenna loaded with a stub. (a) E- plane at 6.82 GHz. (b) H- plane at 6.82 GHz. (c) E- plane at 11.29 GHz. (d) H- plane at 11.29 GHz.

The effect of the dimensions of the stub, i.e. the characteristic impedance of the stub has also been investigated. The simulation results show that for

different dimensions of the stub and the slot around the stub, the resonant frequencies of the antenna and the separation between the resonant frequencies changes. Table 2.4 summarizes the change of resonant frequencies with respect to these dimensions.

Table 2.4. Change of the resonant frequencies of the rectangular slot antenna with the dimensions of the stub. f_{c_L} and f_{c_H} denotes the lower and higher resonant frequencies, and S_{t_l} denotes the stub length.

S_{t_w} (μm)	S_{l_w} (μm)	S_{t_l} (μm)	f_{c_L} (GHz)	f_{c_H} (GHz)
200	150	2975	6.82	11.29
300	100	2975	6.46	11.16
400	50	2975	5.94	10.89
400	150	2975	6.69	11.25

As a result of these examinations, the separation between the resonant frequencies decreases as the characteristic impedance of the stub increases. Also, both resonant frequencies shift when the characteristic impedance of the stub changes. Therefore, one can have a tunable antenna by changing the characteristic impedance of the stub. Using this concept, the stub is loaded with tunable MEMS capacitors to change the characteristic impedance and hence the resonant frequencies dynamically.

2.5.4 Loading With Cantilever Type Capacitors

6 MEMS cantilevers are placed periodically onto the stub to modify the characteristic impedance of the stub. The anchors of these cantilevers are attached to the stub. Two cantilevers supported by these anchors are suspended over the conductor carrying the RF signal. As can be seen from the cross-sectional view in Figure 2.35, these cantilever type capacitors resembles to a "T-wing" structure which can be actuated electrostatically by applying DC voltage between the RF signal line and suspended cantilevers [32]. The length of the cantilevers is limited to 500 μm to decrease the possibility of faults during the fabrication process. The capacitance takes place in the overlapping area of the cantilevers and the conductor carrying the RF signal. The width of the cantilevers is 200 μm each, resulting in a capacitive area of 200 μm × 250 μm. The cantilevers are designed at 2 μm when they are not actuated. Since MEMS cantilevers can only use 1/3 of their initial height because of the mechanical instability, they have been lowered down to 1.4 μm height to achieve the maximum loading on the stub. The MEMS cantilevers are electrostatically actuated using DC voltage applied between the signal and ground of CPW using bias tee. The loading capacitance increases resulting in a change in the characteristic impedance of the stub by bending cantilevers from 2 μm to 1.4 μm to simulate the actuated case. Due to this capacitive loading, the characteristic impedance of the stub is modified resulting in shift in the resonant frequencies.

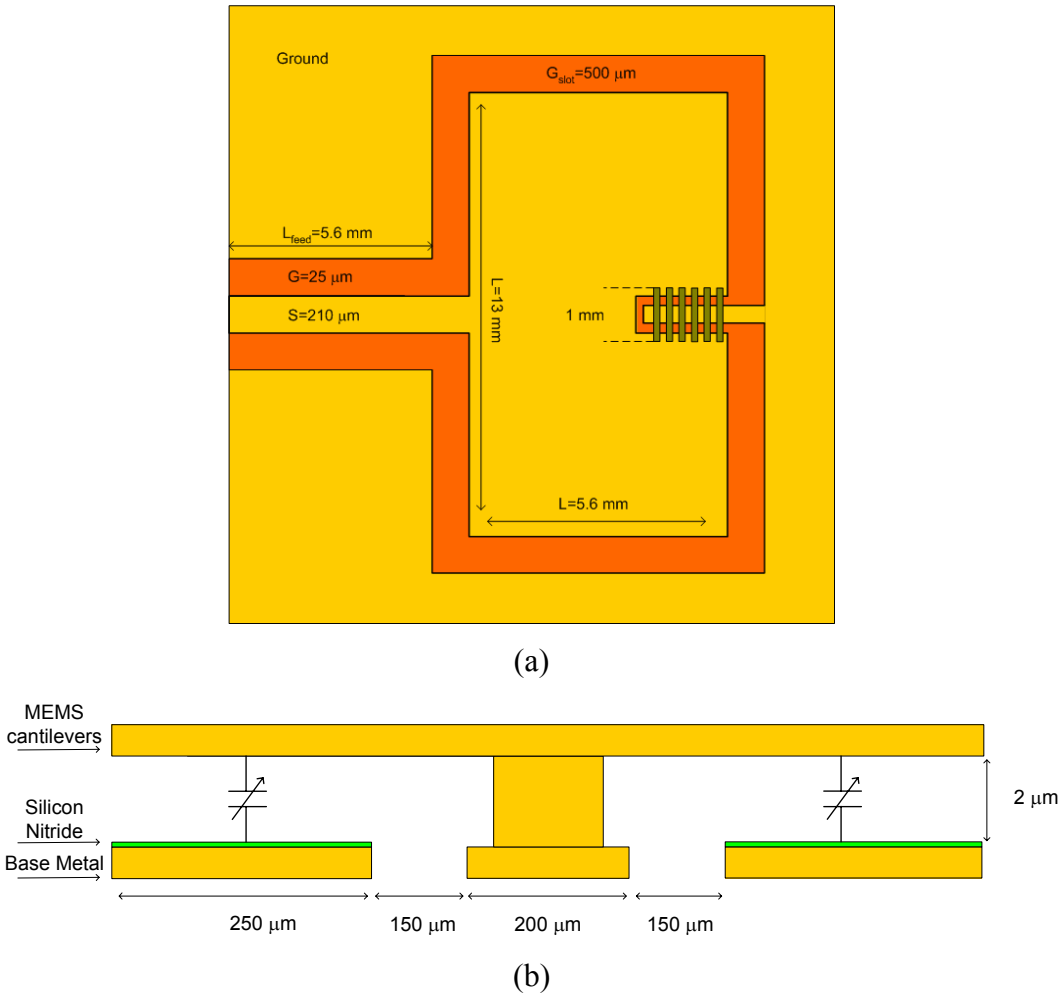

Figure 2.35. (a) The rectangular slot antenna loaded with 6 MEMS capacitors over the stub. (b) The cross-sectional view of the cantilever type capacitors over the structure.

The reflection coefficient characteristics when the bridge is at 2 μm is given in Figure 2.36. Radiation patterns for the resonant frequencies in the E- and H- planes are presented in Figure 2.37. It is understood from the figures that the resonant frequencies at 8.48 GHz and 10.53 GHz have quite similar radiation characteristics in both E- and H- planes, so the rectangular slot antenna shows a dual-frequency behavior. 10 dB bandwidth for the resonant frequency at 10.53 GHz is 10% whereas it is 4.2% for the resonant frequency at 8.48 GHz. The

radiation patterns for the resonant frequency at 14.57 GHz show that the antenna does not radiate broadside. Besides, the antenna radiates broadside with low cross-polar component at 20.4 GHz.

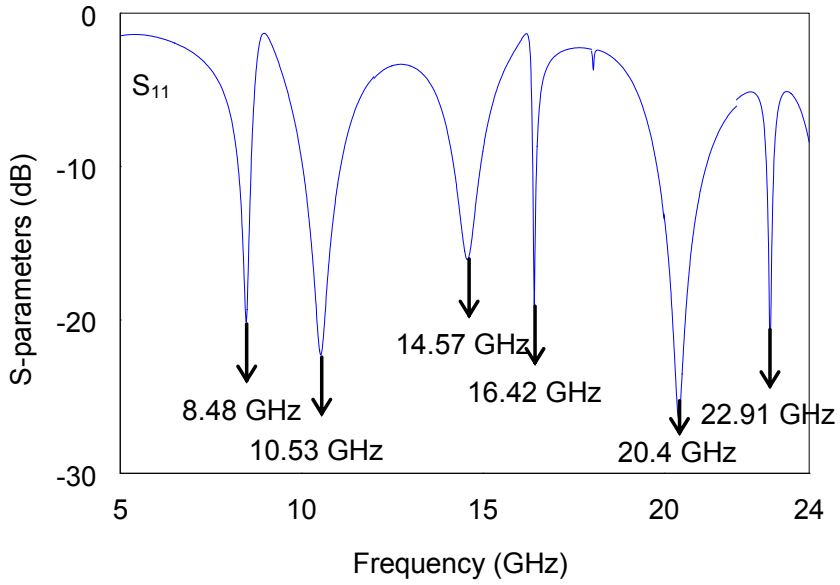

Figure 2.36. Reflection coefficient characteristic of the structure when the MEMS capacitors are at 2 μm height.

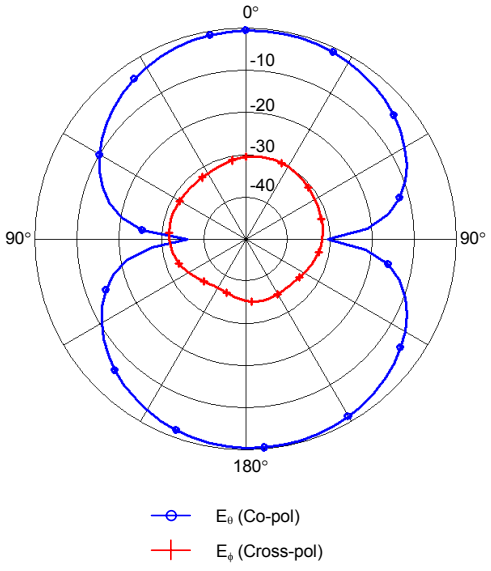

(a) E- plane at 8.48 GHz

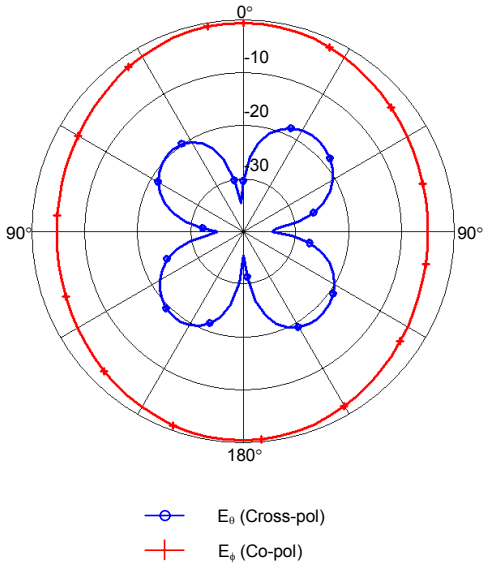

(b) H- plane at 8.48 GHz

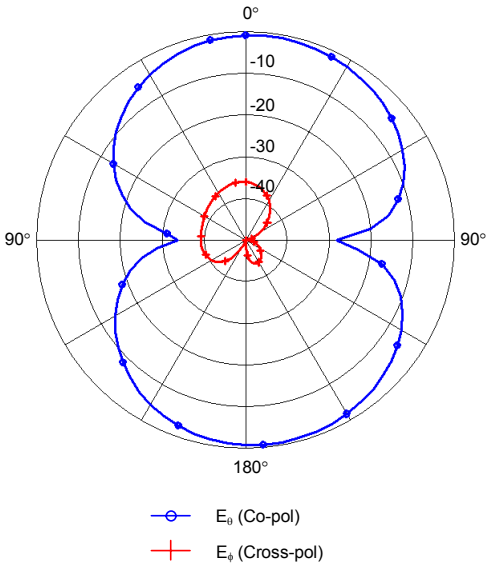

(c) E- plane at 10.53 GHz

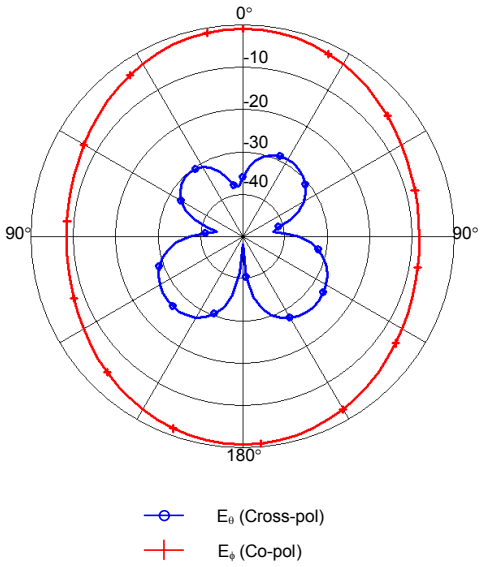

(d) H- plane at 10.53 GHz

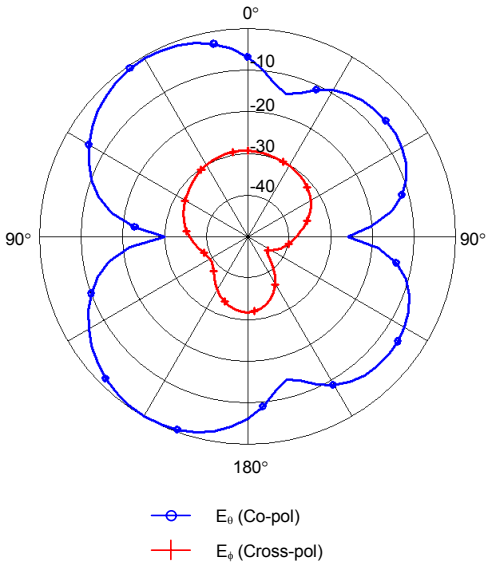

(e) E- plane at 14.57 GHz

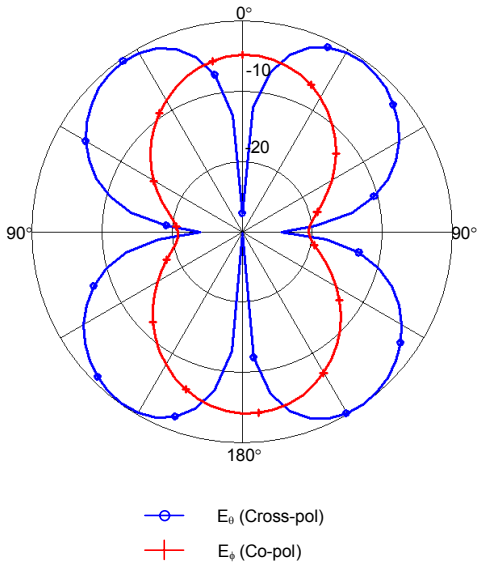

(f) E- plane at 14.57 GHz

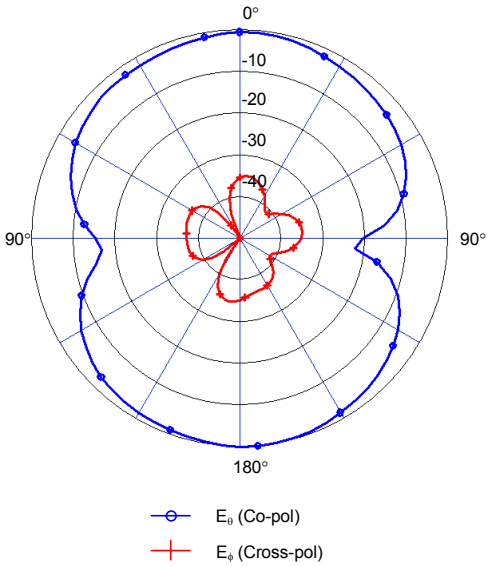

(g) E- plane at 20.4 GHz

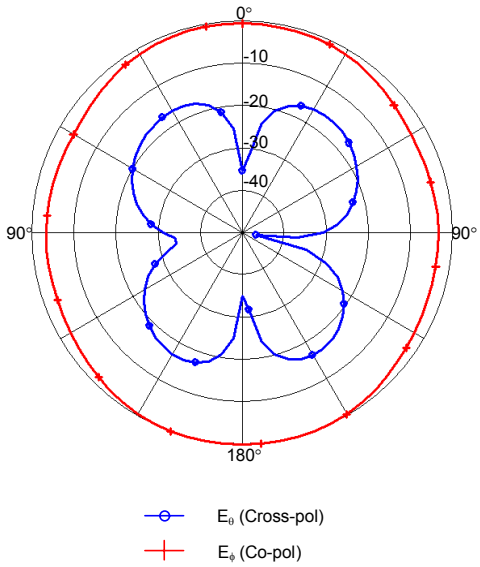

(h) H- plane at 20.4 GHz

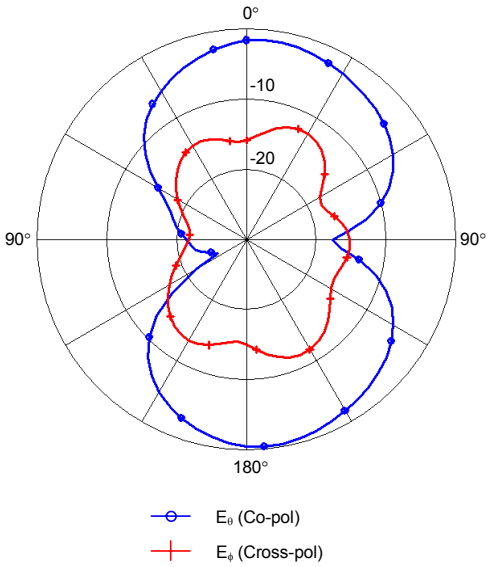

(i) E- plane at 22.91 GHz

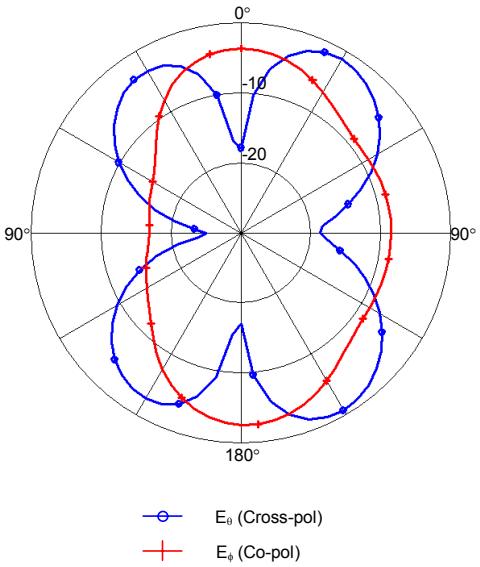

(j) H- plane at 22.91 GHz

Figure 2.37. The radiation characteristics for the resonant frequencies in Figure 2.36. (a) E- plane at 8.48 GHz. (b) H- plane at 8.48 GHz. (c) E- plane at 10.53 GHz. (d) H- plane at 10.53 GHz. (e) E- plane at 14.57 GHz. (f) H- plane at 14.57 GHz. (g) E- plane at 20.4 GHz. (h) H- plane at 20.4 GHz. (i) E- plane at 22.91 GHz. (j) H- plane at 22.91 GHz.

Figure 2.38 shows the reflection coefficient characteristic of the structure when the capacitors are at 1.4 μm height from the stub. According to the figure, the lower resonant frequency shifts from 8.48 GHz down to 7.3 GHz, corresponding to 13.9 % change, and the higher resonant frequency shifts from 10.53 GHz down to 10.2 GHz, corresponding to 3.1 % change. 10 dB bandwidth for the resonant frequency at 10.2 GHz is 11.7% whereas it is 1.6% for the resonant frequency at 7.3 GHz. The radiation patterns for the resonant frequencies at 13.6 GHz and 15 GHz show that the antenna does not radiate broadside. Figure 2.39 shows the radiation characteristics resonances occurring when the bridges are taken into 1.4 μm height.

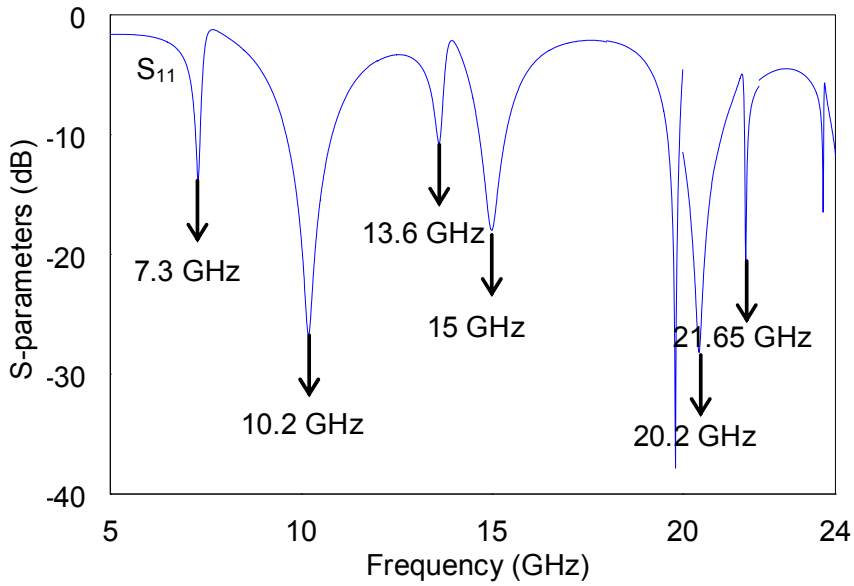

Figure 2.38. Reflection coefficient characteristics of the structure when the MEMS capacitors are at 1.4 μm height.

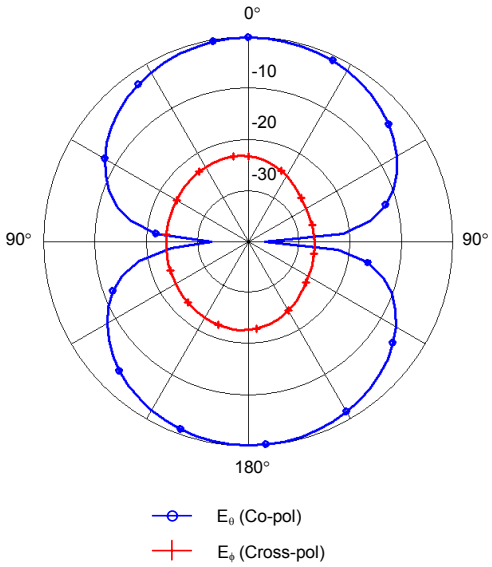

(a) E- plane at 7.3 GHz

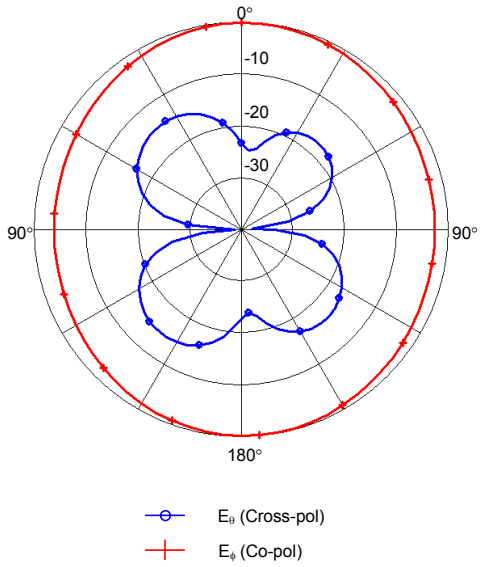

(b) H- plane at 7.3 GHz

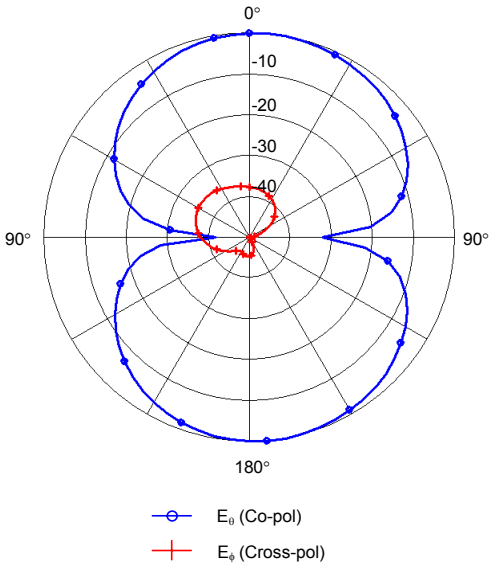

(c) E- plane at 10.2 GHz

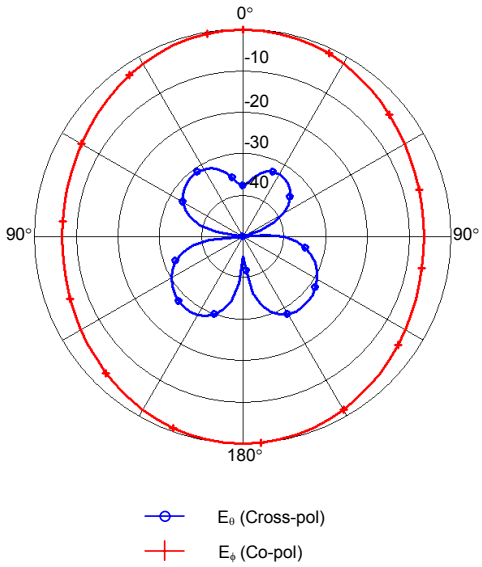

(d) H- plane at 10.2 GHz

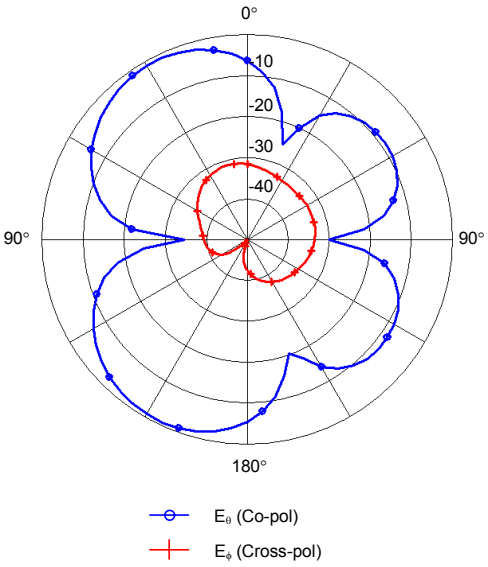

(e) E- plane at 13.6 GHz

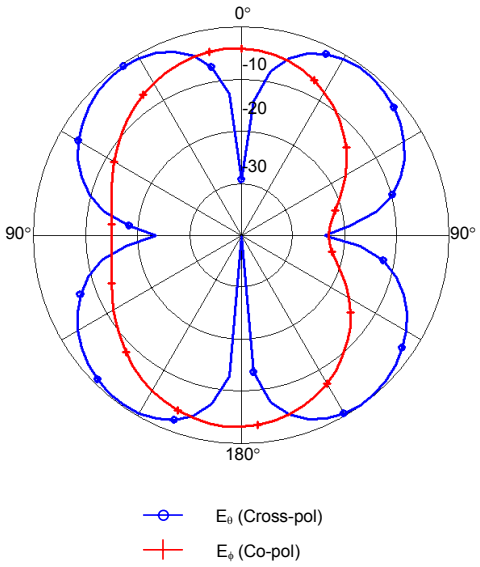

(f) H- plane at 13.6 GHz

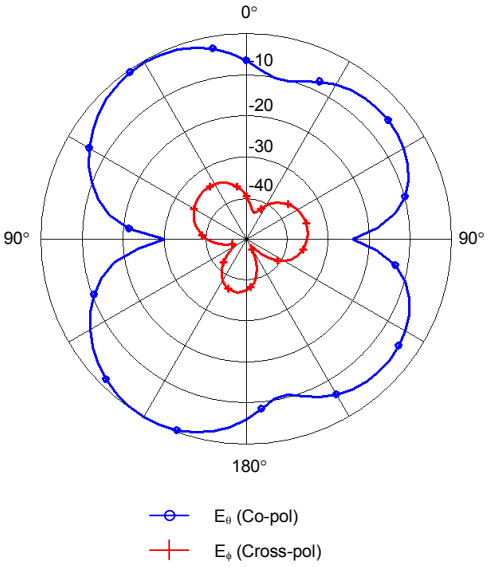

(g) E- plane at 15 GHz

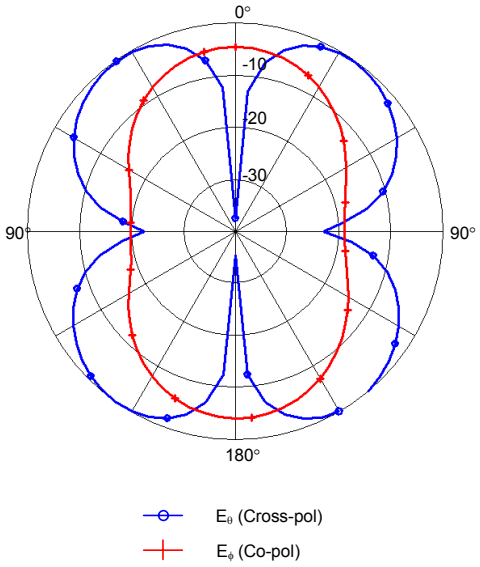

(h) H- plane at 15 GHz

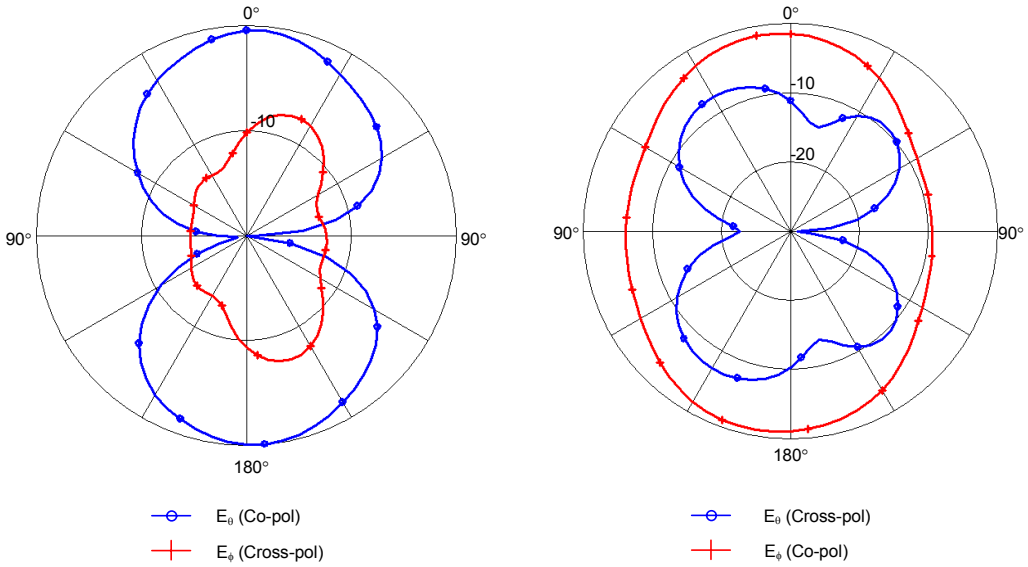

(i) E- plane at 21.65 GHz (j) H- plane at 21.65 GHz

Figure 2.39. The radiation characteristics for the resonant frequencies in Figure 2.38. (a) E- plane at 7.3 GHz. (b) H- plane at 7.3 GHz. (c) E- plane at 10.2 GHz. (d) H- plane at 10.2 GHz. (e) E- plane at 13.6 GHz. (f) H- plane at 13.6 GHz. (g) E- plane at 15 GHz. (h) H- plane at 15 GHz. (i) E- plane at 21.65 GHz. (j) H- plane at 21.65 GHz.

2.5.5 Simulation Results for Loading With Bridge Type Capacitors

Bridge type capacitors are also used to provide loading. Different numbers of capacitors are placed over the stub for different slot gaps to have the idea about the effect of capacitive loading and the slot gap. The results of these simulations are given in Table 2.5. By these simulations it is observed that the MEMS bridge type capacitors have an effect on tuning the resonant frequencies of the structure. However, the shift of the resonant frequencies is far less than the shift done with the cantilever type capacitors. Since the overlapping area forming the capacitance is 200 μm × 200 μm which is smaller regarding to the overlapping area formed by cantilever type capacitors, the amount of loading is smaller in bridge type design.

The effect of slot gap has more significant effect on matching than the shift in the resonant frequency. Lower reflection can be achieved when slot gap is beyond 300 μm which has been observed by simulation results.

Table 2.5. Change of the resonant frequencies of the rectangular slot antenna with respect to the number of bridge type capacitors and the slot gap.

# of MEMS capacitors	MEMS bridge height (μm)	G_{slot} (μm)	f_c (GHz)	Reflection (dB)
6	2	100	9.40	-6.74
6	1.4	100	9.40	-6.78
2	2	300	10.15	-15.94
2	1.4	300	10.05	-28.75
4	2	300	10.00	-18.82
4	1.4	300	10.00	-20.62
6	2	300	9.80	-16.12
6	1.4	300	9.70	-15.62
2	2	500	10.20	-17.75
2	1.4	500	10.05	-18.18
4	2	500	10.00	-21.24
4	1.4	500	9.90	-40.79
6	2	500	9.85	-22.25
6	1.4	500	9.65	-23.59

CHAPTER 3

FABRICATION PROCESS AND MEASUREMENT RESULTS

This chapter presents the fabrication process used to manufacture the designed antenna structures, the measurement results, and the comparison between simulation and measurement results. The fabrication processes have been completed in the facilities of METU MET (Mikroelektronik Tesisleri), the clean room and chemical room located at the Department of Electrical and Electronics Engineering at METU. Antenna structures are fabricated on Pyrex 7740 glass substrates having a thickness of 500 μm. The process flow used in the fabrication of antennas has already been optimized during the research on RF MEMS at METU.

3.1 Fabrication

Figure 3.1 shows the main steps of process flow: (a) 300/3000 Å Cr/Au is evaporated which is required for electroplating of Au. Cr layer is used to promote stiction of Au to the glass surface which is pretreated with buffered HF to increase roughness. The area that will be electroplated Au is determined by thick photoresist (SJR 5740) which is compatible to the cyanide gold electroplating bath. (b) Au is coated using the electroplating technique inside the regions defined by mold SJR 5740 photoresist. (c) SJR 5740 mold photoresist is removed in acetone and the excessive seed layer to be etched is defined with a lithography using S1828 photoresist. Cr/Au layers are etched using wet etching with selective

Au and Cr etchants. (d) Si_3N_4 layer is coated as the isolation layer using plasma enhanced chemical vapor deposition technique (PECVD). S1828 photoresist is coated for patterning of Si_3N_4. (e) Si_3N_4 is patterned using the reactive ion etching (RIE) technique. S1828 photoresist is removed with acetone after Si_3N_4 is removed. (f) 125/2500 Å Ti/Cu layer is sputtered as the seed layer for sacrificial layer plating. Ti/Cu layer in the anchor regions are etched after the patterning of these regions with a lithography using S1828 photoresist. The removal of Ti/Cu layer inside the anchor regions will ensure the direct contact of base metal to the structural (bridge) metal. Otherwise, the sacrificial layer removal process will not be a secure process due to the undercut of the copper etching towards the anchor regions. The photoresist used for anchor etch is removed using acetone. The areas to be Cu plated are defined with a lithography using S1828 photoresist. Deposition of copper sacrificial layer is implemented in copper sulfamate electroplating bath. The photoresist used as sacrificial layer mold is removed using acetone. (g) The areas to be gold plated for bridge formation is defined with a lithography using SJR 5740 photoresist. Au gold plating is completed in cyanite gold electroplating bath using the proper current density to obtain stress free bridges after release. The photoresist used as structural layer mold is removed using acetone. (h) The sacrificial layer is etched and the structures are released. The drying process is performed using critical point drying equipment.

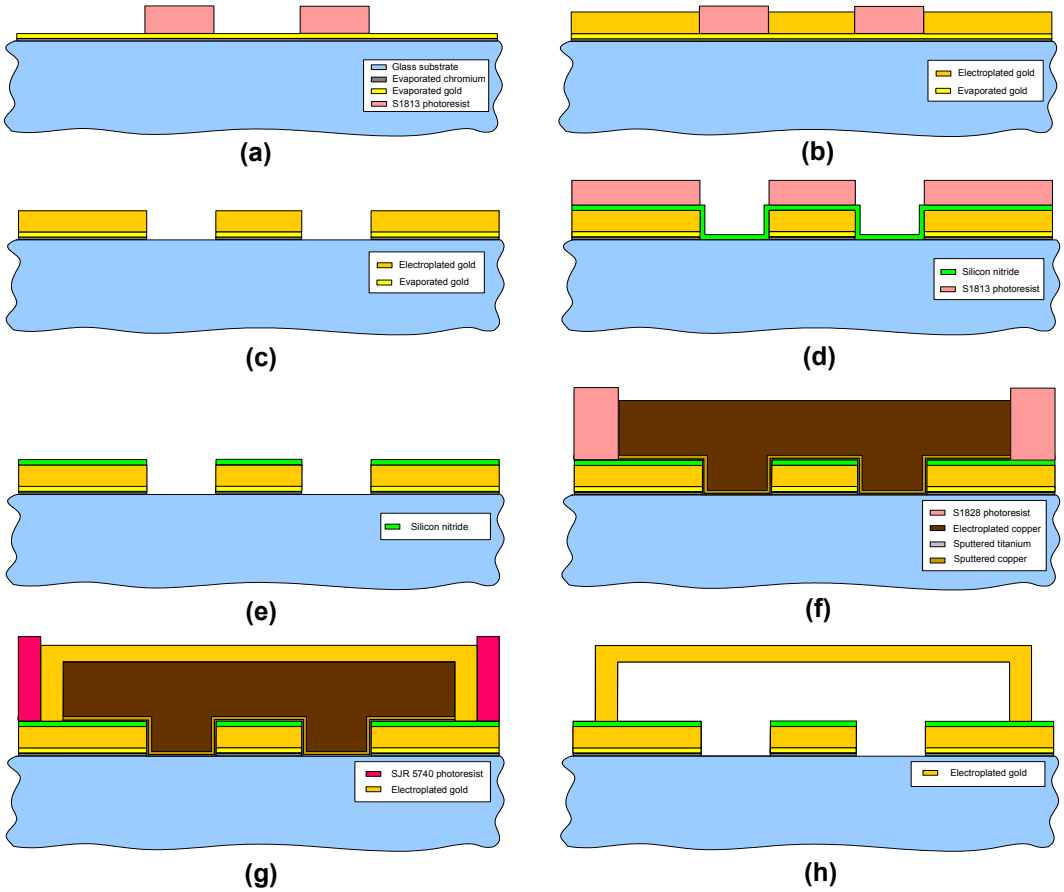

Figure 3.1. Fabrication process flow.

For the lithography steps of the fabrication process, there is a requirement to use special masks with the patterns defined by the layout drawings. The patterns on the masks define the regions of the photoresist to be illuminated by UV light in the exposure step. A mask set which includes the microstrip patch antenna loaded with CPW stub and tunable frequency CPW fed rectangular slot antenna designs is prepared. Since the process steps consist of 6 lithographies, there are 6 masks included in the set. The masks are used for:

1) Mold layer mask of the base metallization for gold electroplating.
2) Post-etch mask of the base metallization to get rid of the excessive seed layer.

3) Silicon nitride mask for RIE patterning.
4) Anchor etch mask on the Ti/Cu seed layer.
5) Sacrificial layer mask defining the region to be copper electroplated.
6) Mold layer mask for structural layer gold electroplating.

The layout drawings are accomplished in the Cadence Layout Virtuoso™ tool environment. The layout drawings of the microstrip patch antenna loaded with CPW stub and tunable frequency CPW fed rectangular slot antenna are given in Figure 3.2 and Figure 3.3, respectively.

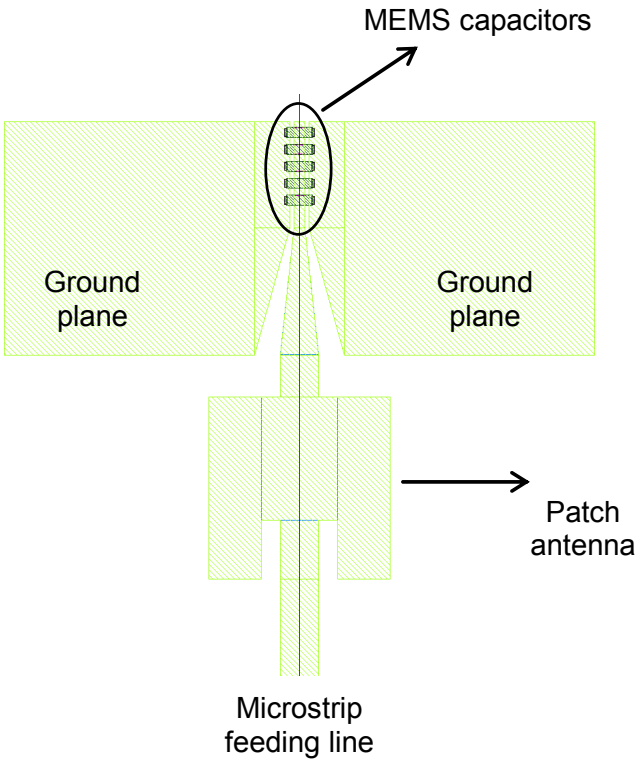

Figure 3.2. Layout drawing of microstrip patch antenna loaded with five MEMS capacitors distributed on CPW.

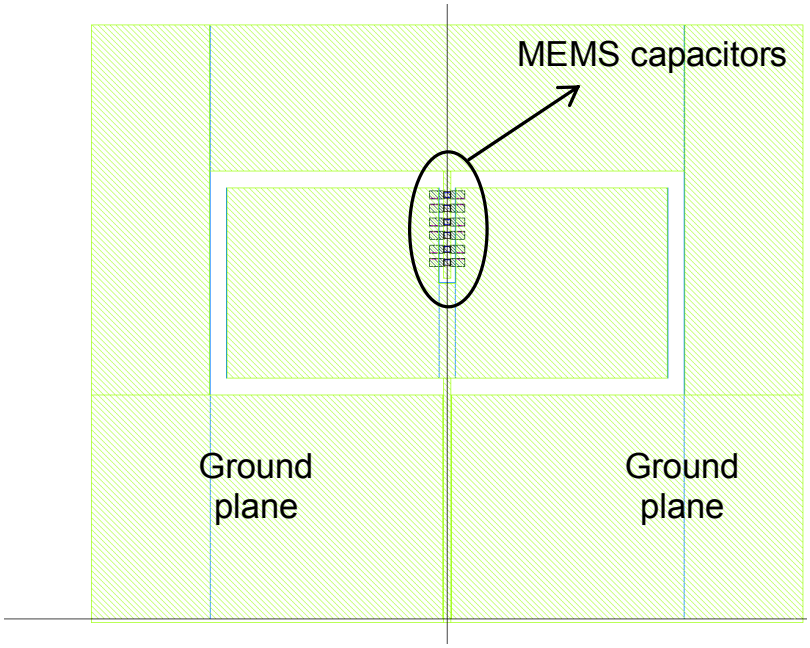

Figure 3.3. Layout drawing of the rectangular slot antenna loaded with six MEMS capacitors distributed on the stub implemented inwards the antenna.

3.2 Measurement Results

3.2.1 Measurement Setup

The RF measurements of the rectangular antenna structure are performed using HP 8720 D 0.05-20 GHz vector network analyzer and Cascade Microtech Summit 9000 manual probe station. As the RF measurement of the rectangular slot antenna is done with probes, Picoprobe 40-A-GSG-150P CPW probes are used at the connection points of the probes to the feeding line of the antenna. Probes are connected to the ports of the network analyzer via HP 85131C 3.5-mm-width semi-rigid cable, Picosecond 5542-230 bias tee, and 101-162 WL GORE 65474 cable. The bias tee is used to actuate the MEMS cantilevers during RF measurements without any adverse effect on the RF signal. Configuration of the measurement setup is shown in Figure 3.4. The calibration method used in our

tests is short-open-load-thru (SOLT). Short-open-load-thru each represents the standards used during the calibration.

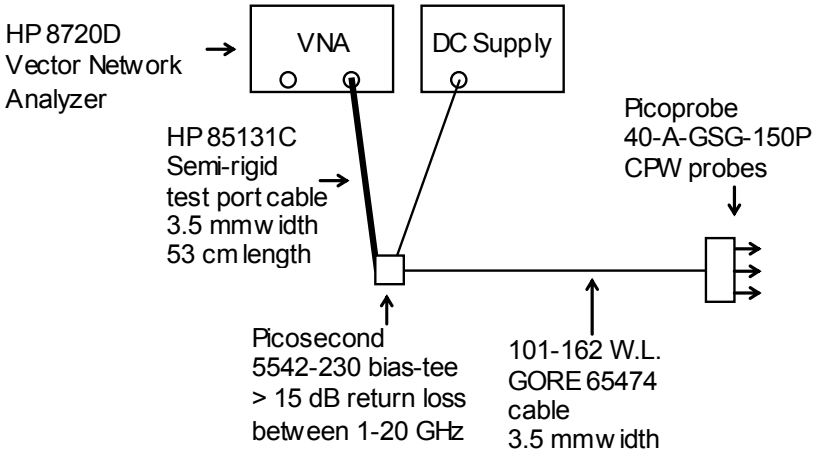

Figure 3.4. Schematics of the measurement setup.

3.2.2 Measurement Results of Rectangular Slot Antenna

Rectangular slot antenna shown in Figure 2.35 (a) is manufactured. Figure 3.5 shows the photograph of the fabricated structure taken with optical microscope.

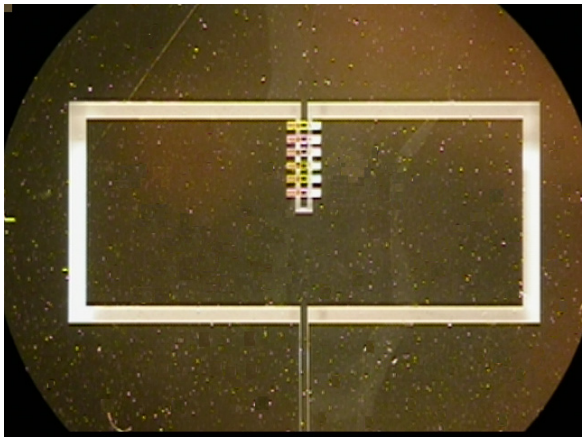

(a)

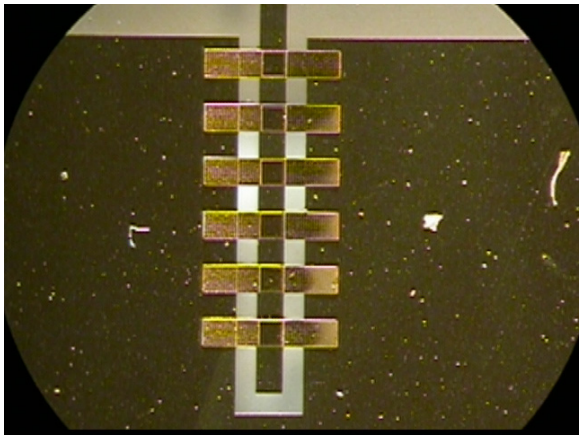

(b)

Figure 3.5. (a) Photograph of the fabricated rectangular slot antenna structure. (b) Close-up view of the six RF MEMS cantilever type capacitors loading the antenna.

During the fabrication process, first the structure without MEMS capacitors is measured. Figure 3.6 shows the reflection coefficient characteristics of the unloaded structure. As seen from the figure, measurement results are compatible with the simulation results. The deviation between the measurement and simulation at the maxima of the reflection coefficient characteristics is due to the conductor losses since the conductivity of the gold base layer is smaller than the perfect electric conductor used in the simulations.

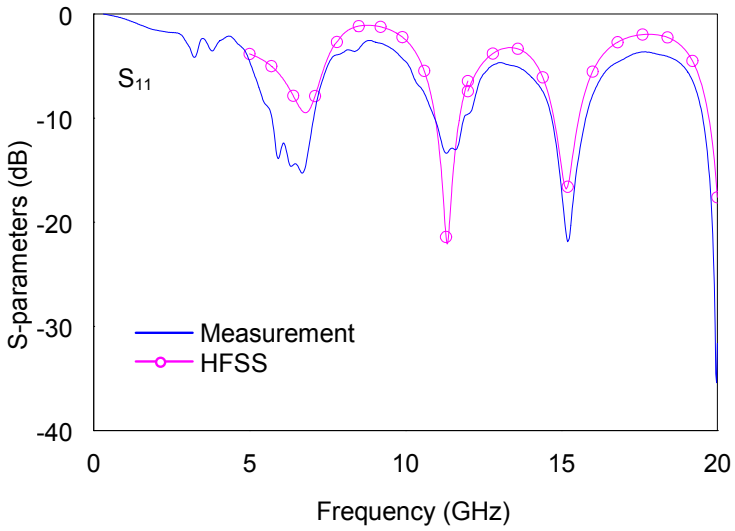

Figure 3.6. The measurement and simulation result for the unloaded antenna.

In the first manufacturing run, 4 antennas were realized. The reflection coefficient characteristics of 4 antenna structures are measured and plotted in Figure 3.7. It is seen that all of the fabricated antenna structures show nearly identical characteristics. The similarity of the characteristics verifies the uniformity of the fabrication process.

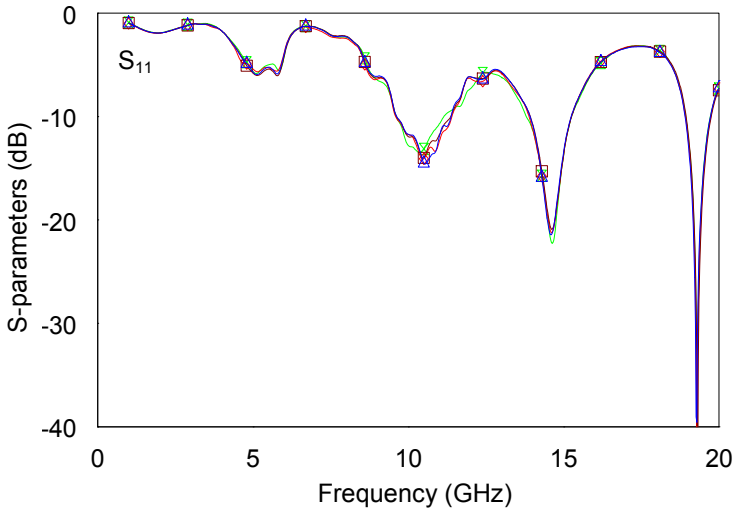

Figure 3.7. The reflection coefficient characteristics of 4 loaded antenna structures manufactured in the first run.

Figure 3.8 shows the comparison between the measured reflection coefficient characteristics of the unloaded antenna and the antenna loaded with MEMS capacitors. The resonant frequencies of the loaded antenna shift towards the lower frequencies due to the capacitive loading, as expected.

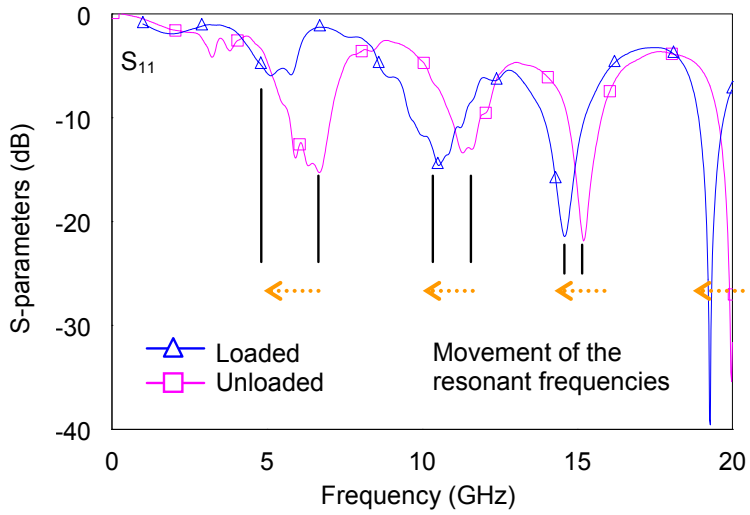

Figure 3.8. A comparison between unloaded and loaded antenna measurements.

Figure 3.9 shows the comparison between the simulation results of the antenna when the cantilever height is at 2 μm and measurement result when the cantilevers are not actuated. It is observed that resonant frequencies at 8.48 GHz and 16.42 GHz seen in the simulation results are not seen in the measurement. To understand the difference between the simulation and measurement results, SEM pictures of the structure shown in Figure 3.10 and Figure 3.11 are investigated. As can be seen, the cantilevers are curled up due to the stress gradient occurred in the structural layer gold plating. Their height is not equal to the designed value which is 2 μm. This problem can be solved by applying proper current density during gold electroplating of the structural layer to achieve stress free cantilevers.

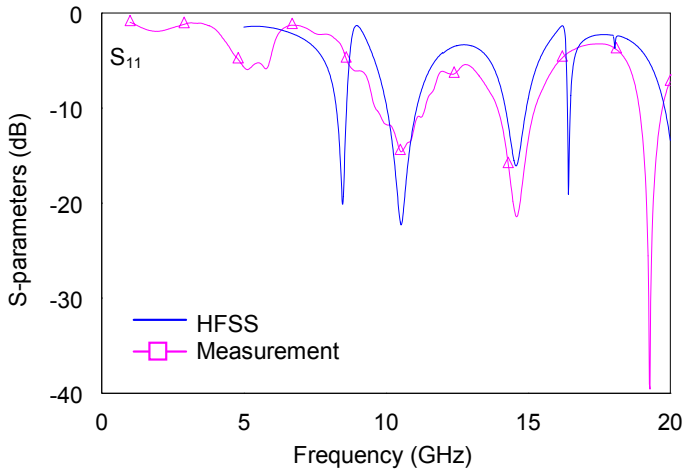

Figure 3.9. A comparison between the simulation result for a cantilever height of 2 μm and measurement result.

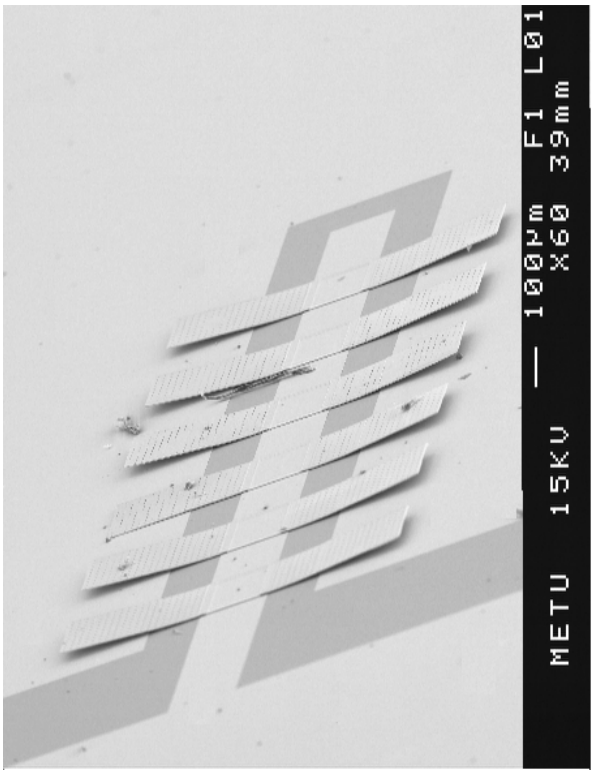

Figure 3.10. SEM view of the loading section of the CPW-fed rectangular slot antenna. The MEMS cantilevers are bended due to the stress gradient occurred during the deposition of structural layer via gold plating.

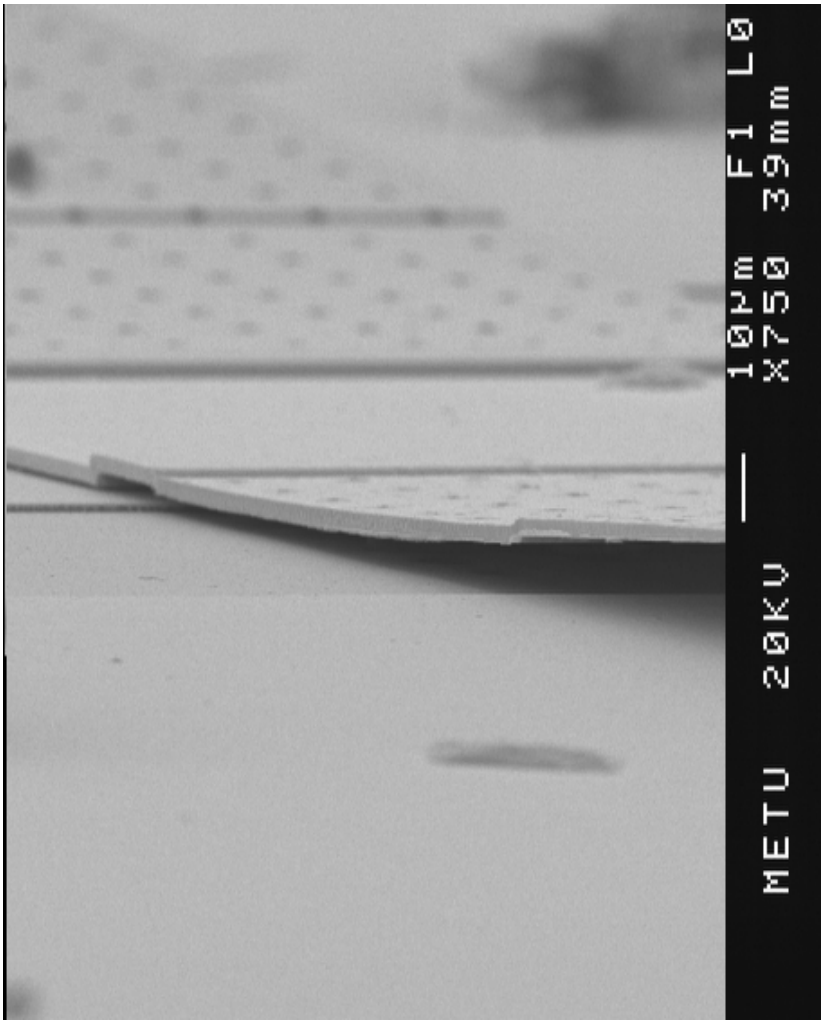

Figure 3.11. A close up view of the one of the MEMS cantilevers at the loading section of the CPW-fed rectangular slot antenna.

Since the fabricated structures could not be realized with the designed cantilever height, various simulations are performed on the antenna structures with different cantilever heights such as 30, 20, 10, 5, 2.5 μm. The agreement between the measurement and simulation result is achieved when the simulation at 20 μm height is considered, as shown in Figure 3.12. This set of solution also verifies that the amount of shift is not dependent on the ratio of the capacitances in different heights but on the value of the capacitance at these states. For

example, the ratio of the capacitance of cantilevers at 30 µm to the capacitance at 20 µm is 1.5 resulting in a shift of resonant frequency from 10.5 GHz to 10.3 GHz. The same ratio can also be maintained by the cantilevers at 2 µm and 1.4 µm yielding a shift of the resonant frequency from 8.48 GHz to 7.3 GHz. As can be concluded the shift in the latter case is higher than the shift in the former one which is a consequence of the significance of the initial capacitance. This information is also discussed in the analyses on transmission line model given in Section 2.2.2. Figure 3.13 shows the reflection coefficient characteristics at 7-12 GHz band for 30, 20, 10, 5, 2.5, 2, and 1.4 µm which verify the discussion above. In order to have a complete picture, the characteristics in 12-18 GHz for the mentioned simulations are also provided in Figure 3.14. Considering these characteristics, it can be concluded that the lowest resonances in 12-18 GHz band for 30, 20, 10, 5 µm shifts down to the 7-12 GHz as the cantilever height is varied as 5, 2.5, 2, and 1.4 µm. These results prove that the concept of tuning the resonant frequency of a slot antenna can be accomplished using RF MEMS technology.

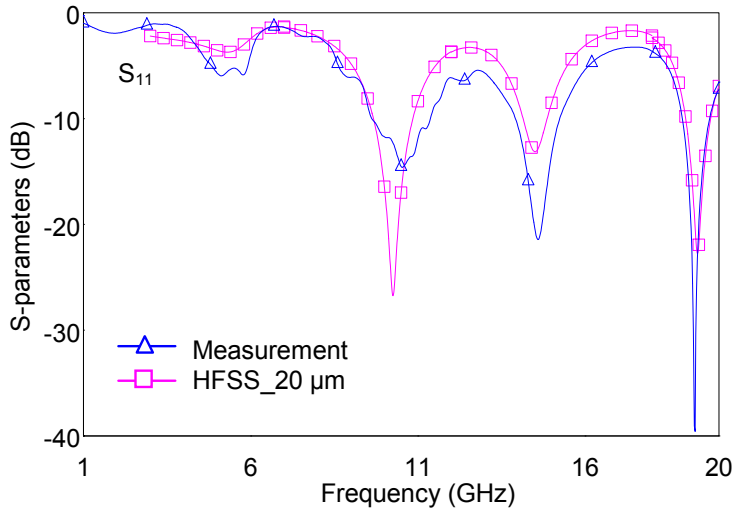

Figure 3.12. A comparison between the measurement result and the simulation result for a cantilever height 20 µm.

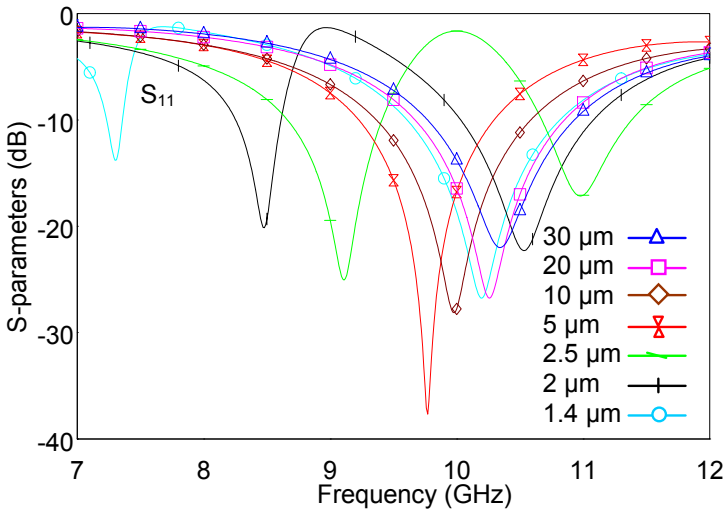

Figure 3.13. Reflection coefficient characteristics for the cantilever heights 30, 20, 10, 5, 2.5, 2, and 1.4 µm in 7-12 GHz band.

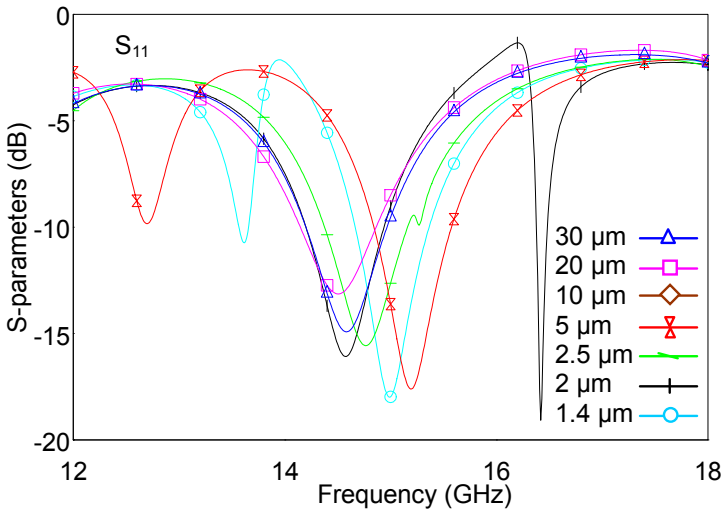

Figure 3.14. Reflection coefficient characteristics for the cantilever heights 30, 20, 10, 5, 2.5, 2, and 1.4 µm in 12-18 GHz band.

The next step is to perform measurements by applying DC voltage in order to observe the reconfigurability of the antenna. The pull-in voltages for samples are 63, 70, 71 and 81 volts. The common behavior shown by all of the samples is

the collapse of first cantilever, which is shown in Figure 3.15, for mentioned voltages. The reason might be that the thickness and the stress distribution of this cantilever are different than the other 11 cantilevers due to a change in the current distribution occurred during the structural metal plating.

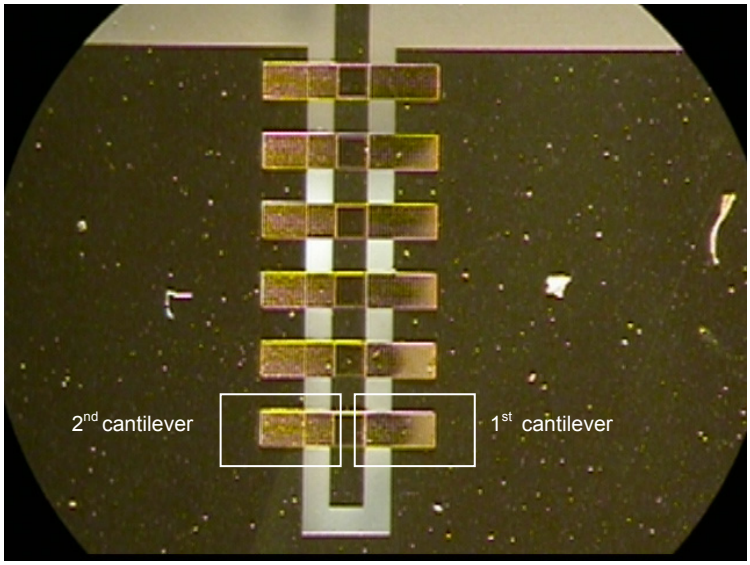

Figure 3.15. The close-up view of the loading section.

The reflection coefficient characteristics of one of the samples for different actuation voltages are shown in Figure 3.16. As can be seen from the figure, at 55 V, the resonant frequency at 19.288 for unactuated case shifts towards 19.121 GHz with an analog manner as the voltage increased from 0 V to 55 V. At 65 V, the 1st cantilever collapses. The 2nd cantilever also collapses with the help of the probe tip. The resonant frequency at 14.656 GHz when 1st cantilever is down shifts to 15.012 GHz when the 2nd cantilever is down. As the first cantilever collapses, the flowing current passes the current limitation of the DC supply. To get rid of this a 1 MΩ resistor is connected between the DC supply and the bias tee. By this way we can increase the DC voltage up to 95 V as the DC voltage limitation of the bias tee is 100 V. At 95 V it is observed that all other cantilevers but the first cantilever are in the up-state. Then we have touched the second

cantilever with the DC probe to make it collapse. After raising the DC probe the cantilever remains down-state. And measurement result is obtained while the first capacitor is totally collapsed as a switch in down-state position. The related reflection coefficient characteristic is shown in Figure 3.16.

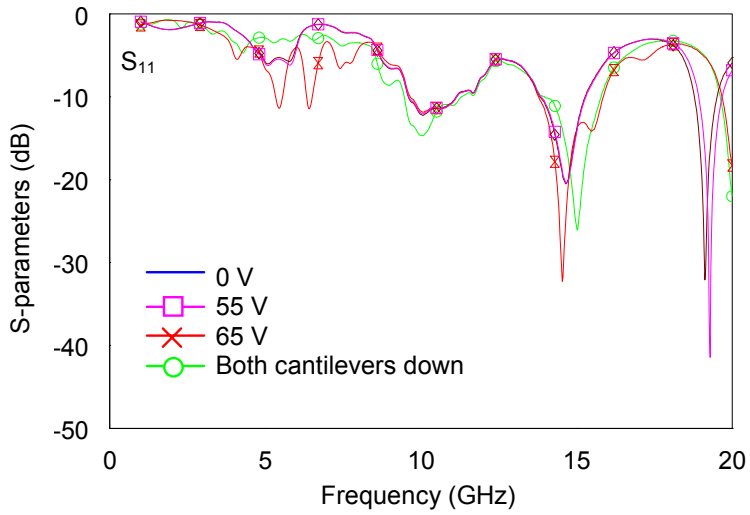

Figure 3.16. The variation of reflection response of one of the samples under actuation.

For the sample whose pull-in voltage is 81 volts, we get the measurement result applying 80 volts, just before the first cantilever collapses. Figure 3.17 gives the reflection coefficient characteristics of the structure for the mentioned condition. As can be seen in the figure, the change in the frequency is more significant for the higher frequency band. The resonant frequency at 19.335 GHz moves in an analog manner to 19.045 GHz by increasing the DC voltage.

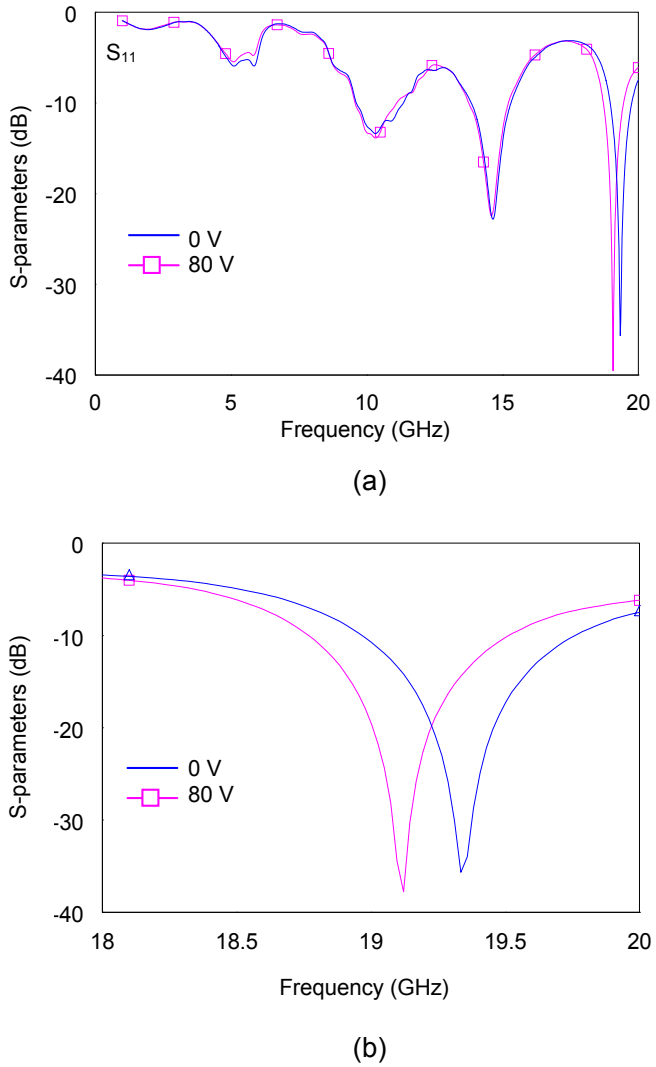

Figure 3.17. The variation of reflection response of the sample with 81 V pull-in voltage. (a) At 0-20 GHz band. (b) At 18-20 GHz band.

In order to measure the radiation pattern, RF connectors are attached to the antenna system. Since the RF connectors can be attached to the microstrip lines, a separate substrate is considered on which a 50 Ω microstrip line is implemented. The general view of the final product can be seen in Figure 3.18. The additional substrate is RO4003 (ε_r=3.38) with a thickness of 500 μm which is equal to that of glass substrate on which the antenna is fabricated. The ground underneath this

substrate is connected to upper grounds using via holes. The microstrip line and the ground planes of external substrate is wire bonded to the signal line and the ground planes of the CPW fed of the antenna. The additional substrate and the antenna substrate are aligned and attached to each other using non-conductive white epoxy.

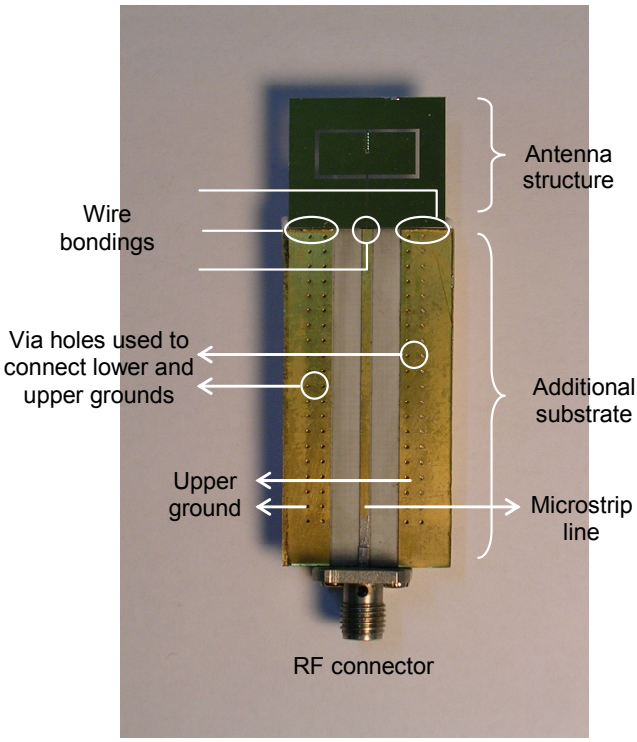

(a)

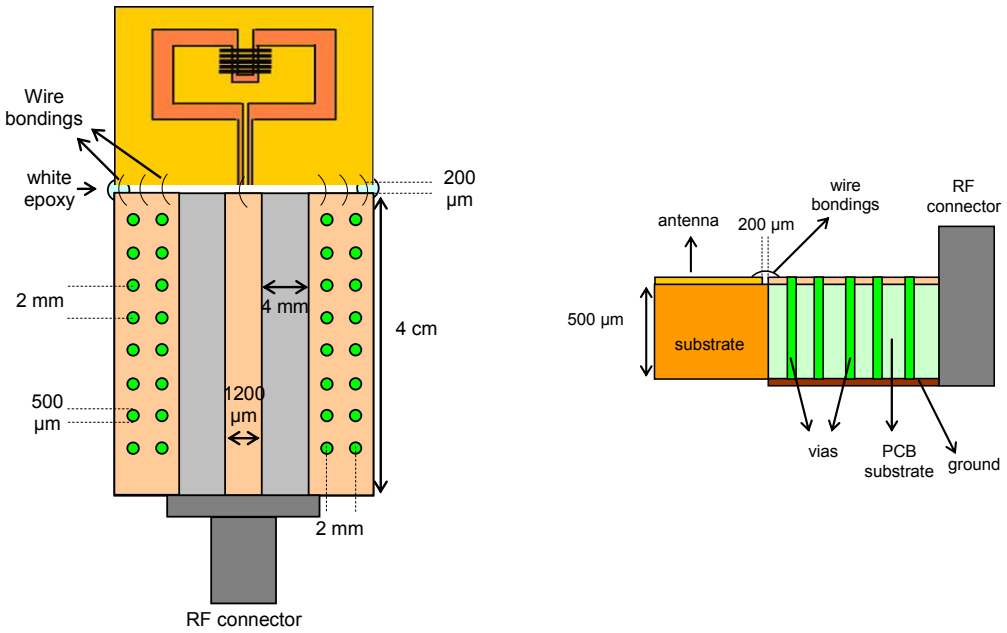

(b) (c)

Figure 3.18. (a) Photograph of the setup used for the radiation pattern measurements of the CPW-fed rectangular slot antenna. (b) Top view of the structure. (c) Side view of the structure.

Figure 3.19 shows the reflection coefficient characteristics of the structure given in Figure 3.18. The response has a minimum around 12 GHz which is different compared to the measurements taken with CPW probes. This discrepancy might be due to the inductive effects of wire bonds and the parasitic coupling between the open end of microstrip line on the additional substrate and the ground planes of the antenna as the microstrip line of the additional structure is much wider than the signal line of the antenna. This parasitic coupling can be prevented by tapering the microstrip line of the additional structure to make a good transition from microstrip line to the CPW.

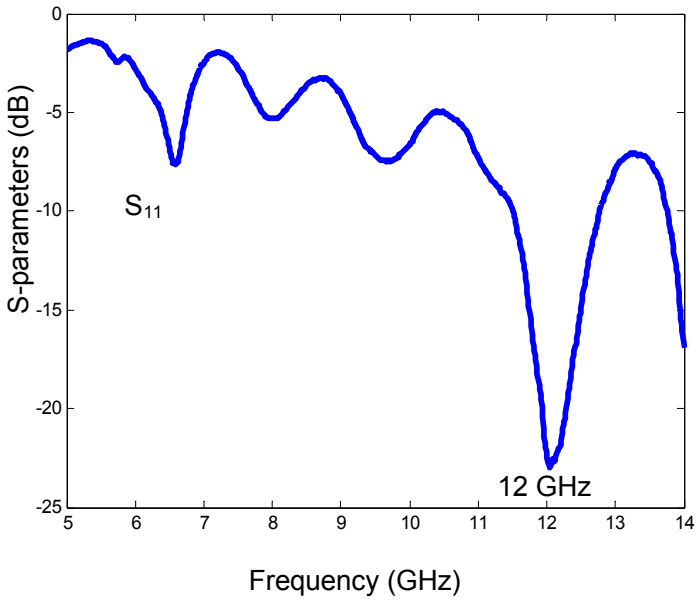

Figure 3.19. The reflection coefficient characteristics of the structure given in Figure 3.18.

The radiation pattern measurements are performed in the anechoic chamber in Middle East Technical University, Department of Electrical and Electronics Engineering Millimeter Wave Laboratory shown in Figure 3.20. During measurements, the additional substrate attached to the antenna is coated with absorber to reduce the parasitic effects. The first radiation pattern measurement is performed at 12 GHz which is resonant frequency of the structure composed of the additional substrate and the antenna structure. Figure 3.21 shows the radiation pattern for H-plane co-polar component measurement and the simulated pattern for the same plane for a cantilever height of 20 μm. Both results show similar characteristics with a small deviation which might be due to the parasitic effects of the additional substrate.

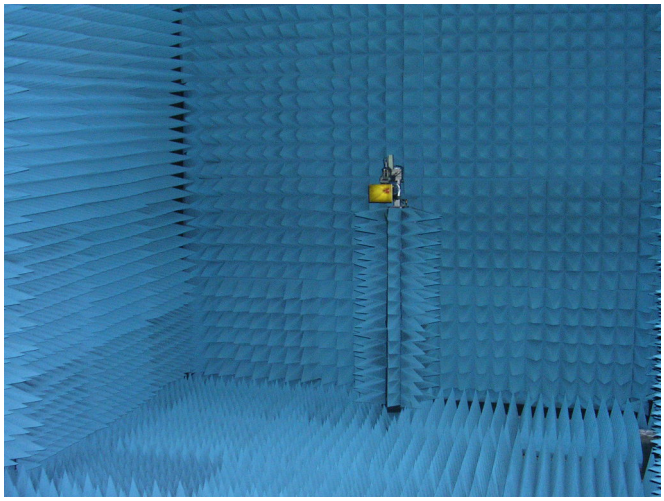

Figure 3.20. The anechoic chamber in METU.

The next measurements are performed at resonant frequencies observed during the measurements with CPW probes, which are shown in Figure 3.7, namely 10.5 GHz, 15 GHz, and 19 GHz. Figure 3.22 shows the radiation pattern at 10.5 GHz for H- plane. The power level of cross-polar component is 7 dB lower than that of co-polar component. It should be noted that since the measurement system assigns the maximum power level to 0°, the pattern for cross-polar component in Figure 3.22 (b) is rotated for proper visualization. The measurement results are in agreement with the simulated patterns, shown in Figure 3.22 (c). The increase in the cross-polar component for the measurement is due to the parasitic effects caused by the additional substrate or due to the limits of the measurement setup.

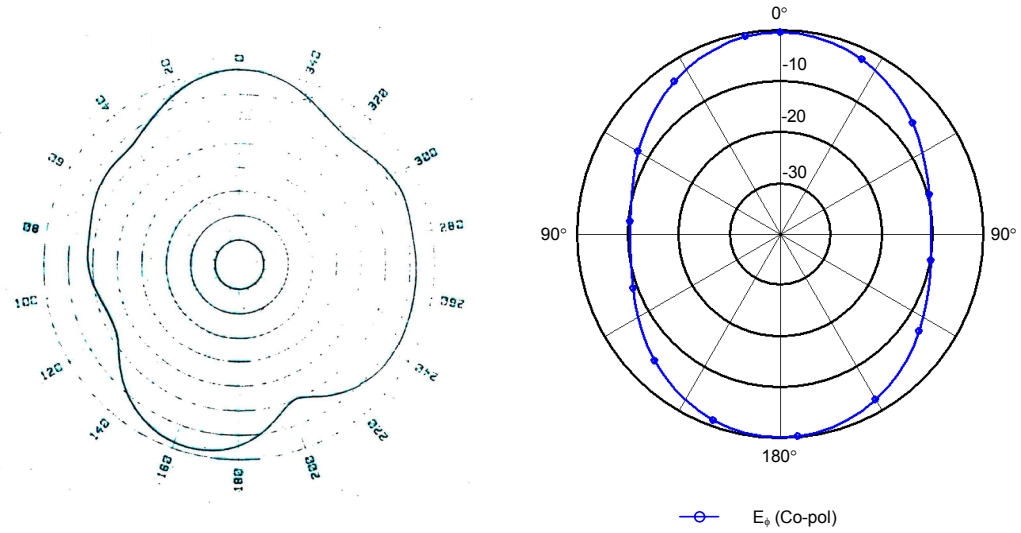

(a) H- plane at 12 GHz (measured) (b) H- plane at 12 GHz (simulated)

Figure 3.21. Comparison of radiation patterns between the measurement and simulation results at 12 GHz for H- plane. (a) Measurement result of the co-polar component at 12 GHz for H-plane. (b) Simulation result of the co-polar component at 12 GHz for H- plane.

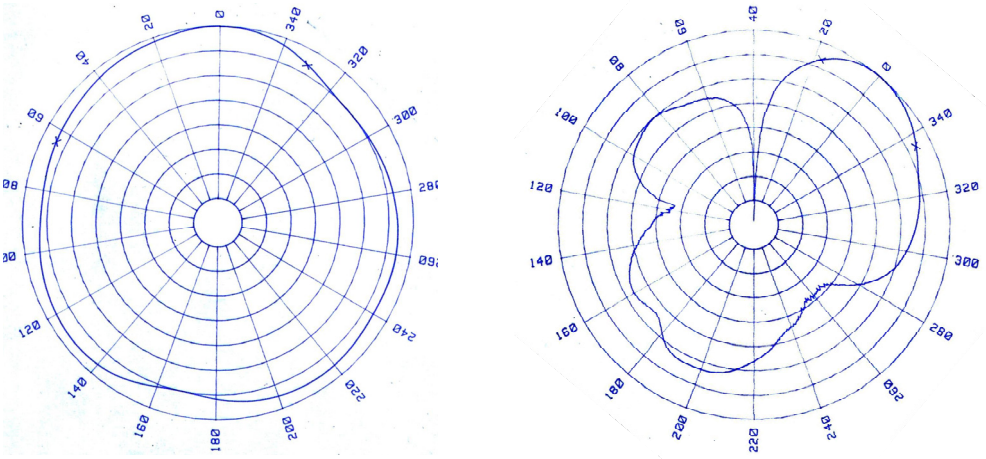

(a) Co-polar component at 10.5 GHz for H- plane

(b) Cross-polar component at 10.5 GHz for H- plane

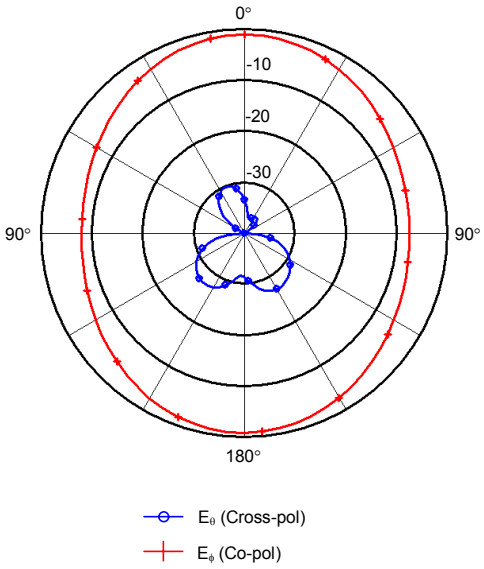

(c) H- plane at 10.5 GHz (simulated)

Figure 3.22. Comparison of radiation patterns between the measurement and simulation results at 10.5 GHz for H- plane. (a) Measurement result of the co-polar component at 10.5 GHz for H-plane. (b) Measurement result of the cross-polar component at 10.5 GHz for H-plane (c) Simulation result at 10.5 GHz for H- plane.

Figure 3.23 shows the radiation pattern at 15 GHz for H- plane. The power levels of co-polar and cross-polar components are approximately equal. These results are also in agreement with the simulated patterns as can be seen in Figure 3.23 (c). The measurement can not be obtained at 19 GHz due to very low measured power which might be because of high reflected power at this frequency.

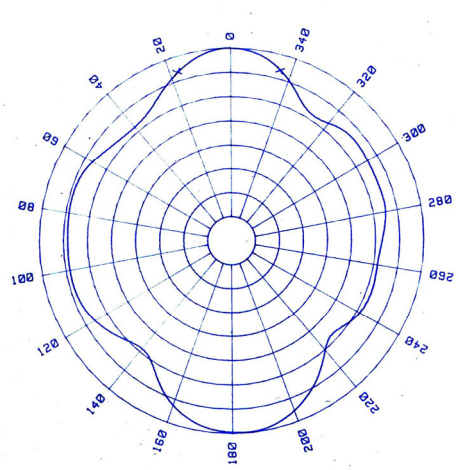

(a) Co-polar component at 15 GHz for H- plane

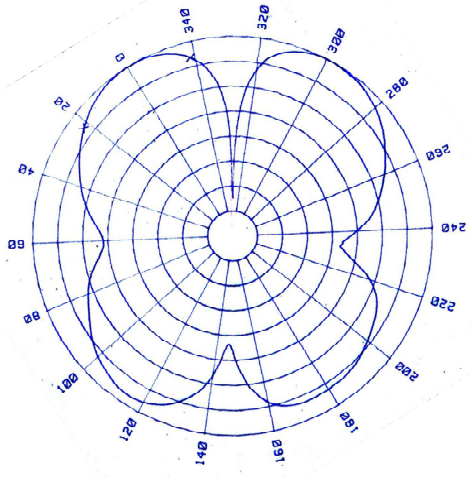

(b) Cross-polar component at 15 GHz for H- plane

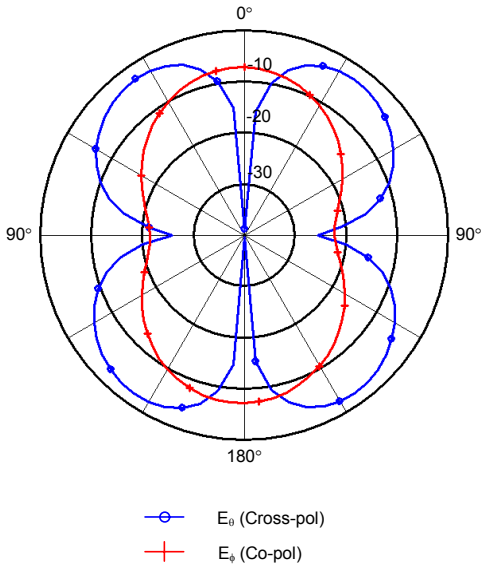

(c) H- plane at 15 GHz (simulated)

Figure 3.23. Comparison of radiation patterns between the measurement and simulation results at 15 GHz for H- plane. (a) Measurement result of the co-polar component at 15 GHz for H-plane. (b) Measurement result of the cross-polar component at 15 GHz for H-plane (c) Simulation result at 15 GHz for H- plane.

Figure 3.24 shows the radiation pattern at 10.5 GHz for E-plane. The power level of cross-polar component is 4 dB lower than that of co-polar component. The simulated patterns are shown in Figure 3.24 (c). The discrepancy between the measurement and the simulation results is due to the damage on the cantilevers occurred before this measurement. The damage is the break of two cantilevers which might totally disturb the radiation pattern characteristics of the antenna.

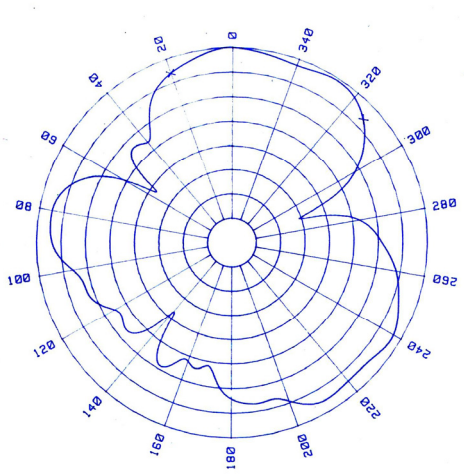

(a) Co-polar component at 10.5 GHz for E- plane

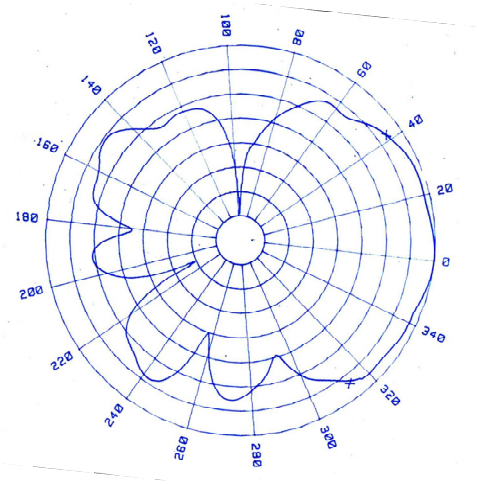

(b) Cross-polar component at 10.5 GHz for E- plane

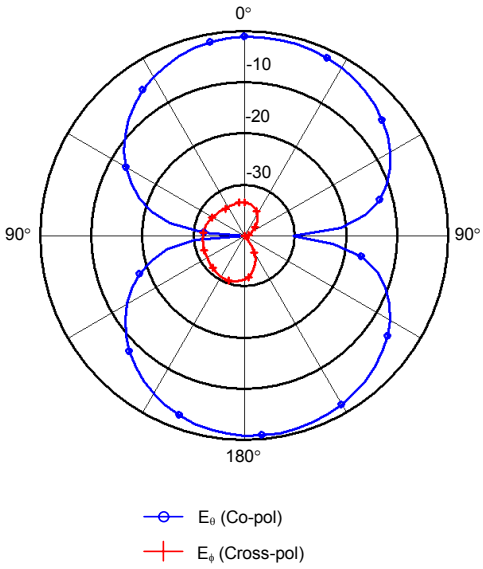

(c) E- plane at 10.5 GHz (simulated)

Figure 3.24. Comparison of radiation patterns between the measurement and simulation results at 10.5 GHz for E- plane. (a) Measurement result of the co-polar component at 10.5 GHz for E- plane. (b) Measurement result of the cross-polar component at 10.5 GHz for E- plane (c) Simulation result at 10.5 GHz for E- plane.

3.2.3 Modified Design with Different Type of MEMS Capacitor

To solve the problem of curling of cantilevers during fabrication process, antenna design can be modified. For instance, ends of the cantilevers can be connected to the substrate via anchors. By this way, as the ends of the cantilevers are connected to the substrate, MEMS capacitors will not curl up, so the fabrication of the capacitors at the designed values can be accomplished. Figure 3.25 shows the side view of the MEMS capacitor. To connect the capacitors to the substrate, slots have been opened in the metal conductor, and anchors are placed in these openings between the substrate and the bridge.

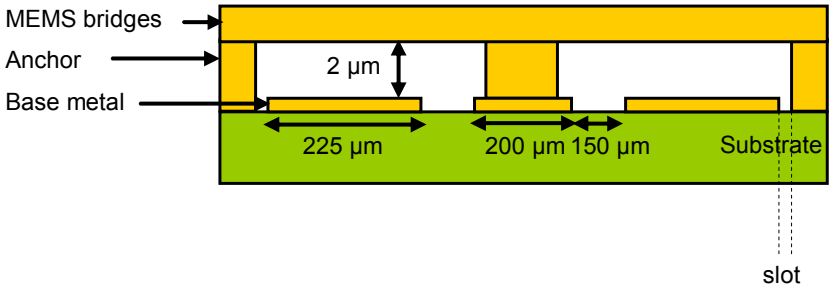

Figure 3.25. Side view of the MEMS capacitor whose ends are connected to the substrate via anchors.

Figure 3.26 shows the reflection coefficient characteristics of the rectangular slot antenna loaded with 6 MEMS capacitors whose ends are connected to the substrate. According to the simulation results, changing the bridge height from 2 µm to 1.4 µm, the lower resonant frequency shifts from 8.58 GHz to 7.88 GHz corresponding to 8.2% change, and the higher resonant frequency shifts from 10.6 GHz to 10.3 GHz corresponding to 2.8% change.

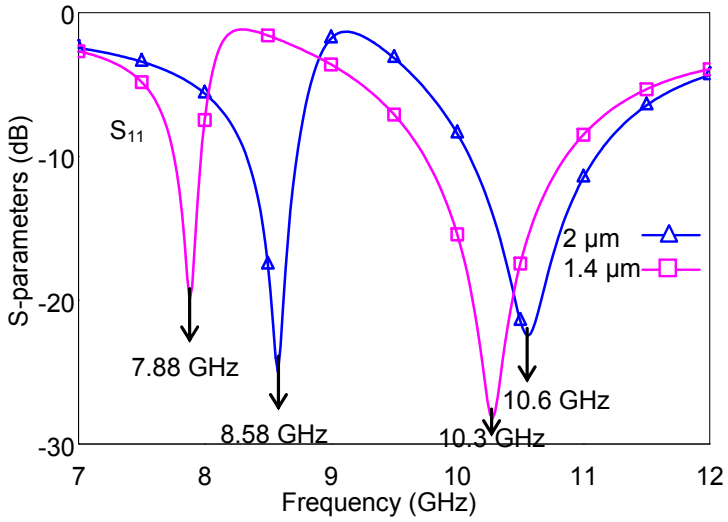

Figure 3.26. Reflection coefficient characteristics of the rectangular slot antenna loaded with 6 MEMS bridge type capacitors whose ends are connected to the substrate via anchors for the capacitor heights 2 µm and 1.4 µm.

CHAPTER 4

CONCLUSION

Throughout this thesis, frequency tunable antenna structures are investigated, designed and fabricated. RF MEMS switches and capacitors are used to tune the resonant frequency. RF MEMS capacitors are placed onto CPW and microstrip stubs to provide capacitive loading. By changing the height of the capacitors, i.e. changing the capacitance value, the resonant frequency of the antenna can be tuned.

During this thesis study, following conclusions are drawn:

1. Loading a microstrip antenna with a capacitor, the input impedance of the antenna is changed resulting in change in the resonant frequency. The shift in the resonant frequency is directly related to the change in the amount of the capacitance value.

2. Microstrip antenna which is loaded by RF MEMS bridge type capacitors distributed periodically onto an open ended CPW stub is designed. Simulation results show 1 GHz shift in the resonant frequency by changing the capacitor height from 2 μm to 1.4 μm. However, the major drawback of this configuration is as microstrip antenna is loaded with CPW stub, to make a good transition between

the microstrip antenna and CPW a tapered line is used which makes the system volume large.

3. Rectangular slot antenna which is loaded by RF MEMS cantilever type capacitors distributed periodically onto the stub is designed and fabricated in the facilities of METU. The stub is realized with the insertion of the ground plane into the conductor carrying the RF signal which reduces the system size compared to tunable microstrip antenna designs. The rectangular slot antenna without the stub shows a dual frequency behavior with a large cross-polar component in the H-plane at the higher resonant frequency. The stub also reduces this cross-polar component for the H-plane significantly by changing the equivalent magnetic current distribution on the slots parallel to the feeding line of the antenna. In the simulations of the loaded antenna structure, a shift of 1.2 GHz for the lower resonant frequency and 330 MHz for the higher resonant frequency is achieved. The reason that we could not achieve such a shift in the measurement results is due to the stress gradient occurring in the cantilever during the fabrication process resulting curling of the cantilever upwards making the cantilever height much more than 2 μm for the unactuated condition. This error due to fabrication can be solved if the current density of the structural layer plating is adjusted properly to yield stress-free cantilevers or different type of capacitors can be designed to solve the problem. For instance, to get rid of curling, ends of the cantilevers can be connected to the substrate via anchors which are placed between the slots opened in the metal conductor and the substrate.

4. For a microstrip antenna whose operating frequency is higher, more shift in the resonant frequency can be achieved with respect to the microstrip antenna operating at lower frequencies for the same amount

of change in the capacitance value since the loading impedance for capacitive loading depends on frequency. Consequently, implementing the configuration proposed to a microstrip antenna operating at higher frequencies can be considered as a future work.

5. To avoid mechanical instability the height of the RF MEMS capacitors used in our designs are lowered to 2/3 of its maximum height which is constraining the amount of shift in the resonant frequency. Design and implementation of RF MEMS capacitors having higher gap variations can also be considered as a future work.

REFERENCES

[1] G. Kumar, K. P. Ray, "Broadband microstrip antennas" Norwood, MA: Artech House, 2003.

[2] G. M. Rebeiz, "RF MEMS theory, design, and technology," Hoboken, NJ: John Wiley & Sons, 2003.

[3] S. P. Pacheco, L. P. B. Katehi, and C. T.-C. Nguyen, "Design of Low Actuation Voltage RF MEMS Switch," 2000 IEEE MTT-S Digest, pp. 165-168.

[4] E. R. Brown, "RF-MEMS Switches for Reconfigurable Integrated Circuits," IEEE Transactions on Microwave Theory and Techniques, vol. 46, no. 11, Nov. 1998, pp.1868-1880.

[5] C. Chang and P. Chang, "Innovative Micromachined Microwave Switch With Very Low Insertion Loss," Sensors and Actuators 79 (2000), pp. 71-75.

[6] S.-C. Shen and M. Feng, "Low Actuation Voltage RF MEMS Switches With Signal Frequencies from 0.25 GHz to 40 GHz," Proc. IEEE 1999.

[7] J. B. Muldavin and G. M. Rebeiz, "Inline Capacitive and DC-Contact MEMS Shunt Switches," IEEE Microwave and Wireless Components Letters, vol. 11, no. 8, Aug. 2001.

[8] J. Y. Park, G. H. Kim, K. W. Chung, and J. U. Bu, “Electroplated RF MEMS Capacitive Switches,”

[9] C. L. Goldsmith, Z. Yao, S. Eshelman, and D. Denniston, “Performance of Low-Loss RF MEMS Capacitive Switches,” IEEE Microwave and Guided Wave Letters, vol. 8, no. 8, Aug. 1998, pp. 269-271.

[10] J. Y. Park, G. H. Kim, K. W. Chung, and J. U. Bu, “Fully Integrated Micromachined Capacitive Switches for RF Applications,” 2000 IEEE MTT-S Digest, pp. 283-286.

[11] L. Dussopt and G. M. Rebeiz, “High-Q Millimeter-Wave MEMS Varactors: Extended Tuning Range and Discrete-Position Designs,” 2002 IEEE MTT-S CDROM, pp. 1205-1208.

[12] J. Y. Park, Y. J. Yee, H. J. Nam, and J. U. Bu, “Micromachined RF MEMS Tunable Capacitors Using Piezoelectric Actuators,” 2001 IEEE MTT-S Digest, pp. 2111-2114.

[13] H. D. Wu, K. F. Harsh, R. S. Irwin, W. Zhang, A. R. Mickelson, and Y. C. Lee, “MEMS Designed for Tunable Capacitors,”

[14] Z. Feng, W. Zhang, B. Su, K. F. Harsh, K. C. Gupta, V. Bright, and Y. C. Lee, “Design and Modeling of RF MEMS Tunable Capacitors Using Electro-thermal Actuators,” 1999 IEEE MTT-S Digest, pp. 1507-1510.

[15] J. B. Rizk and G. M. Rebeiz, “Digital-Type RF MEMS Switched Capacitors,” 2002 IEEE MTT-S CDROM, pp. 1217-1220.

[16] G. V. Ionis, A. Dec, and K. Suyama, “Differential Multi-Finger MEMS Tunable Capacitors for RF Integrated Circuits,” 2002 IEEE MTT-S CDROM, pp. 345-348.

[17] Z. Feng, H. Zhang, W. Zhang, B. Su, K. C. Gupta, V. M. Bright, and Y. C. Lee, “MEMS-Based Variable Capacitor for Millimeter-Wave Applications,” Solid-State Sensor and Actuator Workshop, Hilton Head Island, South Carolina, June 4-8, 2000, pp. 255-258.

[18] K. F. Harsh, B. Su, W. Zhang, V. M. Bright, and Y. C. Lee, “The Realization and Design Considerations of a Flip-Chip Integrated MEMS Tunable Capacitor,” Sensors and Actuators 80 (2000), pp. 108-118.

[19] H. A. C. Tilmans, “MEMS Components for Wireless Communications (invited paper),” EUROSENSORS XVI The 16th European Conference on Solid-State Transducers, Prague, Czech Republic, Sept. 15-18 2002.

[20] J. J. Yao, S. T. Park, and J. DeNatale, “High Tuning-Ratio MEMS-Based Tunable Capacitors for RF Communications Applications, Solid-State Sensor and Actuator Workshop, Hilton Head, SC, USA, June 8-11 1998, pp. 124-127, 1998.

[21] R. N. Simons, D. Chun, and L. P. B. Katehi, “Microelectromechanical Systems (MEMS) Actuators for Antenna Reconfigurability,” 2001 IEEE MTT-S Digest, pp.215-218.

[22] R. N. Simons, D. Chun, and L. P. B. Katehi, "Polarization Reconfigurable Patch Antenna Using Microelectromechanical Systems (MEMS) Actuators," Proc. IEEE. 2002.

[23] Daniel Llorens, Pablo Otero, and Carlos Camacho-Peñalosa, IEEE Trans. on Antennas and Propagation, Vol. 51, Jan. 2003, pp.137-139.

[24] C.A. Balanis, "Antenna Theory: Analysis and Design," 2nd ed., John Wiley & Sons, 1997.

[25] R. Garg, P. Bhartia, I. Bahl, A. Ittipiboon, "Microstrip Antenna Design Handbook," Norwood, MA: Artech House, 2001.

[26] A.Z. Elsherbeni, A.A. Eldek, B.N. Baker, C.E. Smith, and K. Lee, "Wideband Coplanar Patch-Slot Antennas for Radar Applications," Proc. IEEE, 2002.

[27] A.A. Eldek, A.Z. Elsherbeni, C.E. Smith, and K. Lee, "Wideband Rectangular Slot Antenna for Personal Wireless Communication Systems," IEEE Antenna's and Propagation Magazine, Vol. 44, No. 5, October 2002.

[28] K. Li, C.H. Cheng, T. Matsui, and M. Izutsu, "Coplanar Patch Antennas: Principle, Simulation and Experiment," Proc. IEEE, 2001.

[29] B.K. Kormanyos, W. Harokopus, L.P.B. Katehi, and G.M. Rebeiz, "CPW-Fed Active Slot Antennas," IEEE Transactions on Microwave Theory and Techniques, Vol. 42, No. 4, April 1994.

[30] J.Y. Sze, K.L. Wong, and C.C. Huang, “Coplanar Waveguide-Fed Square Slot Antenna for Broadband Circularly Polarized Radiation,” IEEE Transactions on Antennas and Propagation, Vol. 51, No. 8, August 2003.

[31] A.U. Bhobe, C.L. Holloway, M. Piket-May, and R. Hall, “Coplanar Waveguide Fed Wideband Slot Antenna,” Electronics Letters, 3rd August 2000, Vol. 36, No. 16.

[32] M. Unlu, K. Topalli, H. Sagkol, S. Demir, O. Aydin Civi, S. Koc, and T. Akin, "New MEMS Switch Structures for Antenna Applications," *2002 IEEE AP-S International Symposium and USNC/URSI National Radio Science Meeting*, p.134, San Antonio, Texas, 16-21 June 2002.